

Diss. ETH No. 24602

**Development of Model Complexes for the Study of the Transmetalation Step
in Palladium Catalyzed Cross-Coupling Reactions**

A thesis submitted to attain the degree of

DOCTOR OF SCIENCES of ETH ZURICH

(Dr. sc. ETH Zurich)

presented by

RAPHAEL JOSEPH OESCHGER

MSc in Chemistry ETH

born on April 26th, 1987

citizen of Mettauertal, AG

accepted on the recommendation of

Prof. Dr. Peter Chen, examiner
Prof. Dr. Hansjörg Grützmacher, co-examiner

2017

"The miracle isn't that I finished. The miracle is that I had the courage to start."

- John Bingham, marathon runner

Acknowledgements

I would like to thank *Prof. Dr. Peter Chen* for giving me the opportunity to work in his group. His broad knowledge, sense for the right experiment, and allowance for scientific freedom made him a great research advisor, and his trust, passion for chemistry, along with his unforgettable stories, made him an exceptional supervisor.

I also thank *Prof. Dr. Hansjörg Grützmacher* for being my co-examiner and for his interest in my work.

Many thanks to *Dr. Andreas Bach, Mirella Rutz, Anke Witten, and Gabriela Schenk* for their administrative work and for organizing group events.

Armin Limacher has provided great technical support and he was always ready to help when an equipment did not work the way it should.

Dr. Tim den Hartog, Dr. Erik Couzijn, Dr. Adil Zhugralin, Dr. Laurent Batiste, and Dr. Marija Jović helped me a lot when I first arrived in the group. Thanks for guiding me in the laboratory or discussing my experiments.

Dr. Iliia Kobylanskiĭ's and *Marek Bot's* knowledge about mass spectrometers is outstanding and they were always ready to share it with me. Lessons about Eastern European history, politics and culture by Marek Bot were also highly appreciated.

Thanks a lot to *Lukas Fritsche* for the ping-pong lessons, running sessions and organizing my favorite Chen-group event: the SOLA run. The summer outings and ski trips organized by *Dr. David Ringger* were awesome and the cheerful characters of *Dr. Augustin Tchawou* and *Inesa Hadrovic* created a very pleasant atmosphere in our group.

It was fantastic to work together with *Joël Gubler, Stefan Jungen* and *Yannick Stöferle* in the Swiss Lab. They taught me how to work with Swiss precision and that "the early bird catches the worm" - thanks a lot.

Dr. Renana Poranne's, Stefan Künzi's, Robert Pollice's, and Eno Paenurk's enthusiasm for chemistry was contagious and I greatly benefited from scientific discussions.

I also want to thank *Dr. Krista Vikse, Dr. Mihai Răducan, Dr. Juan Manuel Sarria Toro, Yanan Miao, Dr. Alexandra Tsybizova, Dr. Larisa Miloglyadova, and Kevin Breitwieser* for their support and for creating a great atmosphere in our group.

The work of my semester students *Adrian Mühlbach, Evelyn Parmentier, and Tom Schatteburg* was highly appreciated. Results from *Raphael Bissig's* master thesis even made it into this dissertation and I wish him an exciting and successful Ph.D. time in the Chen-group.

I want to thank *Leslie Hansen* for endless support over the last years, particularly when it became stressful at work. Finally, I would like to thank my *parents and sisters* for their support and for always be there for me.

Published Parts of the Thesis

Reviewed Articles

- [Raphael J. Oeschger](#), David H. Ringger, Peter Chen, Gas-Phase Investigations on the Transmetalation Step in Sonogashira Reactions, *Organometallics* **2015**, 34, 3888
- [Raphael J. Oeschger](#), Peter Chen, Structure and Gas-Phase Thermochemistry of a Pd/Cu Complex: Studies on a Model for Transmetalation Transition States, *J. Am. Chem. Soc.* **2017**, 139, 1069
- [Raphael J. Oeschger](#), Peter Chen, A Heterobimetallic Pd–Zn Complex: Study of a d^8 – d^{10} Bond in Solid State, in Solution, and in Silico *Organometallics* **2017**, 36, 1465

Poster Presentations

- [Raphael J. Oeschger](#), Peter Chen, “Heterobimetallic d^8 – d^{10} complexes as intermediates, transition states, and transition state analogs for the transmetalation step in Sonogashira and Negishi coupling reactions, SCS Fall Meeting 2017, Bern, Switzerland
- [Raphael J. Oeschger](#), David H. Ringger, Peter Chen, Gas-phase “Investigations on Transmetalation step in Sonogashira reactions”, OMCOS 2015, Sidges, Spain

Table of Contents

Abstract	1
Zusammenfassung	3
1 Introduction	5
2 Gas-phase investigations on the transmetalation step in Sonogashira reactions	19
3 Investigations on the mechanism of Pd-Cu transmetalation reactions	39
4 Study of a model complex for transmetalation TS in Negishi couplings	73
5 Conclusions and Outlook	87
6 Appendix	91

Abstract

Palladium catalyzed cross-coupling reactions are mild, chemoselective, functional group tolerant, and practical protocols for the formation of C-C bonds. Of the three main steps within a typical catalytic cycle for Pd catalyzed cross-couplings, oxidative addition, transmetalation, and reductive elimination, previous mechanistic studies have identified the transmetalation step to be the key step for the successful outcome of most reactions of this type. This thesis explores the detailed reaction mechanism of the transmetalation processes in Pd catalyzed Sonogashira and Negishi couplings.

Chapter 1 describes the gas-phase investigations on the microscopic reverse of the Pd/M (M: Cu, Ag, Au) catalyzed Sonogashira transmetalation. For that, heterobimetallic Pd(II)/M(I) (d^8 - d^{10}) model complexes were synthesized, their reactivity was studied qualitatively and quantitatively in the gas-phase, and the mechanism of the reaction pathways was explored by density functional theory (DFT) calculations. Thereby it was found that the activation energy for the actual M-C bond breaking, Pd-C bond forming process is surprisingly low and we postulated that the low reaction barriers are due to favorable Pd-M metal-metal interactions.

To study in more detail the crucial interactions between d^8 - and d^{10} -metals in the transition state (TS) for transmetalations, we established bimetallic model systems designed such that they closely resemble the proposed transition state structures of the Sonogashira transmetalation. Chapter 2 describes the development, synthesis and study of a heterobimetallic Pd(II)/Cu(I) complex. The crystal structure of the Pd/Cu complex contains a short metal-metal bond that is bridged over the carbon atom of the benzo[h]quinolinato (bhq) ligand,

looking very similar to the TS's proposed for the Sonogashira transmetalation. Therefore, the quantification of metal-metal bond strength in the gas-phase allowed us to estimate the net stabilization energy of the transition state for Pd-Cu transmetalations due to the close Pd(II)-Cu(I) contact.

The (bhq)₂Pd fragment used in the Pd/Cu model complex turned out to be exceptionally practical and it was also applicable to study the interaction between Pd(II) and other d¹⁰ metals, namely Au(I) and Zn(II). Chapter 3 deals with the synthesis and structural characterization of the first example of a dinuclear complex containing an unsupported Pd(II)-Zn(II) bond. The [Pd]...[Zn] dissociation energy in solution was measured by NMR spectroscopy and the bonding was analyzed by computational methods. The results led to a better understanding of Pd/Zn transmetalations and will be used for rational optimization of the reaction conditions for Negishi type couplings.

Zusammenfassung

Palladium katalysierte Kreuzkupplungsreaktionen zur Synthese von C-C Bindungen sind mild, chemoselektiv, tolerieren viele funktionelle Gruppen und sind einfach durchführbar. Ein typischer Katalysezyklus beinhaltet oxidative Addition, Transmetallierung und reduktive Eliminierung. Mechanistische Studien haben gezeigt, dass der Transmetallierungsschritt besonders wichtig für den Ausgang der Reaktion ist. Die vorliegende Arbeit erforscht den detaillierten Mechanismus vom Transmetallierungsschritt in Pd katalysierten Sonogashira und Negishi Kupplungsreaktionen.

Kapitel 1 beschreibt die Untersuchungen der Umkehrreaktion des Transmetallierungsschritts der Pd/M (M: Cu, Ag, Au) katalysierten Sonogashira Reaktion in der Gasphase. Dafür wurden heterobimetallische Pd(II)/M(I) (d^8 - d^{10}) Modellkomplexe synthetisiert, deren Reaktivität wurde in der Gasphase qualitativ und quantitativ untersucht, und der Mechanismus des Reaktionsverlaufs wurde mittels Dichtefunktionaltheorie (DFT) untersucht. Dabei wurde herausgefunden, dass die Aktivierungsenergie für den Schritt, in welchem die M-C Bindung gebrochen und die Pd-C Bindung gebildet wird, unerwartet niedrig ist. Wir haben postuliert, dass die niedrige Reaktionsbarriere durch Pd-M Metall-Metall Wechselwirkungen zustande kommt.

Um diese wichtigen Wechselwirkungen zwischen d^8 - und d^{10} Metallen in Übergangszuständen (ÜZ) von Transmetallierungsreaktionen detailliert zu untersuchen, haben wir bimetalliche Modellsysteme entworfen, die so konzipiert sind, dass sie den Strukturen der ÜZ der Sonogashira Transmetallierung ähnlich sind. Kapitel 2 beschreibt die Entwicklung, die Synthese und die Studie eines heterobimetallischen Pd(II)/Cu(I) Komplexes. Die

Kristallstruktur des Pd/Cu Komplexes enthält eine kurze Metall-Metall Bindung, welche über ein Kohlenstoff Atom des benzo[h]quinolino (bhq) Liganden verbrückt ist und ähnelt dabei stark den vorher vorgeschlagenen Strukturen der ÜZ von Sonogashira Transmetallierungsreaktionen. Die Quantifizierung der Metall-Metall Bindungsenergie in der Gasphase erlaubte uns die netto Stabilisierungsenergie des Übergangszustandes aufgrund der Pd(II)-Cu(I) Wechselwirkung abzuschätzen.

Das (bhq)₂Pd Fragment, welches wir für den Pd/Cu Modellkomplex verwendet haben, hat sich als speziell gut geeignet herausgestellt und konnte auch für die Untersuchung von Wechselwirkungen zwischen Pd(II) und anderen d⁸ Metallen, Au(I) und Zn(II), verwendet werden. Kapitel 3 beschreibt die Synthese und Charakterisierung der Struktur vom ersten Beispiels eines dinuklearen Komplexes mit einer freistehenden Pd(II)-Zn(II) Bindung. Die [Pd]...[Zn] Dissoziationsenergie wurde in Lösung mittels NMR Spektroskopie gemessen und die Bindung wurde mit Computermethoden untersucht. Die Resultate haben zu einem besseren Verständnis von Pd/Zn Transmetallierungsreaktionen geführt und werden dafür verwenden, die Reaktionsbedingungen von Negishi Kupplungsreaktionen zu Optimieren.

1 Introduction

1.1 Pd in Cross-Coupling Reactions

The discovery and development of transition metal catalyzed cross coupling reactions have changed the world of synthetic organic chemistry. The first examples go back more than 100 years when Glaser and Ullmann found that copper catalyzes the homocoupling of alkynes and aryl halides. The most innovative period started in the 1960s with the discovery of carbon-carbon bond forming palladium catalyzed reactions and climaxed with the awarding of

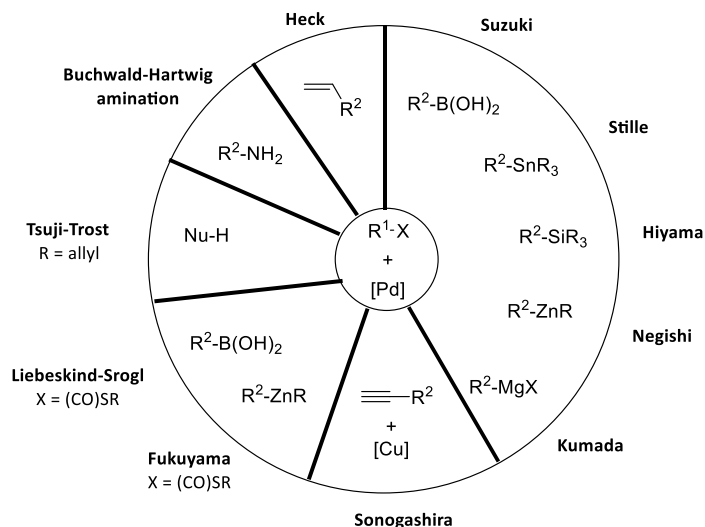


Figure 1: Overview of most common Pd-catalyzed cross-coupling reactions.¹

the Nobel Prize in 2010 to Heck, Suzuki and Negishi “for palladium-catalyzed cross couplings in organic synthesis”. This inspired chemists to develop a wide-range (72 different classes)² of additional Pd catalyzed cross-coupling reactions such as carbon-heteroatom coupling, α -arylation, direct arylation by C-H

activation, decarboxylative couplings and others.³ Figure 1 displays an overview of the most established Pd-catalyzed reactions.

Today, Pd catalyzed cross-coupling protocols are often used as mild, selective, functional group tolerant and reliable processes in complex natural product syntheses, pharmaceutical and agrochemical applications, as well as for the production of new materials.¹ They all have in common that they couple electrophilic with nucleophilic carbon fragments, the most common combinations are organohalides (R-X) with organometallic coupling partners. It is assumed that all these C-C bond forming reactions basically follow a similar generalized catalytic cycle (Figure 2) consisting of oxidative addition, transmetalation, and reductive elimination as elementary steps.⁴

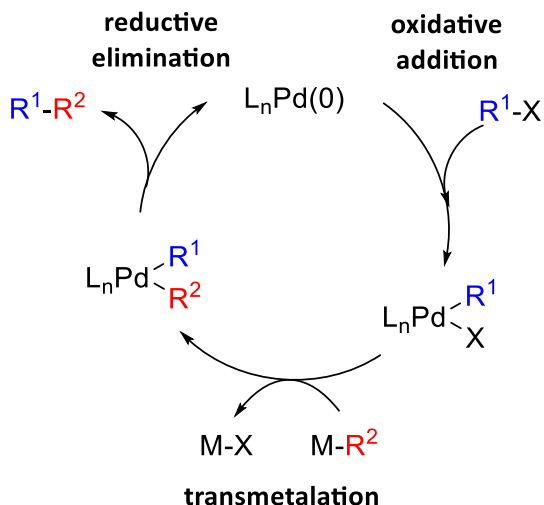


Figure 2: Basic mechanism of Pd-catalyzed cross-coupling reaction

In the oxidative addition step, crudely put, a hydrocarbon fragment is activated. Depending on the particular nature of the catalyst and the substrate, oxidative

addition proceeds either via a concerted 3-center *cis*-addition pathway or nucleophilic substitution (S_N2 type) of the halide by the metal center, followed by coordination of the halide.⁵⁻⁶ The reactivity of C-X bonds towards oxidative addition on Pd(0) normally follows the bond dissociation energy C-I > C-Br = C-OTf > C-Cl and C_{sp^2} -X add faster than C_{sp^3} -X.⁷⁻⁸ The next step in the cycle is transmetalation, a reaction where a second hydrocarbon residue is transferred onto Pd. This step is the topic of this thesis and the current literature is summarized in chapter 1.2. The catalytic cycle is closed by reductive elimination, the process where the new C-C bond is being formed. It is formally the microscopic reverse of oxidative addition; however, unlike the case of oxidative addition, non-polar C-C bonds (and not polar C-X bonds) are involved. Therefore, the reaction is assumed to proceed via a concerted 3-center transition state (TS) where the two M-C bonds are being broken simultaneously.⁹⁻¹⁰ The order of relative rate of reductive elimination follows the bond strength of the newly formed C-C bond aryl-aryl > aryl-alkyl > alkyl-alkyl.¹¹

Depending on the reaction, and the specific conditions, each one of these processes has been claimed, in one circumstance or another, to be rate-limiting. Whereas the mechanisms of oxidative addition and reductive elimination, even though still under investigation, are rather well studied, transmetalation remains relatively poorly understood.

1.2 The Transmetalation Step in Pd-Catalyzed Cross-Coupling Reactions

1.2.1 Transmetalation in Suzuki-Miyaura Reaction

Even though the Suzuki-Miyaura coupling is the most applied cross-coupling procedure, the exact mechanism of its transmetalation step is still under investigation. The main dispute in the literature is about the role of the base and how it initiates the transmetalation event.¹²⁻¹³ Two different pathways (**A** and **B**, Figure 3) are considered. In pathway **A** the base (typically hydroxide or alkoxide, M-OR) activates the boronic acid by forming a negatively charged nucleophilic organoboronate species that reacts with an electrophilic Pd-X. Pathway **B** proceeds via neutral electrophilic boronic acid and nucleophilic Palladium alkoxide/hydroxide. Both routes react to the same intermediate with a characteristic Pd-O-B unit, from which the aryl group is transferred from B to Pd.

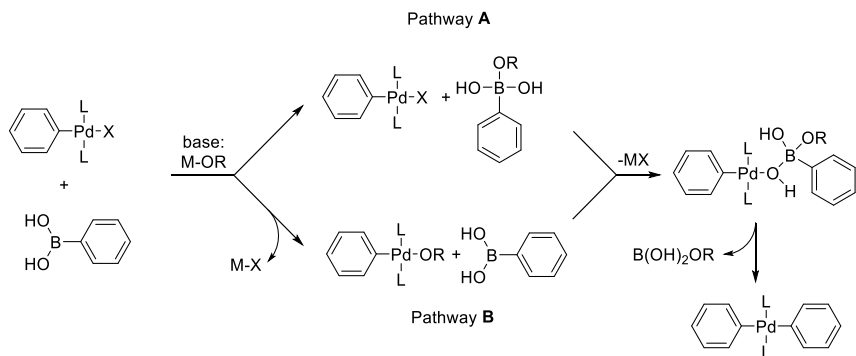


Figure 3: Proposed transmetalation pathways (**A**) and (**B**) for the Suzuki coupling.

Computational studies by Maseras suggested that pathway **A** is active during catalysis, mainly because the direct replacement of palladium halide (X⁻) by the

base (OR) was calculated not to be feasible.^{6, 14} Experimentally the role of the base was investigated by Soderquist¹⁵ and later by Hartwig¹⁶, Amatore and Jutand¹⁷, and Schmidt¹⁸. By investigating stoichiometric reactions of preformed $(\text{Ph}_3\text{P})_2\text{PdPhBr}$ and $(\text{Ph}_3\text{P})_2\text{PdPhOH}$ with $[\text{B}(\text{tol})(\text{OH})_3]\text{K}$ and $\text{B}(\text{tol})(\text{OH})_2$ respectively, Hartwig's group found that, at least for the tested system, Path **B** is faster than Path **A** by more than four orders of magnitude. Extensive kinetic studies by Amatore and Jutand supported this conclusion. Although a pre-transmetalation intermediate containing a Pd-O-B unit has been proposed before, the direct observation and characterization of this short living species succeeded only very recently when Denmark and coworkers identified three different complexes containing a Pd-O-B linkage by rapid injection NMR.¹⁹⁻²⁰

1.2.2 Transmetalation in Stille Reaction

By far the best investigated cross-coupling from a mechanistic viewpoint is the Stille coupling.²¹⁻²³ The detailed kinetic treatment of the Stille coupling by Espinet and coworkers, with a fully elaborated, i.e. not simplified, catalytic cycle, give an unprecedentedly thorough picture of the reaction. Also the isolated transmetalation step has been investigated thoroughly. Stille and Labadie²⁴ found that the reaction proceeds with predominant inversion of configuration whereas Falck et al.²⁵ reported complete retention of configuration in a related process, however, using somewhat different reaction conditions. Based on these findings and additional kinetic results, Espinet and Casado²⁶⁻²⁸ proposed a dual catalytic cycle with two different transition states, one closed (cyclic) and one open (linear) respectively (Figure 4).

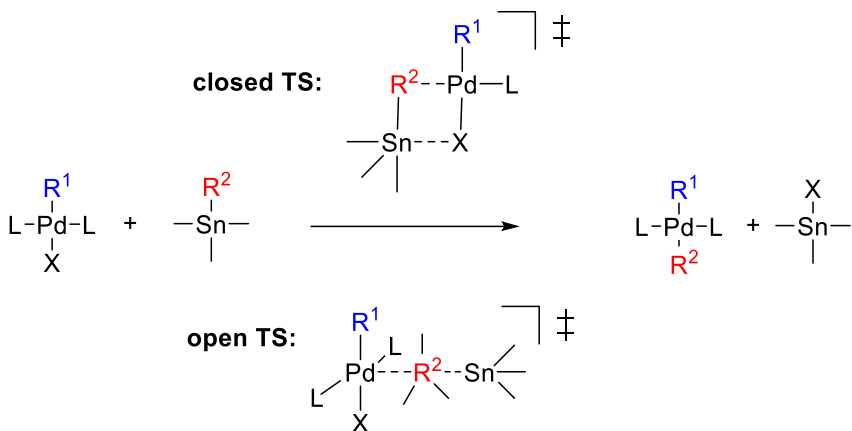


Figure 4: Closed and open TS for the transmetalation in the Stille reaction.

In both cases, cyclic or linear TS, the Pd complex is seen as the electrophile and the Sn moiety as the nucleophile. Which one of the two transition states is favored depends on the exact conditions, but it is assumed that most reactions do proceed by open mechanisms.²²

Even though no one explicitly says that the same transition state is preferred for all cross-coupling reactions, it appears nevertheless to be assumed implicitly by many investigators to apply for most other cases too, including the ones employing isoelectronic Cu(I) (Sonogashira) or Zn(II) (Negishi) instead of Sn(IV).

1.2.3 Transmetalation in Negishi Reaction

The transmetalation step in the Negishi reaction is a complex transformation that has become subject of mechanistic studies only in the recent years and is, therefore, not yet well understood. Most of the work is done by Espinet and coworkers who established 2007 that the kinetics and mechanism of the reaction differ when using ZnMe₂ instead of ZnMeCl.²⁹ They found that the

transmetalation from ZnMe_2^{30} to $(\text{PMePh}_2)_2\text{PdMeCl}$ is faster than from ZnMeCl^{31} , probably because of the formation of highly reactive ionic intermediate $[\text{PdMe}(\text{PMePh}_2)_2(\text{THF})]^+$. This intermediate is not accessible with ZnMeCl , perhaps because of the lower nucleophilicity of the zinc reagent. In any case, transmetalation between Pd and Zn is very fast and this step is therefore, unlike many other Pd-catalyzed cross-coupling reactions, not rate-limiting in the catalytic cycle. Lei et al.³²⁻³³ determined that the turnover-limiting step is most likely reductive elimination, which, by definition, would render the preceding transmetalation step reversible at steady-state. This situation can lead to undesirable side-reactions and will be discussed in more detail in chapter 4.

Despite the importance of the transmetalation step in the Negishi coupling, detailed evidence of intermediates and transition states of Pd-Zn transmetalations are rare and purely based on DFT calculations, even though Espinet points out the eminent importance of a specific element of these proposed structures:

“However, a distinct feature found in the theoretical study of the Negishi transmetalation and absent in the Stille reaction is the existence, in both transition states and in some intermediates, of Pd...Zn bond interactions between the electron-rich Pd center and the fairly positive Zn center. These interactions are deemed responsible for the remarkably low energy of the transmetalation barriers with organozinc compounds as nucleophiles, compared with the noticeably higher barriers for organotin compounds.”³¹

Espinet’s suggestion, that bimetallic interactions are responsible for lowering the barrier of transmetalation processes between Pd(II) and Zn(II), was inspired by recent work done in our group on the isoelectronic Pt-Cu and Pt-Au

systems.³⁴⁻³⁵ Thereby, it was found that the exchange of methyl groups is supported by the formation of metal-metal bonds. Bonds between Pd(II) and Zn(II) had not been observed experimentally (until our recent publication³⁶, see Chapter 4), but examples of isoelectronic d^8 - d^{10} metal-metal bonds are known in the literature.

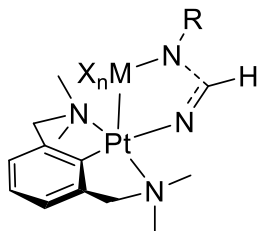
1.3 Heterobimetallic d^8 - d^{10} Complexes

1.3.1 Examples of Pt(II)/Pd(II)(d^8) - M(d^{10}) Complexes

Square-planar Pt(II) complexes that form metal-metal bonds to Lewis acidic d^{10} metals have been known since the 1980s, when Van Koten³⁷⁻³⁸ first reported on Pt(II)-Hg(II) and Pt(II)-Ag(I) complexes; however, it should be noted that those d^8 - d^{10} bonds were supported by bridging formamidino ligands (Figure 5). A few years later, Puddephatt and co-workers³⁹ identified unbridged Pt(II)-Ag(I) and Pt(II)-Au(I) complexes by NMR spectroscopy. A free-standing d^8 - d^{10} bond was shortly thereafter characterized crystallographically in a Pt(II)-Ag(I) complex by Usón and Cotton⁴⁰ (Figure 5).

Since these early examples, numerous bimetallic complexes with a Pt(II)-M bond have been prepared.⁴¹⁻⁴² Different coordination modes for the binding of Pt(II) fragments to Lewis-acidic metals can be distinguished (Figure 6). Type I represents a binding mode where the metal-metal bond stands perpendicular to the coordination plane of the d^8 metal, in type II and III, the Lewis-acidic metal is tilted towards one or two of the ligands on Pt, and in type IV, the metal-metal interaction is stabilized by one or more covalent bridges. The most common d^{10} metal has been Ag(I)^{40, 43-46}, but also examples featuring unbridged metal-metal

van Koten (1982):



MX_n : HgBrCl, AgBr

Usón, Cotton (1985):

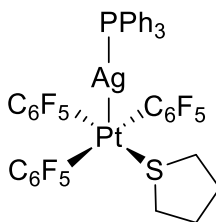


Figure 5: Early examples of heterobimetallic complexes with Pt(II)- d^{10} .

bonds to Cu(I)^{35, 44}, Au(I)⁴⁷, Zn(II)⁴⁸⁻⁴⁹, Hg(II)⁵⁰⁻⁵¹, Cd(II)⁵² are known. Some landmark examples of bimetallic complexes featuring unsupported Pt(II)-M bonds are shown in Figure 7.

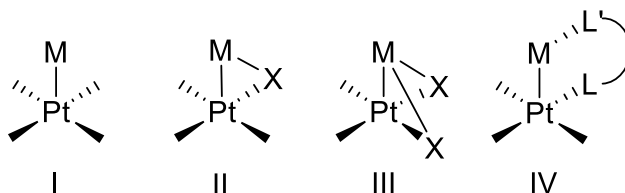


Figure 6: Possible binding modes of square-planar Pt(II) complexes to Lewis-acidic metals M.

Heterobimetallic complexes with a d^8 - d^{10} bond to Pd(II) as the d^8 component are far less common, as the metal-metal interaction is significantly weaker. Only a handful structural analyses of unsupported metal-metal bonds have been reported, with Cu(I)⁵³, Ag(I)⁵⁴⁻⁵⁶, Au(I)⁵⁷, and Hg(II)⁵⁸, and some selected examples are shown in Figure 8. The Pd-Ag complex by Heckenroth and Albrecht⁵⁵ is particularly outstanding since dicationic Pd(II) acts as Lewis acid towards a cationic silver(I) complex. The unusual interaction probably becomes

possible because of the exceptionally strong σ -donor property of the abnormal NHC-ligand.

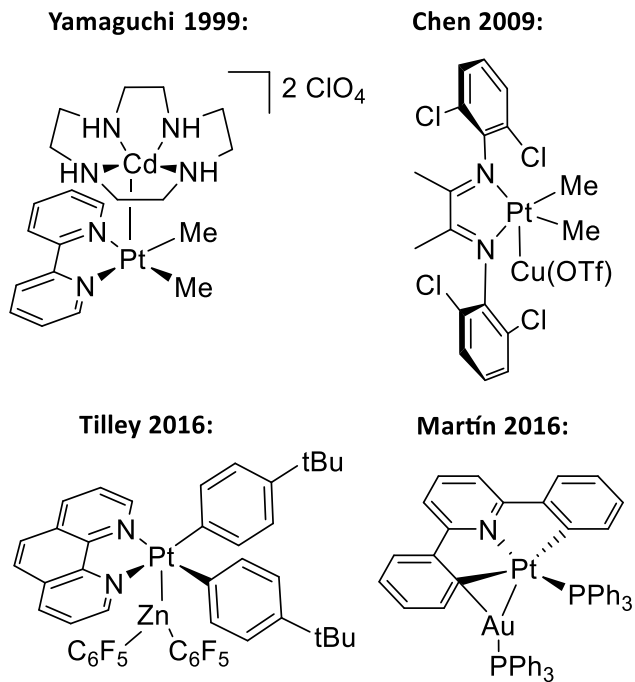


Figure 7: The first bimetallic complexes featuring a unsupported Pt(II)-Cd(II), -Cu(I), -Zn(II) and -Au(I) bond.

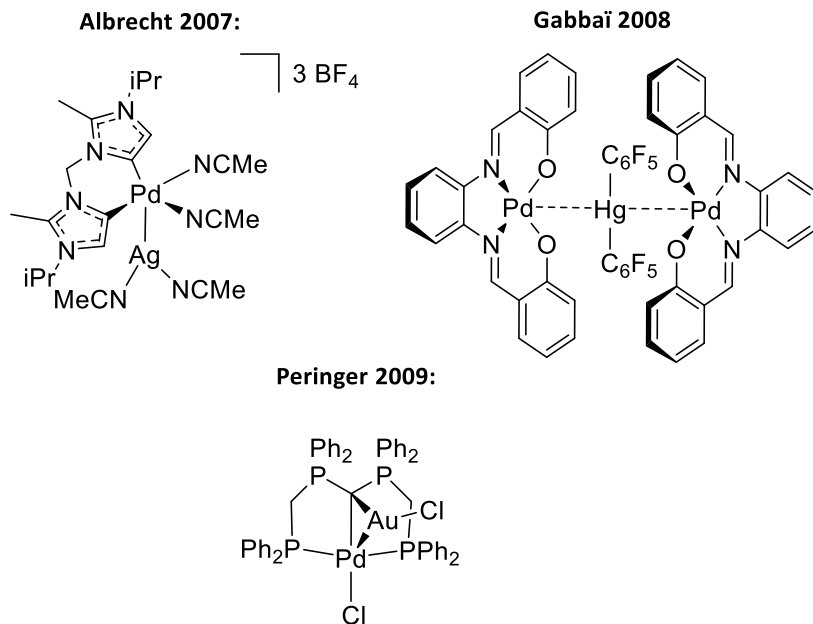


Figure 8: Heterobimetallic complexes of Pd(II)-Ag(I), -Hg(II), and -Au(I).

1.3.2 Bonding in d^8 - d^{10} Complexes

The electronic configuration of Palladium(II) and Platinum(II) is d^8 . With strongly donating ligands, d^8 -metals preferably form square-planar low-spin complexes where the d_{xz} , d_{yz} , d_{xy} and d_{z^2} are filled and the $d_{x^2-y^2}$ is empty. In a strong ligand field, the unoccupied $d_{x^2-y^2}$ -orbital is further destabilized and thus, even though square planar d^8 complexes are electronically unsaturated 16 electron complexes, they behave as pseudo-closed-shell species.⁵⁹ The highest molecular orbital (HOMO) is, in a simple picture, the d_{z^2} -orbital. It points perpendicular to the coordination plane of Pt/Pd, towards an empty region of space, and is, therefore, able to interact with Lewis-acidic species and form dative bonds. This qualitative orbital picture has been used for the studies of

associative ligand exchange on square-planar complexes⁶⁰⁻⁶¹, but it is also adapted to metallophilic⁶² bonds, meaning attractive interactions between closed shell transition metals.⁴¹⁻⁴² This simple picture of the bonding is commonly used to explain empirical observations, like for example that hard (C-, N- or O-donor) ligands stabilize metal-metal bonds by interacting with the “donut” of the d_{z^2} -orbital and thereby raising of the energy of the HOMO.

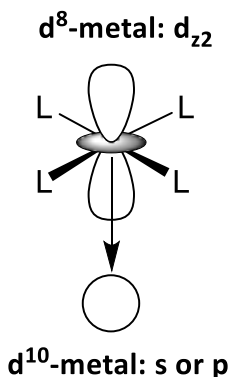


Figure 9: Interaction of the filled d_{z^2} -orbital with an empty s (or p)-orbital.

Others have explained the nature of the bond with distinct frontier molecular orbitals (FMO).⁶³⁻⁶⁷ This picture of the bonding is similar to the Lewis-acid/-base approach, however, it is more detailed, since molecular orbitals are calculated and analyzed instead of simply assuming that only one donor and one acceptor orbital is involved in the bonding.

This explanation of the bonding has been questioned by more recent work of theoretical chemists.^{59, 68-70} Calculations suggest that the attractive metallophilic bonding is not (only) due to orbital interaction, but predominantly because of dispersion effects, i.e. dynamic correlation of electrons.

In general, experimental data on d^8 - d^{10} systems are rare, especially such that are relevant for (Pd-) catalysis. Most of the knowledge is purely empirical, i.e. hard donor ligands on the d^8 -metal are stabilizing the M-M bond, or soft d^{10} -metals (Hg(II), Cd(II)) are better because of a better overlap with the large (soft) d_{z^2} -orbital. The only reported experimental study of a Pd-Au bond has been done by Laguna et al.. They crystallographically characterized a bridged Pd-Au complex, measured the metal-metal bond energy in solution to be 13 kcal/mol and analyzed the bonding by calculations (Figure 10).⁷⁰

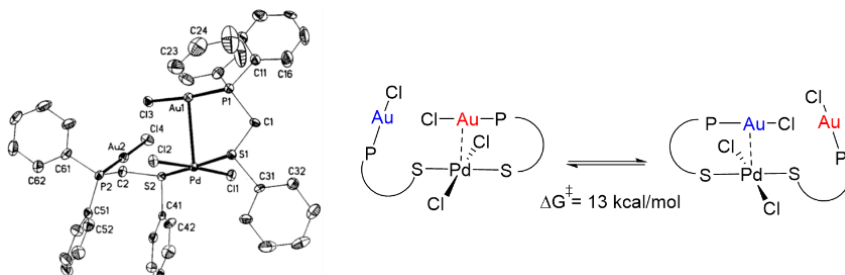


Figure 10: X-Ray structure (left) and NMR-experiment of Pd-Au system by Laguna.⁷⁰

1.4 Scope and Outline of Thesis

When reviewing the literature about metal-metal interactions in Pd-catalysis, it becomes evident, that there is literature about this topic in different fields of chemistry. Organic chemists report about mechanistic experiments, structural inorganic chemists are interested in the structure of bimetallic complexes and theoretical chemist study the bonding by computational methods. The drawback, however, is that these communities are largely isolated from each other. This leads to the situation in which e.g. structural chemist study systems

not relevant to mechanistic investigators or theoretical chemist do not know that their knowledge might be relevant to synthetic applications.

The aim of this thesis is to combine synthetic work, structural studies, thermochemical measurements and the application of computational methods to first develop model systems and then use them to study crucial effects and properties of transmetalation processes in Pd catalyzed cross-coupling reactions.

Chapter 2 describes the gas-phase and computational investigation of the transmetalation step in the Sonogashira reaction. Chapter 3 presents the thorough structural, gas-phase, solution-phase and computational study of bimetallic Pd-Cu complexes. In Chapter 4, a heterobimetallic Pd-Zn complex is analyzed by X-ray, by NMR spectroscopy and by computational methods. Chapter 5 gives a short discussion of possible future explorations and Chapter 6 consists of details about experimental and computational methods used in this work.

2 Gas-phase investigations on the transmetalation step in Sonogashira reactions

Dr. David Ringger is acknowledged for help with the gas-phase experiments. Parts of the work presented in this chapter is published: Raphael J. Oeschger, David H. Ringger, Peter Chen, Gas-Phase Investigations on the Transmetalation Step in Sonogashira Reactions, *Organometallics* **2015**, *34*, 3888.

2.1 Threshold-CID Measurements by ESI-MS/MS

Electrospray-ionization (ESI) is a technique to transfer ions from solution into the gas-phase. This “soft” ionization method in combination with tandem mass spectrometry (MS/MS) to separate charged molecules by mass to charge ratio, followed by fragmentation by collision induced dissociation (CID), has turned out to be particularly useful. While qualitative CID experiments can be performed on most commercially available instruments, for quantitative CID some customized modifications are required. Within the Chen group, a TSQ-700 ESI-MS/MS equipped with 24-pole ion guide (see Figure 12) is routinely used to obtain gas-phase thermochemical data.⁷¹⁻⁸¹

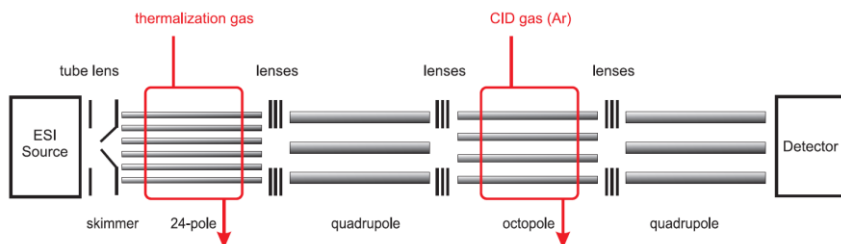


Figure 11: Schematic representation of customized TSQ-700 ESI-MS/MS.

First, ions are electrosprayed from a solution and introduced to the 24-pole where the ions are being thermalized to 70 °C by collision with Ar. Then the parent ions are mass-selected in the quadrupole and accelerated with a defined

collision-offset into the collision chamber that is filled with a gas (Ar, Xe, Ne). Upon collision, the ions are fragmented and the resulting daughter ions are analyzed with the second quadrupole. The parent and daughter intensities are measured as a function of collision offset and at 5 to 7 different collision gas pressures between 20 and 110 μ Torr. Using Lambert-Beer law, reactant and product intensities are converted into reactive cross-sections, the quantity describing the probability that two particles collide and react to product. The cross-sections at different gas-pressures are extrapolated to zero pressure in order to avoid effects from multiple collisions (see e.g. Figure 17) and these data are fitted using the software L-CID⁸⁰⁻⁸¹. In the L-CID program, cross-sections are simulated and the parameters (i.e. threshold energy) are optimized until they fit the experimental data. As input, L-CID needs little information, one being the nature of the rate-limiting transition state. For intramolecular rearrangements connecting two local minima on the potential energy surface prior to dissociation, a “tight” transition state model is used. A “loose” transition state model is appropriate for simple dissociations without reverse activation barrier.

2.2 Introduction

C-C bond forming reactions catalyzed by bimetallic Pd/M (M: Cu, Ag, Au) complexes have recently been investigated with high interest.⁸²⁻⁸³ A well-known variation of such a transformation is the Sonogashira reaction,⁸⁴ using mostly Cu(I) or alternatively Ag(I)⁸⁵⁻⁸⁹ and Au(I)⁹⁰⁻⁹⁴ salts as cocatalyst. The detailed mechanisms of these reactions are still not well understood. Nevertheless, a mechanism consisting of a Pd- and a M-cycle that are linked via a transmetalation step (Figure 12) is generally accepted.⁹⁵⁻¹⁰³

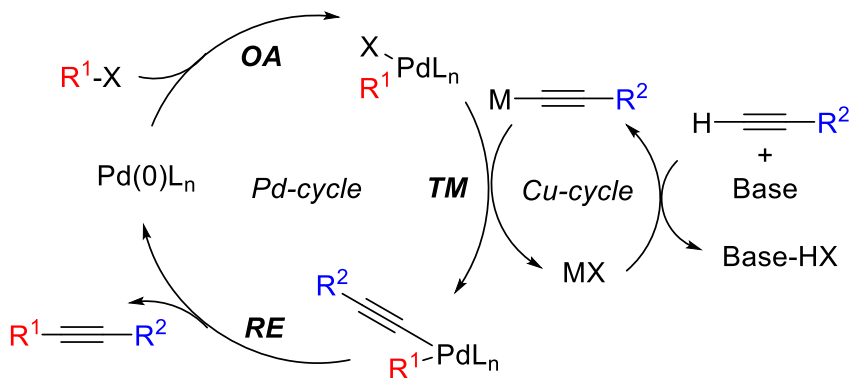


Figure 12: Catalytic cycle of the Sonogashira reaction with oxidative addition (OA), transmetalation (TM), and reductive elimination (RE).

Comparing to the more thoroughly studied Pd(0)/Pd(II) catalytic cycles, fewer experiments on Pd/coinage metal acetylide transmetalation investigations have been reported. A better understanding of the mechanisms underlying the transmetalation step will help to design rationally more efficient Sonogashira and related cross-coupling reactions.

Mechanistic studies by Osakada and Yamamoto¹⁰⁴⁻¹⁰⁶ showed that transfer of acetylides from Cu(I) to Pd(II) is reversible and goes via the formation of bimetallic intermediates. Espinet and coworkers¹⁰⁷ reported crystal structures of such previously proposed intermediates and found copper and silver chlorides coordinating to the π -bond of the Pd-acetylide. Lei et al.¹⁰⁸ performed the only quantitative kinetic study from which he proposed the transmetalation step to be the rate-limiting step of the Sonogashira reaction. Our group recently studied the transmetalation of methyl groups from Pt(II) to Cu(I)³⁵ or Au(I)³⁴ in the gas-phase and the results indicated that such a process occurs through the formation of bimetallic Pt-Cu/Au (d^8 - d^{10}) bonds. Similar findings were reported

by Espinet et al.¹⁰⁹ and Hashmi et al.¹¹⁰ for the Pd(II)/Au(I)-catalyzed cross-coupling reactions using density functional theory (DFT) calculations; their optimized intermediate and transition state structures revealed Pd-Au distances below the sum of their respective van der Waals radii. Additionally, Hashmi and coworkers demonstrated that transmetalation from Au to Pd requires simultaneous transfer of a halide from Pd to Au to be thermodynamically feasible. To further elucidate the mechanism of the Pd/coinage metal transmetalation, we wanted to study this step by mass spectrometric and computational means. We decided to investigate the microscopic reverse of the Sonogashira transmetalation because it is experimentally more convenient. The outcome is not dependent on the direction because in both ways (forward or backward) the same TSs and intermediates are accessed.

The starting point for the investigation of the retro transmetalation step are acetyldearyldiphosphine Pd(II) and a copper(I) complex. According to the catalytic cycle of the Sonogashira reaction (Figure 12), this system in principal can react in two ways: a) forwards, by reductive elimination or b) backwards, by retro transmetalation. Since reductive eliminations to form C_{sp2}-C_{sp} bonds are usually very fast (rendering acetyldearyldiphosphine Pd(II) unstable in solution) and because we were solely interested in the transmetalation step, we suppressed the reductive elimination reaction channel by building the aryl ligand into a chelating pincer ligand framework. Nevertheless, it is assumed that pincer complex **1** has very similar electronic and steric properties as the intermediates of the Sonogashira reactions (Figure 13).¹¹¹

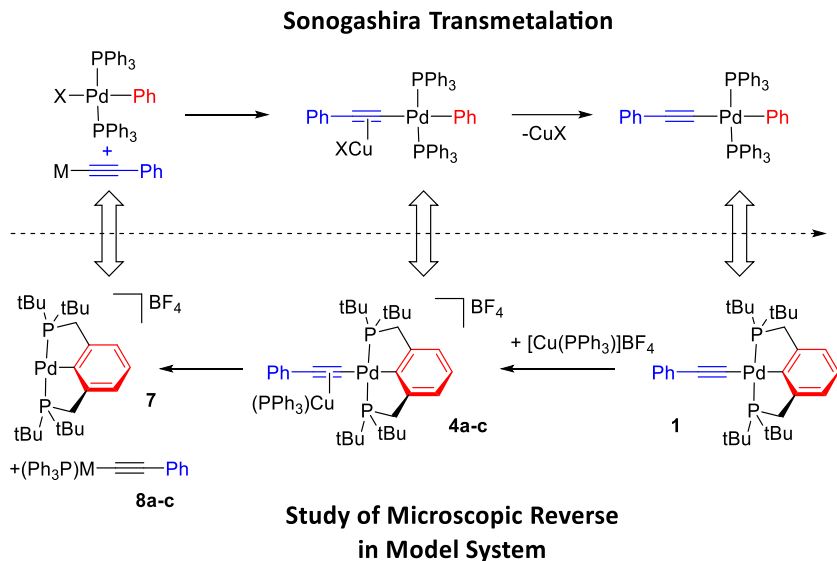


Figure 13: Comparison of intermediate structures in Sonogashira transmetalation (top) and model system (bottom).

2.3 Results

The cationic heterobimetallic complexes **4a-c**, Figure 14, were synthesized in acetonitrile solution by mixing equimolar amounts of Pd(II)

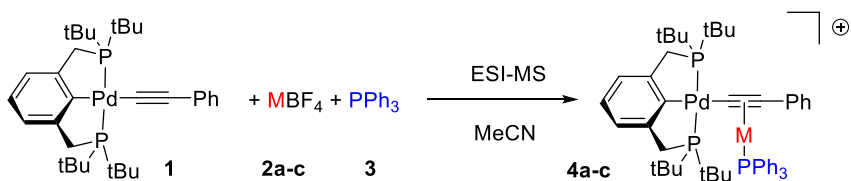


Figure 14: Generation of Cations **4a-c**.

pincer complex **1**¹¹² with MBF₄ (M = Cu(I) (**2a**), Ag(I) (**2b**), Au(I) (**2c**)) salts and triphenylphosphine **3**.

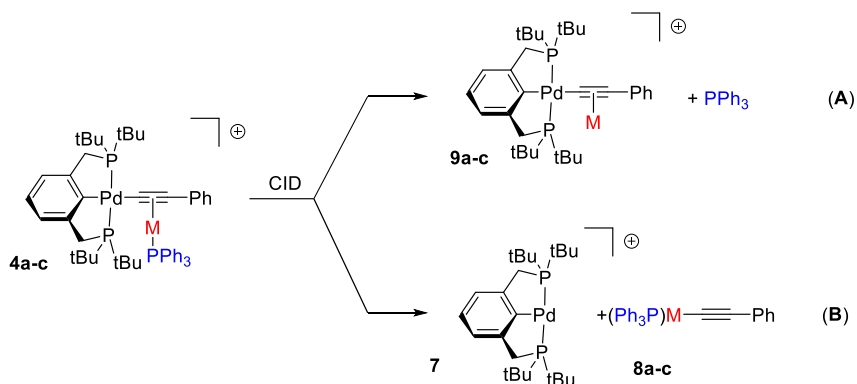


Figure 15: Reaction Pathways of **4a-c** upon CID with Ar.

The resulting charged bimetallic complexes **4a-c** were then analyzed in the gas phase by means of ESI-MS/MS techniques and the bimetallic complexes **4a-c** were identified by their *m/z* ratio. The measured isotope patterns (inset Figure 16) were found to be in good agreement with the simulated patterns, which further confirms their identity. Upon collision-induced dissociation (CID) with Argon, **4a-c** furnished two daughter signals (Figure 15 and 16). The first **(A)** corresponds to loss of the neutral PPh₃ ligand (**3**), and the second **(B)** to the transmetalation of phenylacetylide from Pd(II) to M(I), and subsequent dissociation of uncharged (PPh₃)M-C≡C-Ph **8a-c**, to form coordinatively unsaturated [(PCP)Pd]⁺ **7**. The signals resulting from PPh₃ ligand loss **(A)** are observed only for Cu and Ag but not for Au, perhaps due to the relatively high Au-P bond strength. The detection of no more than two competing dissociation pathways stemming from the same parent ion renders these systems suitable for two channel energy-resolved threshold experiments (Chapter 2.1).

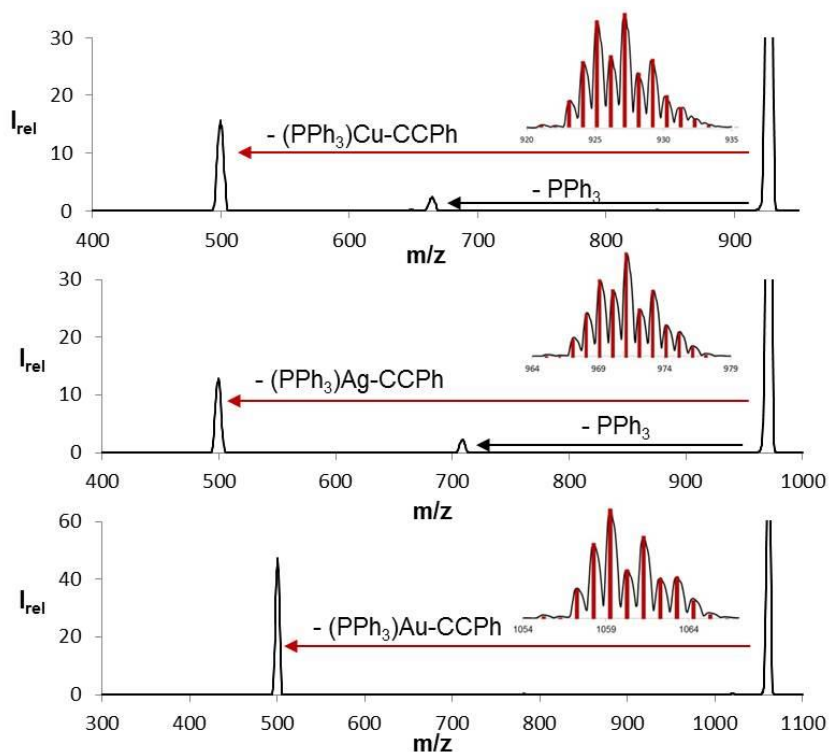


Figure 16: CID spectrum of ions **4a,b,c** at 0.2 mTorr and collision offset 90 V. PPh_3 loss (**A**) is represented by black arrows; transmetalation (**B**), by red arrows. Inset: Experimental (black) and calculated (red) isotope patterns of ions **4a,b,c**.

The gas-phase activation energies for the dissociation of PPh_3 (**A**) and transmetalation (**B**) processes were measured using the customized Finnigan MAT TSQ-700 ESI-MS/MS spectrometer described in chapter 2.1. DFT modeling of the reaction pathways of the three bimetallic complexes reveals that the barriers for the intramolecular Pd-C/M-C σ/π -rearrangements are much lower in energy than those for the subsequent dissociation of the M-acetylides (Figure 20). Based on these results, a loose TS model was chosen to be appropriate for

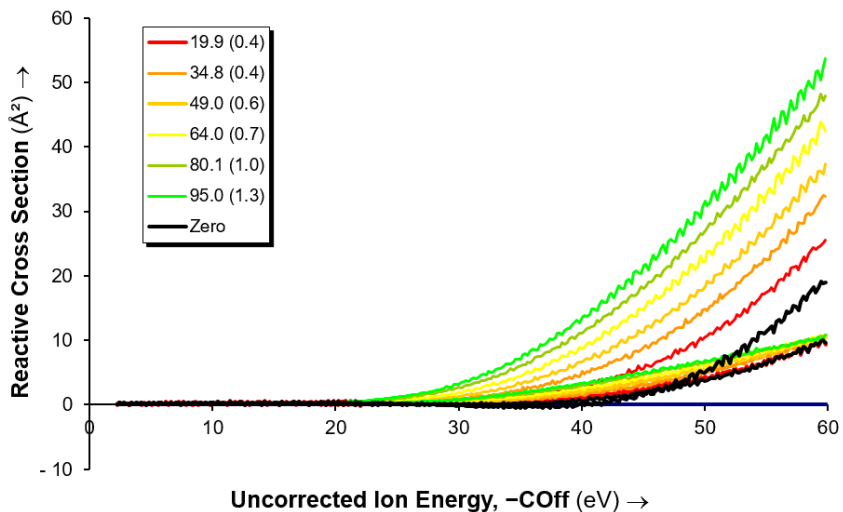


Figure 17: Reactive cross sections at various pressures (colored lines) and zero-pressure extrapolation (black line) of pathway A (lower lines) and pathway B (upper lines) for Pd/Ag. Inset: pressures of collision gas in μTorr .

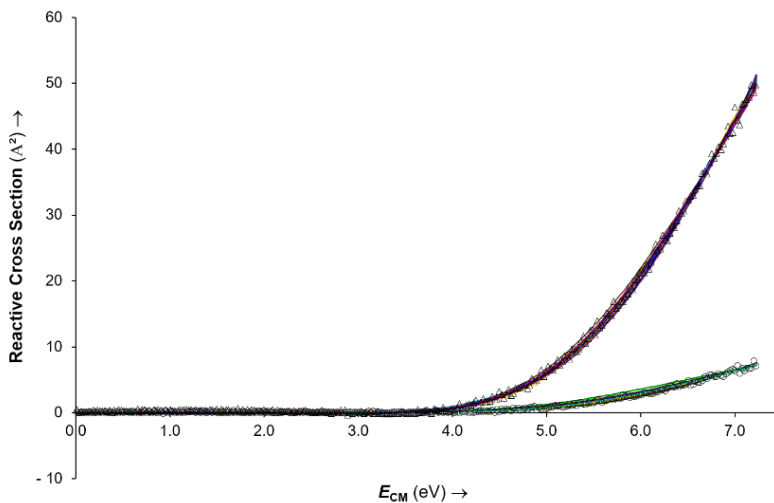


Figure 18: Zero-pressure extrapolated cross sections (circles: pathway A, triangles: pathway B) for Pd/Cu with L-CID-fitted curves (lines).

Pd/Cu	Experiment	M06-L
Pathway (A)	43.0 ± 1.1	52.8
Pathway (B)	47.0 ± 1.0	57.7
Pd/Ag	Experiment	M06-L
Pathway (A)	42.5 ± 1.5	44.3
Pathway (B)	52.8 ± 1.8	58.9
Pd/Au	Experiment	M06-L
Pathway (A)	not observed	58.7
Pathway (B)	37.7 ± 1.0	48.8

Figure 19: Table with experimental and calculated values in kcal/mol for pathways (A) and (B).

all of the reaction pathways observed for the three bimetallic complexes, **4a–c**. The activation energies for the transmetalation process (**B**) were experimentally determined to be 47.0 ± 1.0 kcal/mol for copper, 52.8 ± 1.8 kcal/mol for silver, and 37.7 ± 1.0 kcal/mol for gold. Interestingly, the measured values suggest similar reactivity for Cu and Ag, but a substantially lower reaction barrier for Au. Such an anomaly of the trend within the coinage metals have previously been observed in the investigation of the bonding energies of coinage metal nitrenes⁷⁹ and the ring opening of dimethoxycyclopropane with Cu, Ag, and Au and could be due to relativistic effects on gold.⁷⁶ The measured activation energies for the loss of the PPh₃ ancillary ligand (**A**) were measured to be 43.0 ± 1.1 kcal/mol for Cu and 42.5 ± 1.5 kcal/mol for Ag.

For a more detailed picture of the mechanisms of the observed gas phase reactivities, the potential energy surfaces were modeled by DFT calculations at the M06-L/TZP//M06-L/SDD(d,p) level of theory as implemented in ADF¹¹³ and the Gaussian 09¹¹⁴ suite. All calculated energies were zero-point energy and basis set superposition error corrected. We used the M06-L functional for our

investigation of the transmetalation (**B**) and ligand loss (**A**) reactions, because it has explicitly been designed to describe transition-metal thermochemistry, kinetics, and attractive dispersion effects between dissociating fragments. Furthermore, M06-L has modeled the experimentally obtained bond dissociation energies in previously reported gas-phase and DFT studies adequately. The DFT calculations on our model system for the Sonogashira transmetalation, however, overestimate the energies by 2–11 kcal/mol (Figure 19 and Figure 20). In accordance to the CID experiments, DFT calculations propose that complexes **4a-c** react either by direct loss of PPh₃ to form bimetallic complexes **9a-c** (Pathway (**A**)), or through a stepwise reorganization of the metal-carbon bonds and subsequent decooordination of (PPh₃)M-CCPh **8a-c**. In the latter mechanism, Pd-acetylides **4a-c** rearrange via the formation of a three-membered Pd-C-M ring and an *ipso*-carbon (**5a-c**), to an intermediate that is best described as a coinage metal acetylide with (PCP)Pd⁺ coordinated to the π -bond. The most stable computed bimetallic Pd/Cu and Pd/Ag complexes were found to be the intermediates **4a** and **4b** where [M-PPh₃]⁺ is coordinated to the π -bond of the Pd-acetylide. However, in the case of the bimetallic Pd/Au system, complex **5c**, the intermediate with a three-membered Pd-C-Au ring, was calculated to be the energetically lowest lying structure. This phenomenon could be due to the stabilizing interaction between the metals (Pd-Au, d⁸-d¹⁰). Despite these geometric differences, the loss of the PPh₃ ligand and the decooordination of M-acetylide from [(PCP)Pd]⁺ were found to be the steps with the highest barriers on the calculated potential energy surface for all three bimetallic complexes. Taking into account that the only product ion observed in the gas phase for the transmetalation step (**B**) is the cationic [(PCP)Pd]⁺ complex, in principle, the transmetalation pathways could also

proceed via the loss of the ancillary PPh₃ ligand prior to transmetalation, yielding in [(PCP)Pd]⁺, PPh₃ and M-CCPh. However, such a stepwise reaction pathway, was found to be unlikely, because it is energetically highly unfavorable and does not correlate to our experimentally measured threshold energies.

Several attempts to crystallize the bimetallic complexes **4a-c** failed, however, X-Ray crystal structures of the closely related [(POCOP)Pd-CCPh/AuIPr]OTf complex **13** (Figure 21) could be obtained. Crystals of complex **13** were formed by mixing Pd-pincer complex¹¹⁵ and [Au(IPr)]OTf¹¹⁶ in dichloromethane, followed by layering with hexane and immediate cooling to -35 °C. The structure of Pd/Au complex **13** (Figure 23) can be described as Au-acetylide with [Pd]⁺ coordinating to the triple bond. The Au-C(*C-Ph*) bond distance of 2.00 Å is only marginally elongated with respect to uncoordinated (IPr)Au-CCPh (1.98 Å)¹¹⁷. Upon coordination of Pd, the Au-acetylide fragment is somewhat distorted from linearity (Au-C-C(-*Ph*): 163.1 °) and also the geometry around Au is not exactly linear (C-Au-C: 167.1 °). The Pd-π bond is slightly asymmetric (Pd-C(-*Ph*): 2.36 Å vs. Pd-C(-*Au*): 2.30 Å).

We also managed to crystallize the [(POCOP)PdCCPh-Cu(IPr)]OTf complex and its crystal structure shows, as predicted by DFT, the [(IPr)Cu]⁺ fragment coordinated to the triple bond of the Pd-acetylide. Unfortunately, the quality of the crystals were not (yet) good enough to get a publishable X-ray structure. The only bimetallic Pd-acetylide/Cu complex we obtained in good quality is the one of [(dppe)Pd(Me)CCPh-Cu(IPr)]OTf (**14**). Even though this complex is somewhat different from **4a**, we still think that they are comparable, especially

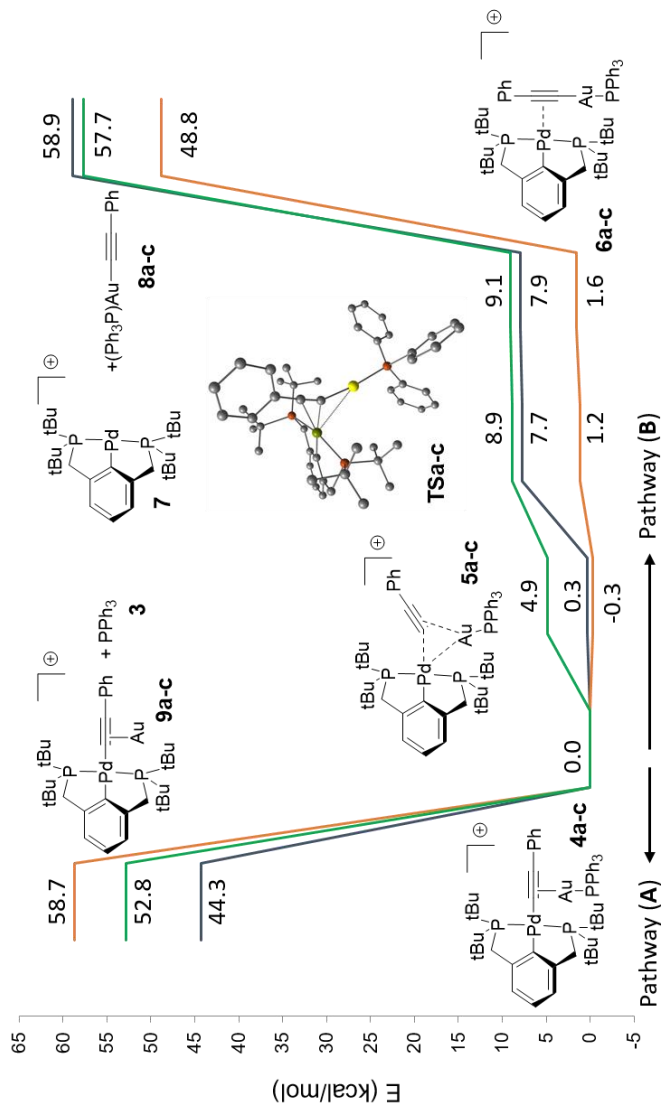


Figure 20: Calculated zero-point energy corrected potential-energy surface (M06-L/TZP//M06-L/SDD(d,p)) in kcal/mol for reaction pathways **A** and **B**. For clarity only structures of Pd/Au are shown and hydrogen atoms are excluded (red: Pd/Au, blue: Pd/Ag, green: Pd/Cu).

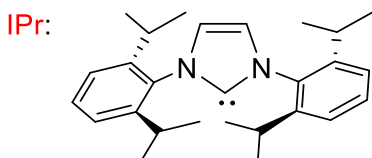
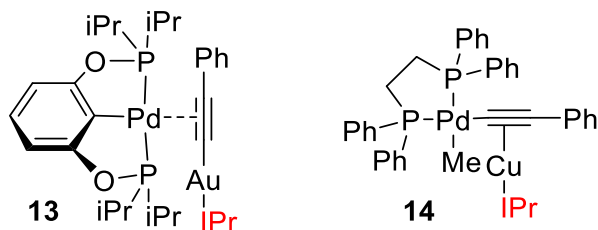


Figure 21: Bimetallic Pd/Cu **13** and Pd/Au **14** complexes for X-Ray analysis.

because the electronics at the Pd-center in **14** are expected to be similar as in **4a**. In both cases, Pd is ligated by two P- and one C-based ligand in addition to the acetylide. Crystals of **14** were grown by dissolving (dppe)Pd(Me)CCPh and [Cu(IPr)]OTf in THF and subsequent layering with diethyl ether at $-20\text{ }^{\circ}\text{C}$. The structure of bimetallic complex **14** in Figure 23 shows Pd-acetylide with [(IPr)Cu]⁺ coordinated to the triple bond. The Pd-C(CPh) bond length of 2.03 Å is in the typical range for Pd-acetylides and therefore not strongly influenced by the coordination of [Cu(IPr)]⁺. The triple bond, however, gets somewhat distorted when binding to [Cu] (Pd-C-C(-Ph): 169.8 ° and Ph-C-C(-Pd): 164.9). [(IPr)Cu]⁺ binds not exactly symmetrically to the triple bond but is slightly tilted towards the carbon bound to Pd (Cu-C(-Pd): 2.05 Å vs. Cu-C(-Ph): 2.09 Å), presumably because this end of the acetylide is more electron rich.

Since triple bonds as in phenyl acetylides have two orthogonal π -systems, the M-fragment could coordinated to either one of them. Interestingly, in the

crystal structures of **13** and **14**, both Cu and Pd coordinate to the π -orbitals not conjugated with the π -system of the phenyl rings. The reason for that observation could be that the π -orbitals not conjugated with the phenyl are higher in energy and therefore form stronger bonds to the electrophilic Cu- and Pd-fragments respectively.

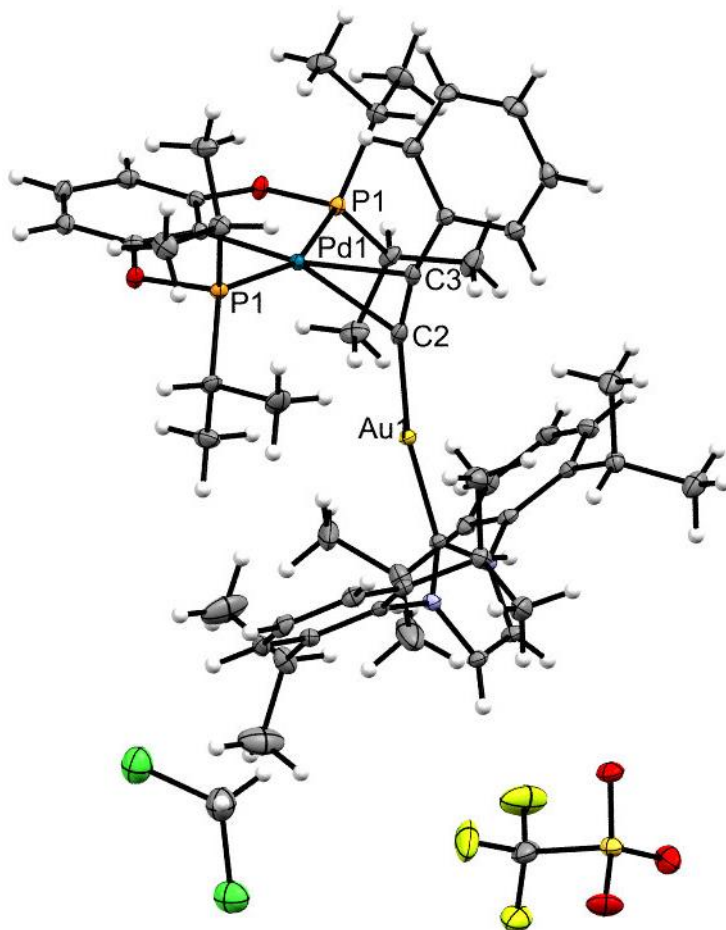


Figure 22: Thermal ellipsoid (50% probability) representation of bimetallic complex **13**.

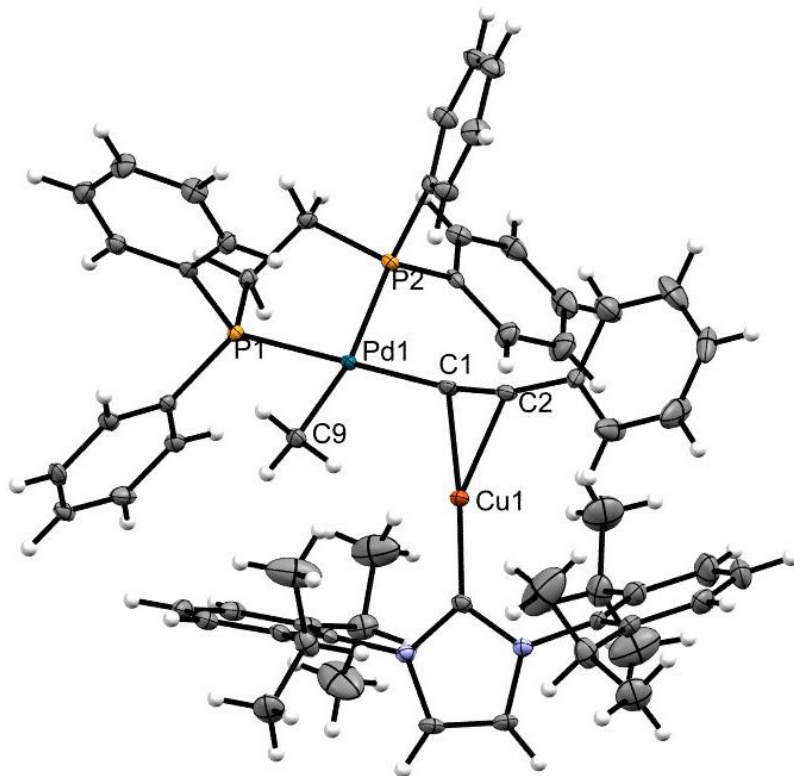


Figure 23: Thermal ellipsoid (50% probability) representation of bimetallic complex **14**.

2.4 Discussion

In the literature, only one structural study of Pd-Acetylide/Au¹¹⁸ and one of Pd-Acetylide/Cu¹⁰⁷ has been reported. Like in our molecules, the Pd-Cu complexes in the literature correspond to a Pd-acetylide with Cu coordinated to the π -bond and the Pd-Au complexes correspond rather to a Au-acetylide with Pd coordinated to the triple bond. Bimetallic complexes **14** and **13** can be seen as representatives of the two intermediates **4** and **6** of the calculated potential energy surface (Figure 20) of our model system. Their experimental structure

indicate that the proposed stepwise mechanism for the transmetalation process (Pd-acetylide - σ/π -rearrangement - M-acetylide) is correct. In the case of Pd/Au **13**, unlike calculated, the product of the transmetalation and not the intermediate with the trigonal carbon (**5c**) is lowest in energy, at least in solid. It should, however, be noted that the calculated complexes **4c**, **5c** and **6c** are all very close in energy (within 1.9 kcal/mol) and that DFT calculated energies can easily be off by a few kcal/mol. Moreover, the electronic and steric properties of the ligands in the calculated and the experimental system used for the crystallization are not identical. Following the empirical knowledge described in Chapter 1.3., it is plausible that the slightly lower electron density of the Pd-center in **13** compared to **5c**, in combination with the stronger donor ligand on Au (NHC vs. PPh₃), is enough perturbation to destabilize the Pd-Au bond.

Except for the M-acetylide dissociation, the overall energy surface for the transmetalation pathway (**B**) is computed to be very flat, even though strong Pd-C bonds are broken and new M-C bonds are formed. We propose that the reaction barriers for the transmetalation are lowered by stabilizing Pd(II)-M(I) (d^8 - d^{10}) interactions. Judging from the calculated distances between Pd and M, the interactions are strongest in the intermediates **5a-c** and **TSa-c** that connect the transmetalation reactant **4a-c** with the products **6a-c**. The shortest Pd-M distances were calculated to be Pd-Au 2.87 Å (**5c**), Pd-Ag 2.91 Å (**5b**), and Pd-Cu 2.68 Å (**5a**) and, thus, they are only slightly longer than the sum of the covalent radii (Pd/Au: 2.75 Å, Pd/Ag: 2.84 Å, Pd/Cu: 2.71 Å).¹¹⁹ DFT modeling is known to have limitations in giving accurate results for metal-metal interactions and, therefore, the computed activation energies and intermediate energies for the transmetalation processes need to be considered with care. The experimentally determined energies for pathways **B** give an upper limit for the transmetalation

TSa-c. The computed potential surfaces suggest that in the gas-phase experiment, we probably measure only the barriers for the “loose” dissociation pathways. For a preceding “tight” **TSa-c**¹²⁰ rearrangement to become slower than the subsequent dissociation (and thus observable during CID experiments as the rate-determining transition state), its activation would have to be at least 15–20 kcal/mol lower in energy than the barrier for dissociation (with a “loose” transition state).⁷⁵ This provides an upper limit of 27–32 kcal/mol for Pd/Cu, 33–38 kcal/mol for Pd/Ag, and 18–23 kcal/mol for Pd/Au. Following the principle of microscopic reversibility, the transition state in the elementary transmetalation step in the Sonogashira reaction is the same as the one involved in our gas-phase experiment, but simply in the reverse direction. From the calculated barriers and, at least for the Pd/Au system also from the crystallization experiment of complex **13** (the σ/π -rearrangement occurs at -35 °C), we see that the internal σ/π -rearrangement, the actual M–C bond breaking, Pd–C bond forming step from **6a-c** to **4a-c** is fast and, therefore, not likely to be rate-limiting in the Sonogashira reaction. At first sight, this result seems to be contradicting with Lei’s findings from solution-phase kinetics¹⁰⁸, however, we suggest that there is an explanation consistent with both results. We propose that it is rather the preceding alkyne coordination step to form **6a-c** that limits the overall rate of the reaction in solution; this ligand exchange is part of the overall transmetalation process in Lei’s mechanism (Figure 24). While the coordination of an incoming acetylide to the coordinatively unsaturated center in $[(PCP)Pd]^+$ is barrierless in the gas phase, it would proceed by associative displacement of a ligand (solvent, halide, ...) on Pd in solution and, hence, would require a substantial activation energy. To investigate the activation energy of ligand displacement on Pd(II) by acetylides, one could

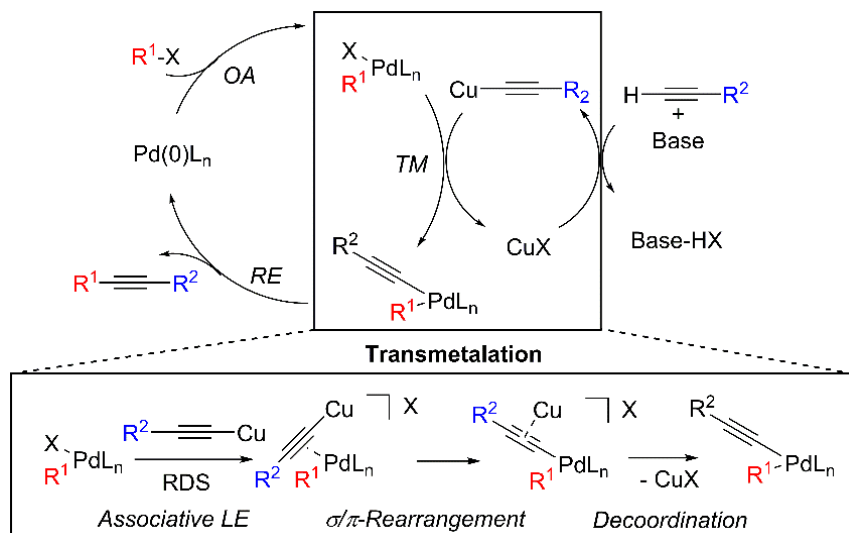


Figure 24: Catalytic cycle of the Sonogashira reaction with oxidative addition (OA), transmetalation (TM), and reductive elimination (RE). Below TM is demerged into its three main steps (LE: ligand exchange).

think of measuring gas-phase energies for decoordination of solvent molecules as a comparison. However, this would not be conclusive because (a) ligand exchange in d^8 square planar complexes is usually associative and (b) dissociation limits are much higher in the gas phase than in solution due to solvation effects, electrostatic screening, and dispersion effects. Lei determined the enthalpy of activation for the transmetalation in solution to be 8.5 kcal/mol,¹⁰⁸ which is in the range of what has previously been reported for associative ligand substitution on square-planar Pd(II) centers in solution. The measured values vary from 4 to 16 kcal/mol, depending on the nucleophilicity of the incoming ligand and degree of steric hindrance at the Pd(II) center, corresponding to a wide range of ligands and complexes.¹²¹⁻¹²³ Therefore, Lei's value would be rather typical. It is noteworthy that associative ligand exchange

being the rate-limiting step of the Sonogashira reaction would also be in agreement with Lei's Hammett correlation plot: Electron accepting substituents on the aryl cause stronger *trans* effects and therefore accelerate the reaction.

3 Investigations on the mechanism of Pd-Cu transmetalation reactions

Raphael Bissig is acknowledged for the synthesis of the substituted 1,10-benzo[h]quinolinato (^Rbhq) ligands, the synthesis of [(^{Me}bhq)₂Pd-Cu(IPr)]X and [(^{OMe}bhq)₂Pd-Cu(IPr)], and the performance of the NMR-titration experiment. Eno Peanurk is acknowledged for providing Figure 37 and two dissociation energies in Figure 41. Parts of the work presented in this chapter is published: Raphael J. Oeschger, Peter Chen, Structure and Gas-Phase Thermochemistry of a Pd/Cu Complex: Studies on a Model for Transmetalation Transition States, *J. Am. Chem. Soc.* **2017**, 139, 1069.

3.1 Introduction

The combination of the reactivities of two different metals into one catalytic transformation has recently emerged as a powerful method.⁸² One of the most practical reaction is the well-known Sonogashira reaction in which a Pd-cycle is linked to a Cu-cycle by a transmetalation step. We investigated its mechanism and showed that the actual Cu-C bond breaking/Pd-C bond forming process is remarkably fast (see Chapter 2). Fast transmetalation between Cu and Pd has also been found in other cases. Marino et al.¹²⁴ discovered an accelerating effect of copper in the Pd-catalyzed Stille reaction (“copper effect”) and Liesbeskind et al.¹²⁵ suggest that the beneficial effect of copper salts, at least under some reaction conditions, is due to Sn to Cu to Pd double transmetalation. More recently, the same effect of copper has also been observed by Deng and coworkers¹²⁶ for Suzuki couplings. Because the rate of a reaction is generally dependent on the relative energy of its transition state, we need to study and compare the TSs of the individual reactions in order to understand why transmetalation between Pd and Cu is faster than between Pd other metals/metalloids (Figure 25).

The reaction mechanism of the Stille-Migita-Kosugi reaction has been proposed to go via either an open or a closed TS. The closed TS consists of a four-membered metallacycle whereas the open TS is linear, similar to a S_N2 -type mechanism, and reacts therefore with inversion of the stereo center at the carbon.

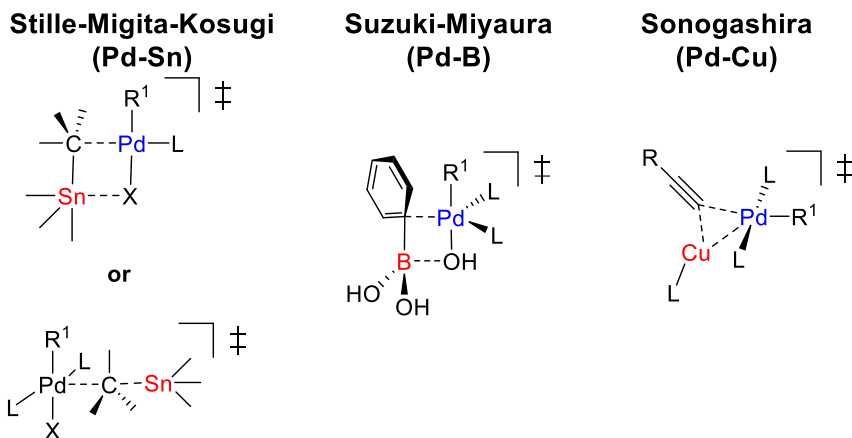


Figure 25: Comparison of proposed transitions stated for Stille, Suzuki and Sonogashira transmetalation.

For the Suzuki-Miyaura transmetalation a similar cyclic TS has been suggested, however, bridged over hydroxide instead of halide. The Pd-Cu catalyzed Sonogashira reaction has been proposed to proceed via an alternative pathway with the formation of a three-membered Pd-C-Cu ring being the most striking feature. When comparing the TS structures of the three reactions (Figure 25), the outstanding difference is the presence of a direct metal-metal bond in the case of Pd-Cu. We believe that transmetalation reactions between Pd(II) and Cu(I) are particularly fast because these d^8-d^{10} bonds are net stabilizing the transition states of the process.

Generally, the only technique to investigate TSs experimentally are kinetic studies, by which relative energies as well as rough ideas about the structure of TSs can be gained. More detailed structural information can nowadays be obtained by computational methods. A somewhat different approach to study TSs is by means of model systems. The basic concept is to establish a system as close as possible to the “real” reaction conditions but designed such that the pathway along the reaction coordinate is blocked. In this way, the TS, or a closely related structure, is trapped and can be analyzed. A classical example for the use of this strategy is the determination of trajectories for the nucleophilic carbonyl addition by Bürgi and Dunitz in the 1970s.¹²⁷ They synthesized 1,8-disubstituted naphthalenes where one substituent was a carbonyl and the other a nucleophile (amine, alcohol, ...), and analyzed the structures by X-Ray crystallography. Because the reaction coordinate for the intramolecular carbonyl addition was frozen, they obtained a snapshot of the reaction pathway based on which they proposed the angle of attack for the incoming nucleophile to be between 107 - 109° (“Bürgi-Dunitz angle”).¹²⁸

We wanted to apply this strategy to study the TSs of transmetalation steps in Pd/Cu catalyzed reaction and, thereby, put our focus on metallophilic interactions. d⁸-d¹⁰ bonds in general are not well investigated and Pd-Cu bonds in particular have experimentally not been investigated at all. We studied metallophilic interactions by structural analysis, quantum mechanical calculations, mass spectrometry and in solution by NMR spectroscopy.

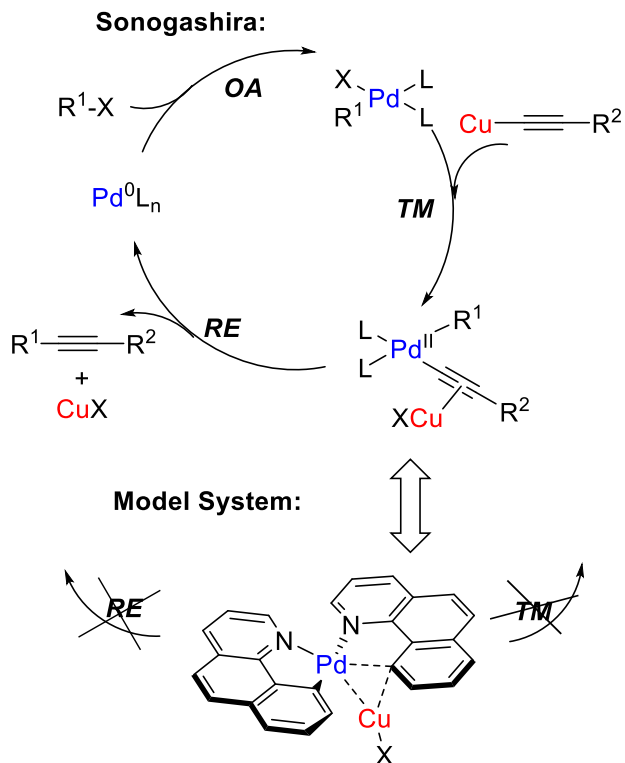


Figure 26: Comparison of Sonogashira reaction (top) and model system (bottom).

3.2 Study of a model complex for transmetalation transition states

3.2.1 Structure

We synthesized *cis*-bis(1,10-benzo[h]quinolinato)palladium, [(bhq)₂Pd(II)] (**15**),¹²⁹ because it is structurally and electronically similar to proposed intermediates in Pd-catalyzed cross-coupling reactions, however, more stable than other L₂Pd(II)R₂ (R = alkyl, alkenyl, alkynyl) complexes. The forward

reaction, reductive elimination, is sterically blocked in the bischelate and also the backward reaction, retrotransmetalation from Pd to Cu, is unfavorable because the chelating bhq-ligand is strongly bound to Pd(II) (Figure 26). A CH₂Cl₂ solution of (bhq)₂Pd **15** was mixed with a solution containing an equimolar amount of (IPr)Cu(I)OTf, [**16**(-OTf)] (IPr = [1,3-bis(2,6-diisopropylphenyl)imidazol-2-ylidene])¹³⁰ (Figure 27), the resulting solution was cooled to -35 °C, and the thereby-formed colorless crystals of

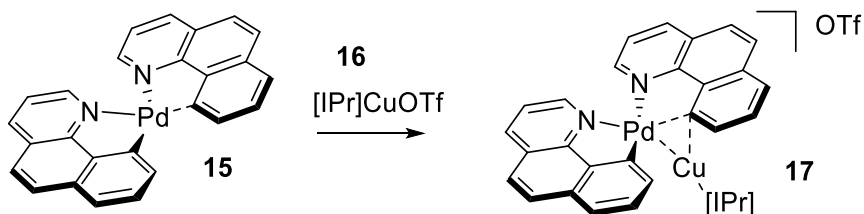


Figure 27: Synthesis of bimetallic complex **17**.

[**17**(-OTf)] were analyzed by X-ray diffraction. The measured crystal structure (Figure 29) displays a short Pd(II)-Cu(I) distance of only 2.55 Å, which is significantly shorter than the sum of the covalent radii (2.71 Å).¹³¹ This criterion has been justified in similar cases as an indication of an attractive bonding interaction.^{109-110, 132} Also striking is the strong interaction between Cu and one of the carbons of the bhq ligand (Cu-C13: 2.025 Å) leading to an enhancement of a slight, already present (see Figure 28 for the crystal structure of (bhq)₂Pd), twisting of the bhq ligand (N2-Pd-C13: 162.6°) and the formation of a trigonal *ipso* carbon.

In the simplest picture of the bonding in d⁸-d¹⁰ complexes, it is understood that the metal fragments are solely held together by the dative interaction of a filled d_{z²} orbital with an empty s or p orbital. This description is generally used to

explain the often-observed geometry with the metal-metal bond standing perpendicular to the coordination plane of the d^8 metal. The coordination mode in complex **17** with the d^{10} moiety tilted toward one of the ligands, had been observed previously in some Pt(II)–M(I) complexes by our group and others.⁴³⁻

47

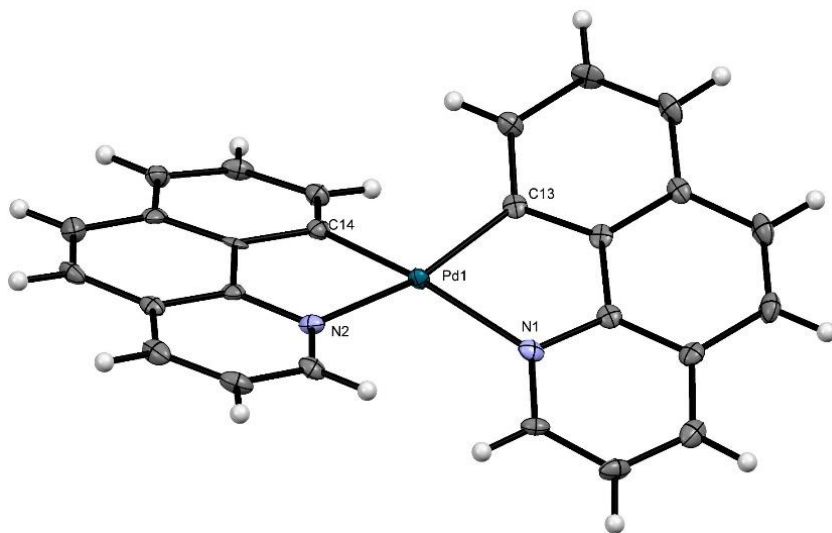


Figure 28: Thermal ellipsoid (50% probability) representation of complex **15**. Selected bond distances (Å) and angles (deg): Pd–C14 1.995, Pd–C13 2.001, Pd–N1 2.146, Pd–N2 2.141, N1–Pd–C52 166.7, N2–Pd–C13 164.4.

To gain further knowledge about the characteristics of Pd–M complexes, we wanted to investigate the structural dependence of these complexes upon variations on the bimetallic system. For that, we synthesized and crystallized Pd/Au complex **18** (Figure 30) in which Cu(I) is exchanged for isoelectronic Au(I), everything else is being kept the same. On first sight, the complex looks similar to the Pd/Cu system with the Au-fragment tilted towards one of the ligands forming a trigonal *ipso* carbon. The Pd–Au distance of 2.68 Å is exceptionally

short and shorter than the sum of their covalent radii (2.75 \AA)¹³¹, indicating a strong interaction between the two metal centers. The most distinctive difference between the geometries of Pd/Cu and Pd/Au is the somewhat elongated Pd-C_{ipso} bond in the case of Pd-Au complex (Pd-C53 2.13 \AA) and the slightly stronger distortion of the square-planar coordination sphere around Pd (N4-Pd-C53 161.1°). It is probably a result of stronger interaction of Au with the *ipso* carbon compared to Cu.

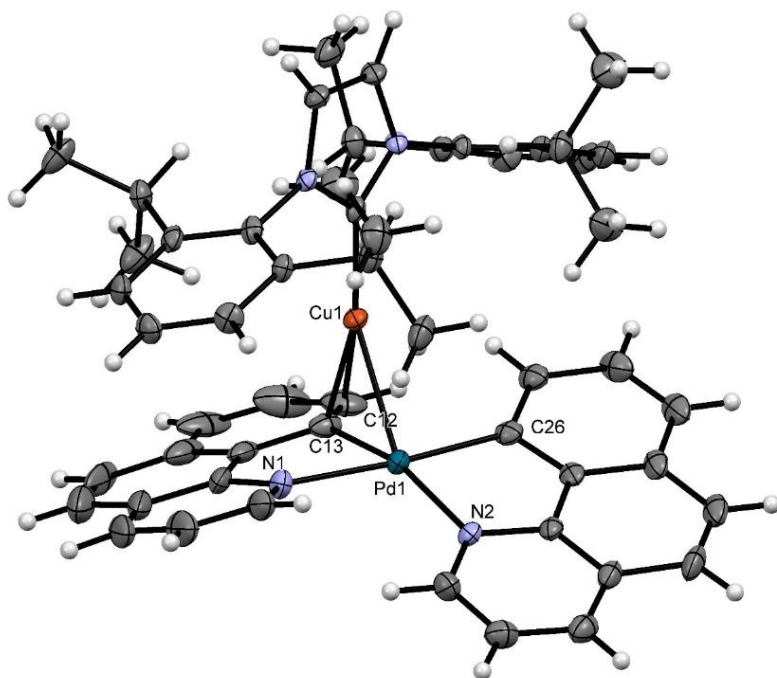


Figure 29: Thermal ellipsoid (50% probability) representation of cationic bimetallic complex **3**. The triflate counterion and one molecule of dichloromethane are omitted for clarity. Selected bond distances (\AA) and angles (deg): Pd-Cu 2.554 , Pd-C13 2.072 , Pd-C26 2.018 , Pd-N1 2.148 , Pd-N2 2.124 , Cu-C13 2.025 , Cu-C12 2.610 , N2-Pd-C13 162.6 , N1-Pd-C26 175.3 , N2-Pd-Cu 146.5 .

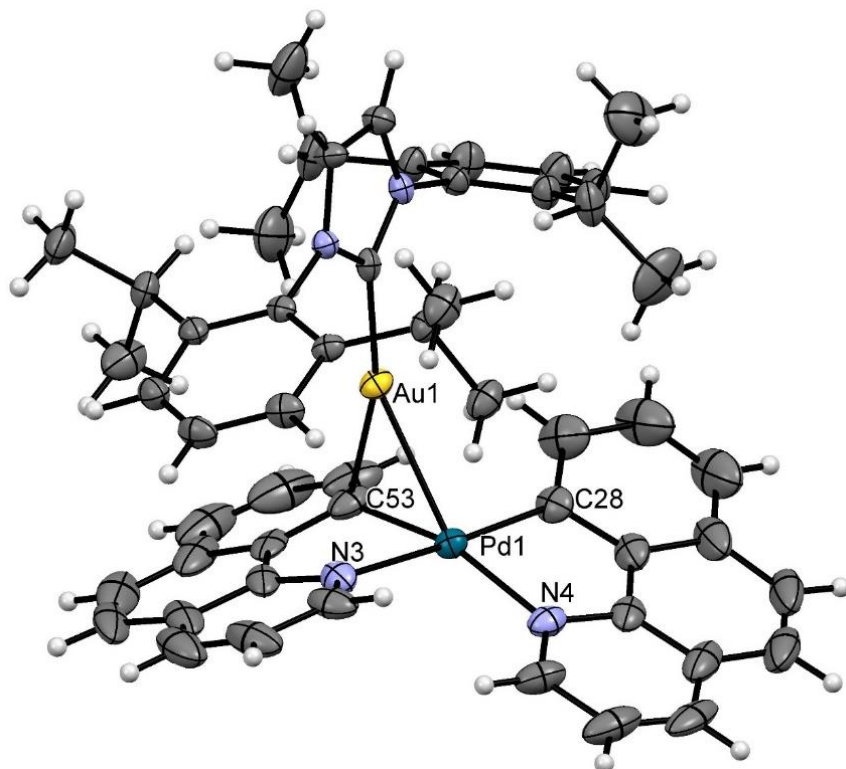


Figure 30: Thermal ellipsoid (50% probability) representation of cationic bimetallic complex **18**. The triflate counterion is omitted for clarity. Selected bond distances (Å) and angles (deg): Pd–Au 2.683, Pd–C53 2.133, Pd–C28 1.996, Pd–N3 2.139, Pd–N4 2.098, Au–C53 2.183, N4–Pd–C53 161.1, N3–Pd–C28 176.9, N4–Pd–Au 146.4.

Next, we synthesized benzo[h]quinolinato ligands with different substituents (-NO₂, CF₃, -CN, -Cl, -F, -Me, -OMe, -NH₂) at the position *para* to the C-Pd bond (position number 7).¹³³ Whereas the synthesis of the different ligands was achieved successfully in all cases, the formation of the Pd-complexes turned out to be more troublesome. Unfortunately, until now only the crystal structures of the bimetallic Pd/Cu complexes with -Me and -OMe substituents could be obtained (Figure 31). The most striking difference between the Me-/OMe-

substituted and the unsubstituted bimetallic complex is the somewhat different coordination mode in the Pd fragment: Whereas the bhq's in **17** form a "twisted" arrangement around Pd with one carbon tilted out-of-plane, a "stepped" coordination mode is observed in the substituted complexes **19** and **20** (Figure 31). In the "stepped" mode, only marginally distortion from planarity around Pd with N-Pd-C angles of almost 180° is observed (**19**: 177.2° and 177.4°, **20**: 172.9° and 175.9 °). The somewhat elongated Pd-Cu distances (**19**: 2.59 Å, **20**: 2.63 Å), the shortened Cu-*C_{ipso}* bond lengths (**19**: 2.04 Å, **20**: 2.03 Å), and especially the shortened distance between Cu and the carbon (C9) next to *C_{ipso}* (**17**: 2.61 Å, **19**: 2.52 Å, **20**: 2.44 Å) could indicate a stronger interaction of Cu with the π -system of the bhq ligands in the substituted complexes than in unsubstituted analogs. A possible explanation for this phenomenon is that the electron donating *para*-substituents are raising the energy of the π -orbitals of the bhq-ligand, thus, leading to a better interaction with the electrophilic Cu fragment and an overall stabilization of the bimetallic complex.

Based on these crystal structures only, it is difficult to explain all structural observations and features, but in general, it is surprising how the geometries of the complexes change upon relatively small perturbations on the system. Our structural analysis suggests the existence of a subtle equilibrium of different forces in the dinuclear system and indicates, that the above mentioned picture of the dative bonding is overly simplistic.⁴⁷

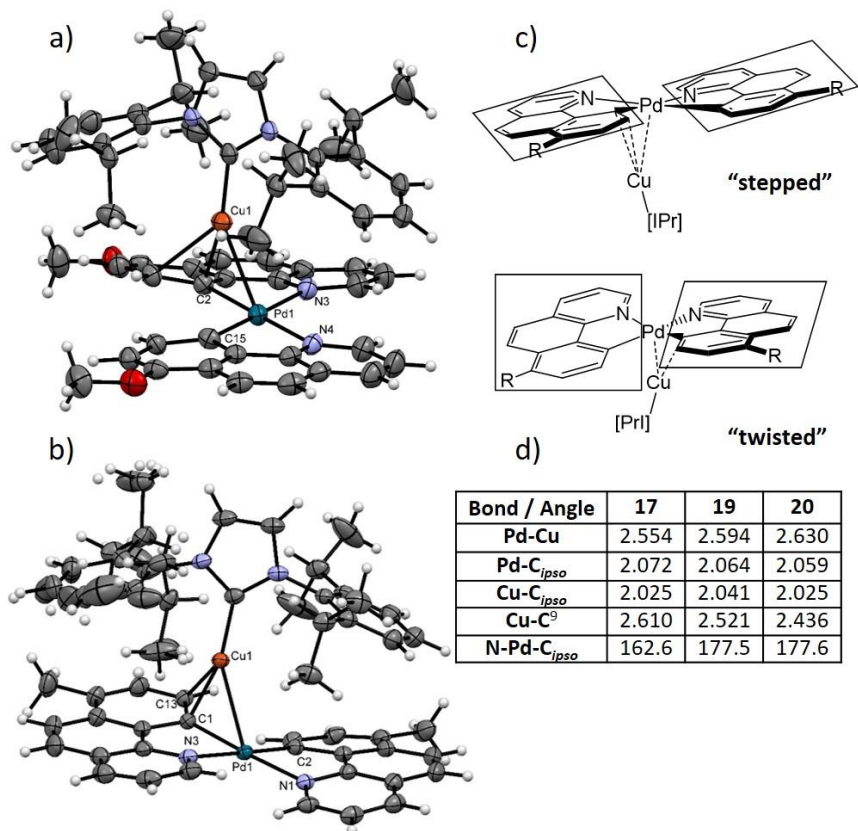


Figure 31: a) Thermal ellipsoid (50% probability) representation of cationic bimetallic complex **19**. The BARF counterion is omitted for clarity. b) Thermal ellipsoid (50% probability) representation of cationic bimetallic complex **20**. The BARF counterion is omitted for clarity. c) Comparison of the “stepped” and the “twisted” coordination mode. d) Comparison of selected bond lengths (Å) and angles (°)

3.2.2 Gas-Phase

The DFT studies of the transmetalation step in the Sonogashira reaction suggested that the reaction starts from a Cu acetylide with Pd coordinated to the π bond and goes through a transition state with a close Pd(II)-Cu(I) contact

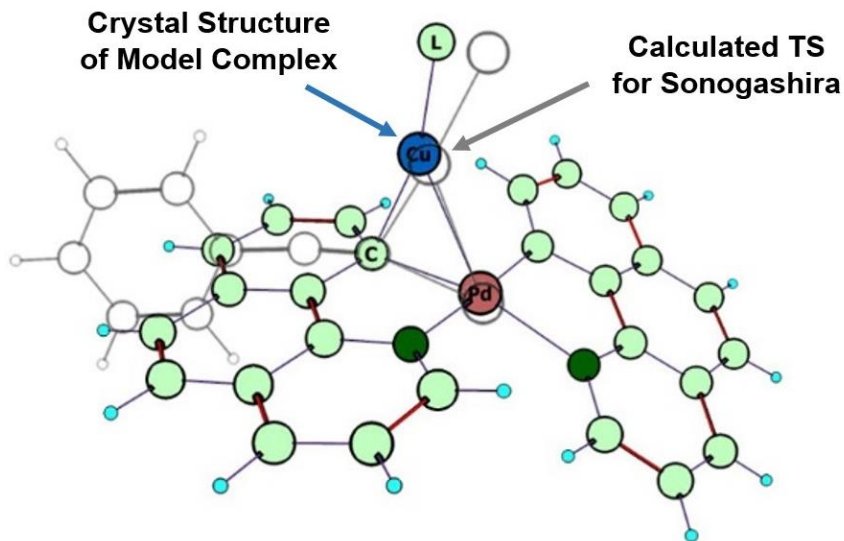


Figure 32: Comparison of crystal structure with calculated TS of Sonogashira reaction.

Pd/M M: Cu(I), Zn(II)	Pd-M	Pd-C _{ipso}	M-C _{ipso}
Pd/Cu (Complex 17 , X-ray)	2.55	2.07	2.03
Pd/Cu (Sonogashira-TS) ^a	2.69	2.14	1.91
Pd/Zn-1 (Negishi-TS) ^b	2.47	2.27	2.16
Pd/Zn-2 (Negishi-TS) ^b	2.65	2.39	2.21

Figure 33: Comparison of selected bond lengths (Å) in the X-ray structure of **17** and three isoelectronic DFT-calculated transmetalation TSs. a) Geometric parameters were taken from our study of the transmetalation step in the Sonogashira reaction (Chapter 2) b) Geometric parameters were extracted from Espinet's study of the transmetalation between *cis*-[PdArMe(PMe₃)₂] and ZnMe₂.¹³⁴

and a trigonal *ipso* carbon to a Pd acetylide with Cu coordinated to the triple bond (Figure 20).⁷³ Experimental results as well as DFT calculations showed that the barrier for the internal rearrangement is exceptionally low, leading us to propose that the favorable metal-metal interaction, which occurs in the

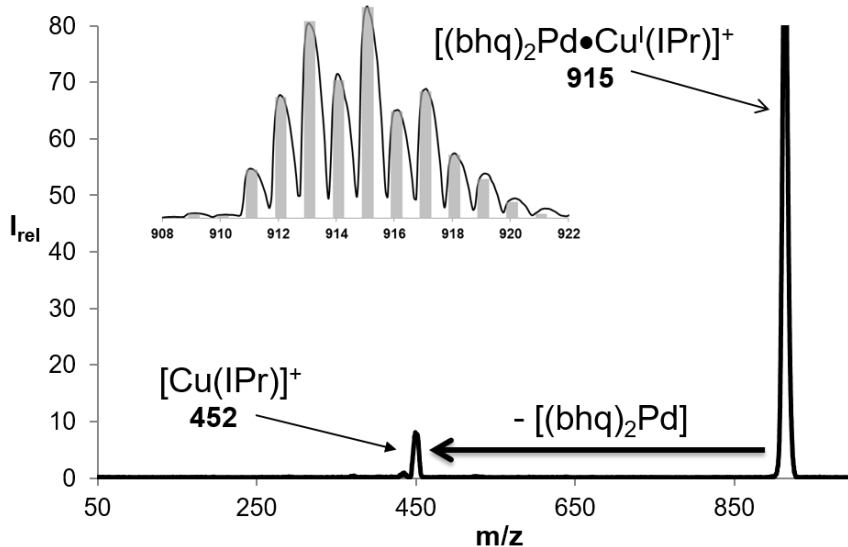


Figure 34: Mass spectrum upon CID of $[(bhq)_2Pd-Cu(IPr)]^+$ (**17**) at 0.1 mTorr and a collision of offset 70 V, showing the clean dissociation to $[(bhq)_2Pd]$ (not visible because it is uncharged) and $[Cu(IPr)]^+$. Inset: Experimental (black) and calculated (red) isotope patterns of **17**.

transition state but not in either of the π complexes, lowers the barrier to rearrangement with respect to the reactant and product. As may be seen in Figure 32 and 33, the crystal structure of **17** looks very similar to the calculated structure of the transition state of the rearrangement in the Sonogashira transmetalation, specifically with regard to the short Pd(II)–Cu(I) distance and the trigonal *ipso* carbon. The transmetalation process has been identified by Lei and co-workers to be rate-limiting in the overall Sonogashira reaction.¹⁰⁸ The computed structures along the reaction coordinate of the transmetalation step in the Sonogashira coupling strongly resemble those computed by Espinet for the Negishi coupling,^{31, 109, 134-135} (see chapter 4) as also seen in Figure 33. Therefore, the quantification of the net stabilization of the transition state due

to the close Pd(II)-Cu(I) contact would not only lead to a better understanding of the mechanisms of transmetalation reactions in general but could also help to develop more efficient catalytic systems for Sonogashira and isoelectronic Negishi type couplings.

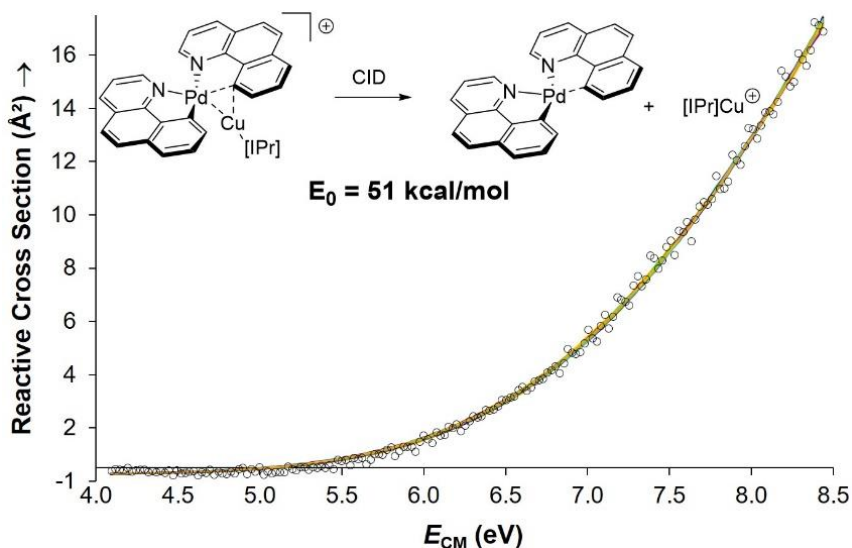


Figure 35: Zero-pressure-extrapolated cross sections (circles) with L-CID-fitted curves (lines). Inset: Reaction scheme for CID of complex $[(\text{bmq})_2\text{Pd}(\text{II})\text{-Cu}(\text{I})(\text{IPr})]^+$ **17** with the corresponding activation energy (E_0).

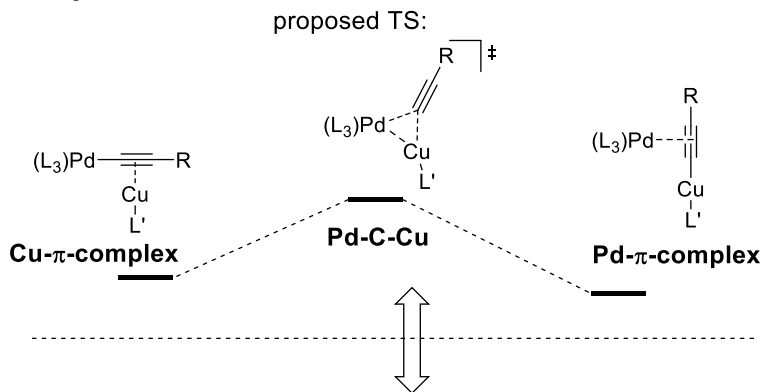
The cationic nature of complex **17** renders it well-suited for ESI-MS/MS investigations (Figure 34). Its composition was confirmed by the m/z ratio as well as by its isotope pattern (inset Figure 34). Upon collision-induced dissociation (CID), $[(\text{bmq})_2\text{Pd}(\text{II})\text{-Cu}(\text{I})(\text{IPr})]^+$ (**17**) reacted to give a single product corresponding to $[(\text{IPr})\text{Cu}]^+$. The activation energy for this gas-phase reaction was determined experimentally by measuring the energy-resolved CID cross section in our customized Finnigan-MAT TSQ-700 ESI-MS/MS mass

spectrometer as described in Chapter 2.1. Reactant and product ion intensities were recorded at different CID gas (Xe) pressures (20 to 110 μTorr) as a function of the collision offset, extrapolated to zero pressure, and subsequently fitted with the L-CID program as a dissociation through a “loose” transition state. In this way, the threshold energy for the dissociation of $[(\text{bhq})_2\text{Pd}]^+\cdots[\text{Cu}(\text{IPr})]$ was determined to be 51 kcal mol^{-1} (Figure 35).

An *estimate* of the net stabilization of the transition state for transmetalation attributable to the close Pd(II)-Cu(I) contact can be obtained by subtracting the binding energy of $[(\text{IPr})\text{Cu}]^+\cdots[\text{Benzene}]$ in $[(\text{IPr})\text{Cu}(\eta^2\text{-C}_6\text{H}_6)]^+$ (**21**) from the binding energy of $[(\text{IPr})\text{Cu}]^+\cdots[\text{Pd}(\text{bhq})_2]$ in our model complex **17** (see Figure 36, bottom). Thereby, complex **21** is the closest, if nevertheless imperfect, model for the interaction without Pd. It should be noted that the structure of a σ -bonded Cu(I)-vinyl species has been reported¹³⁶ in which the Cu–C bond length of 1.919 Å is only marginally shorter than that of 2.025 Å in **17**. However, the angle of the Cu–C bond in **17** with respect to the plane of the aromatic ring (119°) suggests that a π -bonded reference molecule (like e.g., **21**) would be at least as appropriate for the thermochemical comparison. Because an ESI-MS/MS study requires a charged species, we prepared **21** by electrospray of $[\mathbf{16}(-\text{OTf})]$ in benzene and thereby measured a CID threshold of 42 kcal mol^{-1} . Even though the comparison of **17** to **21** is admittedly imperfect, the experimental results suggest that the Pd(II)-Cu(I) contact is accountable for the stabilization of the Sonogashira transmetalation TS by about 9 kcal mol^{-1} . This value is consistent with our expectation based on the single comparable value of 11–12 kcal mol^{-1} determined experimentally for a Pd(II)-Au(I) d^8 – d^{10} system (Figure 10).⁷⁰ At first sight, 9 kcal mol^{-1} may not appear to be a large stabilization energy, however, it should be kept in mind that an alternative transition state

(e.g. a linear TS as proposed for the Stille reaction) would not be stabilized at all, so that one would infer an acceleration of transmetalation by about 6 orders of magnitude.

Sonogashira:



Model System:

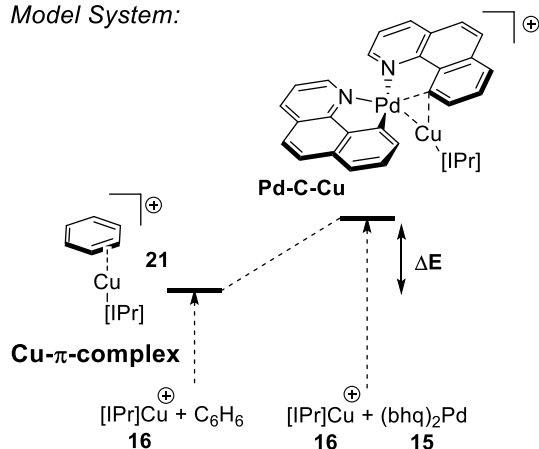


Figure 36: Schematic comparison of the proposed mechanism for the transmetalation step in Sonogashira reaction (top) with the model system (bottom).

3.2.3 Computations

To further characterize the bonding in bimetallic dinuclear complex **17**, we calculated the electron density at the experimental geometry by DFT (TPSS-D3/def2-TZVP(ECP)) and analyzed it with the atoms-in-

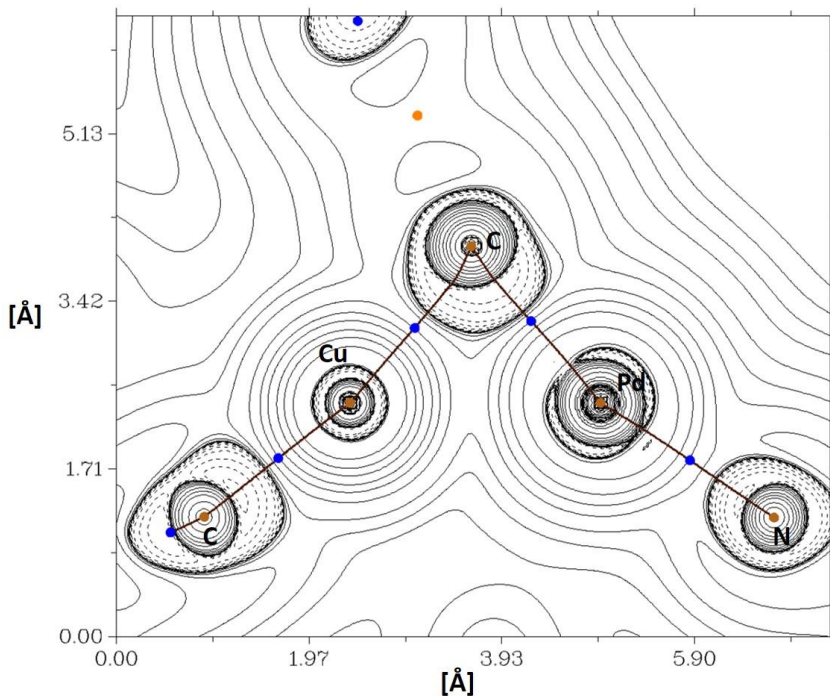


Figure 37: Contour-line diagram of $\nabla^2\rho(r)$ for $[(\text{bhq})_2\text{Pd-Cu}(\text{IPr})]^+$, **17**, with bond paths (brown lines), atom critical points (ACPs, yellow points), and BCPs (blue points), in the Pd-Cu-C13 plane.

molecules (AIM) method.¹³⁷ The contour plot in Figure 37 shows a bond path and a bond critical point (BCP) between Pd and the neighboring carbon atom as well as between Cu and *ipso* carbon. Even though the Pd-Cu distance in the crystal structure of **17** indicates that there must be an interaction between the

two metals, no bond path and no BCP were located between Pd and Cu. A similar finding was reported for the AIM analysis of a Pt-Au complex by Martín and co-workers,⁴⁷ where the AIM method also did not find a BCP between the metal centers. Preliminary results from our group indicate that a BCP can be recovered with thorough analysis of the electron density, which supports the statement that the computational treatment of the metallophilic interactions can be troublesome.^{59, 69}

In the literature, attractive interactions between d^8 - d^{10} (and also the related d^8 - d^8) metals are generally attributed variously to generalized Lewis acid-Lewis base effects,⁶⁰⁻⁶¹ specific frontier orbital overlap,^{65-67, 138} or even predominantly London dispersion (van der Waals) interactions.^{59, 69-70} To get further quantitative information on the nature of the bonding in $(\text{bhq})_2\text{Pd}\cdots^+\text{Cu}(\text{IPr})$, we performed an ETS-NOCV¹³⁹ analysis, an energy partitioning schemes used to interpret total energies coming from quantum chemical calculations. The results in Figure 38 show that the interaction is predominantly of ionic character (ΔE_{elstat} : 50 % of the total attractive interaction), which is not overly surprising because $(\text{bhq})_2\text{Pd}$ and positively charged $^+[\text{Cu}(\text{IPr})]$ were used as fragments in the NOCV bonding analysis. Also high covalent character (35 %) of the bonding was found; dispersive forces (15 %), however, are of less importance.

ΔE_{int}	ΔE_{Pauli}	ΔE_{elstat}	ΔE_{orb}	ΔE_{disp}
-85.4	101.4	-93.0 (50 %)	-65.5 (35%)	-28.4 (15%)

Figure 38: NOCV values in kcal/mol (The percentage values in parentheses give the contribution to the total attractive interactions ($\Delta E_{\text{elstat}} + \Delta E_{\text{orb}} + \Delta E_{\text{disp}} = 186.9$ kcal/mol). The interaction energy, ΔE_{int} , is the sum of the attractive interactions and the repulsive Pauli exchange term.

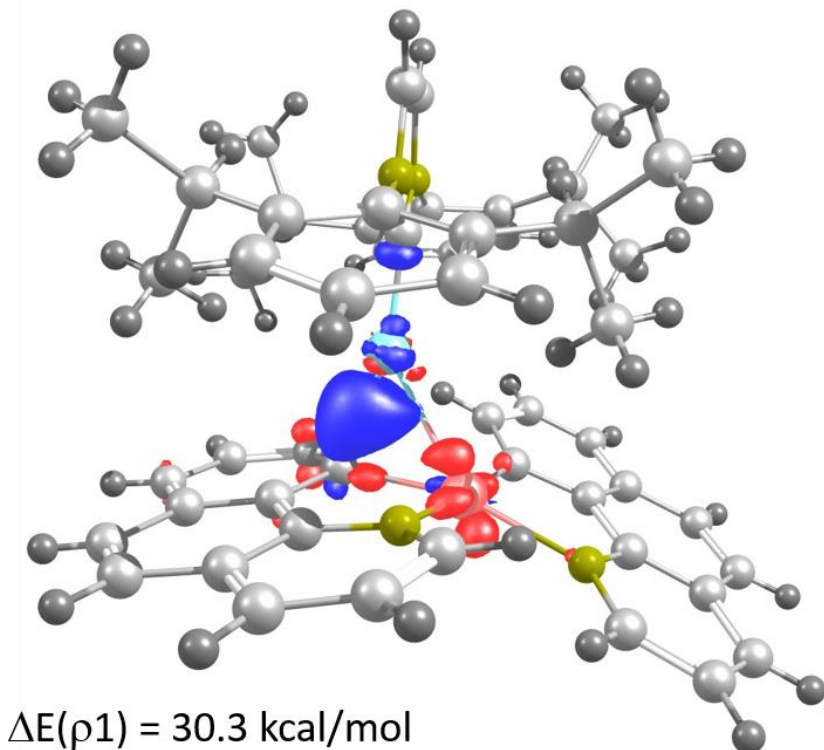


Figure 39: ETS-NOCV computed main deformation density ($\Delta\rho(1)$, largest orbital contribution) for complex **17**. Charge flows from red to blue.

The ΔE_{orb} term can be further subdivided into pairwise energy contributions for each pair of interacting orbitals. The strongest contribution comes from the $\Delta\rho(1)$ interaction (Figure 39) which can be seen as the donation of electron density from a π -MO of $(\text{bhq})_2\text{Pd}$ to the bonding region between the two fragments. When looking more closely it becomes visible that the strongest electron depletion is experienced by a d-orbital of Pd, the Pd-C σ -bond, and the p-orbitals of the carbons *ortho* and *para* to the *ipso*-carbon. The second largest contribution, however significantly lower, comes from the $\Delta\rho(2)$ interaction

(Figure 40) and can be understood as back-donation from a d-orbital of Cu into the bond between the two metal centers.

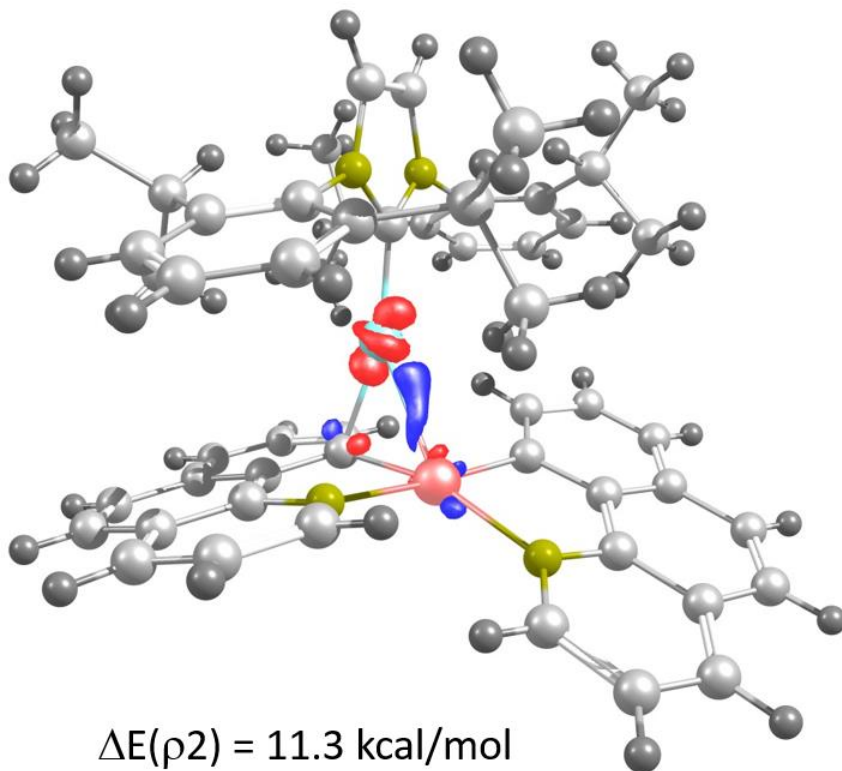


Figure 40: ETS-NOCV computed main deformation density ($\Delta\rho(2)$, second largest orbital contribution) for complex **17**. Charge flows from red to blue.

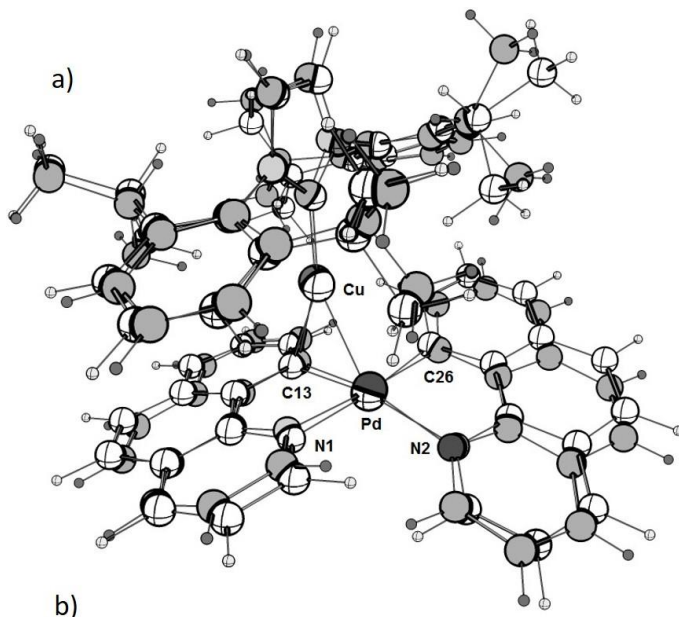
The overall dissociation energy was calculated to be, depending on the particular method, between 75 - 82 kcal/mol (see Figure 34), which is 24-31 kcal/mol higher than the experimental value. We wanted to find out which of the two values is correct (or incorrect). For that, we first sought to ensure that the computationally optimized structure is realistic and compared the

calculated geometry with the experimentally determined structure. As can be seen in Figure 42, the calculated structures and the crystal structures are almost identical and also dispersion corrections seem to have only minor influence on the structural parameters (Figure 42b). Therefore, we think that the structures used for the modeling of the dissociation energies are correct and the discrepancy in the dissociation energies is not due to incorrectly optimized structures.

$(\text{bhq})_2\text{Pd}\cdots^+\text{Cu}(\text{IPr})$	E_{Diss}	$\Delta E_{\text{Exp/Calc}}$
Experiment	51 kcal/mol	-
M06-D3^{a)}	82 kcal/mol	31 kcal/mol
TPSS-D3	75 kcal/mol	24 kcal/mol
DLPNO-CCSD(T)^{a)}	77 kcal/mol	26 kcal/mol

Figure 41: Experimental and calculated zero-point energy corrected dissociation energies of $(\text{bhq})_2\text{Pd}\cdots^+\text{Cu}(\text{IPr})$. $\Delta E_{\text{Exp/Calc}}$ is the difference between calculated and experimental values. ^{a)} These values were calculated by Eno Paenurk

To find out experimentally which of the two numbers, the experimental or the calculated, is incorrect, we designed an intramolecular competition experiment. For that, we synthesized a Pd/Cu system with an “internal standard” in it, a bond that breaks at a lower energy than the $(\text{bhq})_2\text{Pd}\cdots^+\text{Cu}(\text{IPr})$ bond would, if the calculated value was correct. We chose to synthesize the allyl substituted $[(\text{bhq})_2\text{Pd-Cu}(\text{allyl})\text{NHC}]]\text{OTf}$ complex **22** because the side chain is expected to cleave in a CID experiment at low collision energies by forming two allylic radicals (Figure 43). Using TPSS-D3/cc-pVTZ, we calculated the C-C bond dissociation energy (BDE) to be 58 kcal/mol, which is only slightly lower than reported numbers of 62 kcal/mol for the closely related, yet somewhat less electron rich, C-C bond in 1,5-hexadiene¹⁴⁰. The value lies right in-between the



Bond (Å) / Angle (°)	X-Ray	TPSS	Δ	TPSS-D3	Δ
Pd1-Cu1	2.554	2.559	0.005	2.523	-0.031
Pd1-C13	2.072	2.087	0.015	2.069	-0.003
Pd1-C26	2.018	2.015	-0.003	2.016	-0.002
Pd1-N1	2.148	2.163	0.015	2.153	0.005
Pd1-N2	2.123	2.141	0.018	2.129	0.006
Cu1-C13	2.025	2.040	0.015	2.037	0.012
N2-Pd1-C13	162.6	156.6	-6.0	164.3	2.3
N1-Pd1-C26	175.3	176.2	0.9	171.0	-4.3
N2-Pd1-Cu1	146.5	152.1	5.6	142.9	-3.6

Figure 42: a) Overlay of crystal structure and TPSS-D3/SDD(d,p) optimized structure **17** (grey: crystal, white: DFT). b) Comparison of selected bond lengths (Å) and angles (°), Δ : Difference.

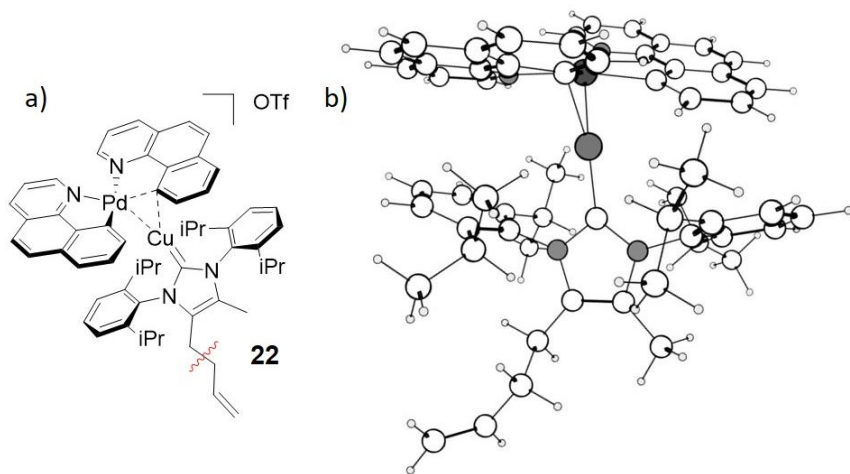


Figure 43: a) Schematic structure of complex **22**. b) DFT (TPSS-D3/SDD(d,p)) optimized structure of complex **22**.

experimental and the calculated number and, thus, if the calculated number was correct, we should observe exclusively C-C-bond cleavage in a CID experiment. The mass spectrum upon CID with Ar is displayed in Figure 44 and shows clean and selective fragmentation of the $(bhq)_2Pd \cdots Cu(iPr)$ bond of **22**. This is a strong evidence that the correct value must lie below ~ 60 kcal/mol and, thus, the calculated dissociation energy of ~ 80 kcal/mol is too high. Actually, if the ~ 80 kcal/mol were correct, not only the C-C bond of the “allyl-tail” of **22** should break, but also the *iPr* groups of the NHC-ligand in **17** and **22**, because the bond dissociation energies of the C-C bond in isopropylbenzene is reported to be ~ 75 kcal/mol kcal/mol.¹⁴⁰ So far, there is no indication that the measured 51 kcal/mol should not be correct. The total dissociation energy of $(bhq)_2Pd \cdots Cu(iPr)$ consists, in a very simple picture, of two stabilizing interactions: a direct Pd-Cu metal-metal bond and a Cu- π interaction. The measured Cu- π dissociation energy of 42 kcal/mol in $[(iPr)Cu-Benzene]^+$ is well

reproduced by TPSS-D3/cc-pVTZ (45 kcal/mol). Since DFT appears to have no problems with calculating Cu- π complexes accurately, the discrepancy with the experimental value presumably comes from the metal-metal bonding part. Detailed analysis of the source of these problems are currently under investigation in our group.

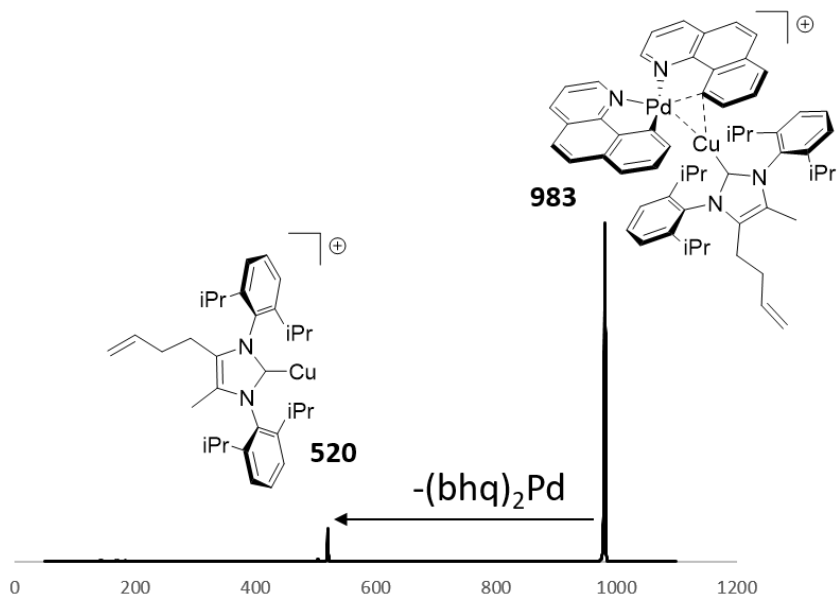


Figure 44: Mass spectrum upon CID of Pd/Cu complex (**22**) at 0.2 mTorr (Ar) and a collision of offset 100 V, showing the clean dissociation to $[(\text{bhq})_2\text{Pd}]$ (not visible because it is uncharged) and substituted Cu-NHC complex. No product of C-C bond cleavage is detected.

3.2.4 Solution-Phase

With the structural and gas-phase results in hand, we also wanted to investigate the characteristics of the bimetallic complex in solution by NMR spectroscopy (for room temperature ^1H NMR see first spectrum in Figure 46b). From the static image of the crystal structure (Figure 29), one would theoretically expect 16

different signals from the benzo[h]quinolinato ligands, 8 from each separately because they are not equivalent. In addition, we would expect 8 signals in the aromatic region, 4 peaks from the tertiary C-H's and 8 (with integral 3) from the methyl groups of the NHC-ligand. In the ^1H NMR spectrum measured in CD_2Cl_2 at room temperature, however, only 8 different signals can be observed that relate to protons from the bhq-ligand, especially characteristic are H2 at 8.68 ppm and H4 at 8.45 ppm. Furthermore, there are only 3 aromatic protons (7.27 ppm, 6.98 ppm, 6.95 ppm), 1 tertiary C-H (2.61 ppm) and 2 corresponding to methyl groups (0.95 ppm, 0.61 ppm) of the NHC-ligand. This behavior can be explained with fast (at NMR-timescale) chemical exchange that occurs in solution at room temperature but not in the crystal. To determine whether these dynamics occur on a single stable bimetallic complex or if they are due to fast dissociation into unbound $(\text{bhq})_2\text{Pd}$ and $[\text{Cu}(\text{IPr})]\text{OTf}$, we did a NMR titration study where we added stepwise from 0 to 2.0 equivalents of $(\text{bhq})_2\text{Pd}$ to a solution of $[\text{Cu}(\text{IPr})]\text{OTf}$ in CD_2Cl_2 . It is clearly visible that upon addition of $(\text{bhq})_2\text{Pd}$, the signals stemming from $[\text{Cu}(\text{IPr})]\text{OTf}$ (i.e. the tertiary C-H at 2.56 ppm) are getting smaller and a second species is being formed that matches with the spectrum of the bimetallic complex. When adding more than one equivalent of $(\text{bhq})_2\text{Pd}$, the free $[\text{Cu}(\text{IPr})]\text{OTf}$ has fully disappeared and uncomplexed $(\text{bhq})_2\text{Pd}$ starts being formed. This is a clear evidence that the equilibrium of $[(\text{bhq})_2\text{Pd}] \cdots {}^+\text{Cu}(\text{IPr})$ lies strongly on the side of the bimetallic complex. Therefore, the observed dynamic processes, which render some protons magnetically equivalent, occur on a single bimetallic complex and are not part of a dissociation equilibrium.

A schematic drawing of expected exchange dynamics in the bimetallic complex is displayed in Figure 45b. The methyls of the *iso* propyl groups are inequivalent but still spectrally close together in free [Cu(IPr)]OTf (at 1.30 ppm and 1.27 ppm,

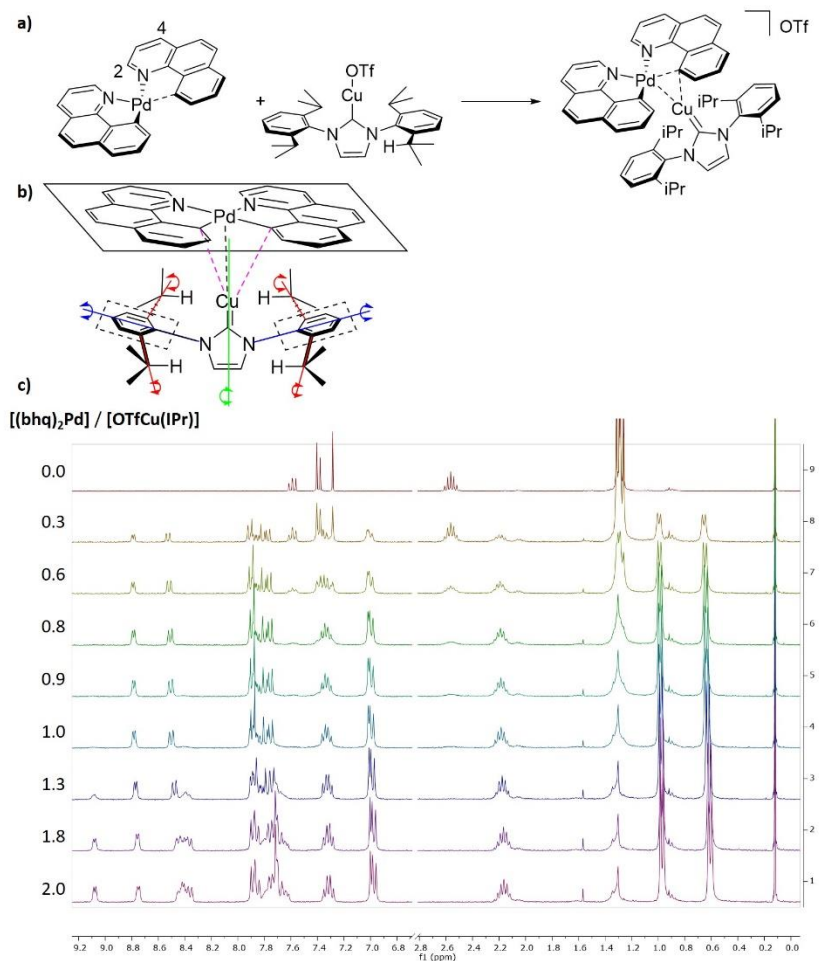


Figure 45: a) Formation of [(bmq)₂Pd-Cu(IPr)]OTf. b) Schematic drawing of expected fast exchange dynamics in the NHC ligand of the bimetallic complex. c) ¹H NMR (300 MHz) titration of OTfCu(IPr) with (bmq)₂Pd in CD₂Cl₂ at 25 °C.

first spectrum in Figure 45c). Coordination to $(\text{bhq})_2\text{Pd}$ leads to significant separation of these two peaks (0.97 ppm and 0.61 ppm) and can be attributed to hindered rotation around the benzylic C-C bonds (red arrow). Even though the rotation around the N-C bond (blue arrow) is presumably very slow, the tertiary benzylic C-H's are all equivalent. This observation is probably due to fast rotation around the Pd-Cu bond (green arrow) in combination with fast isomerization of the bhq-ligands of Pd and fast "hopping" of $^+\text{[Cu(IPr)]}$ between the two Pd-C (purple lines) of $(\text{bhq})_2\text{Pd}$. In the ^1H NMR at room temperature we see only the average of all these processes, which corresponds to square-planar coordination of Pd with an unbridged Pd-Cu bond perpendicular to this plane (see schematic drawing in Figure 41b).

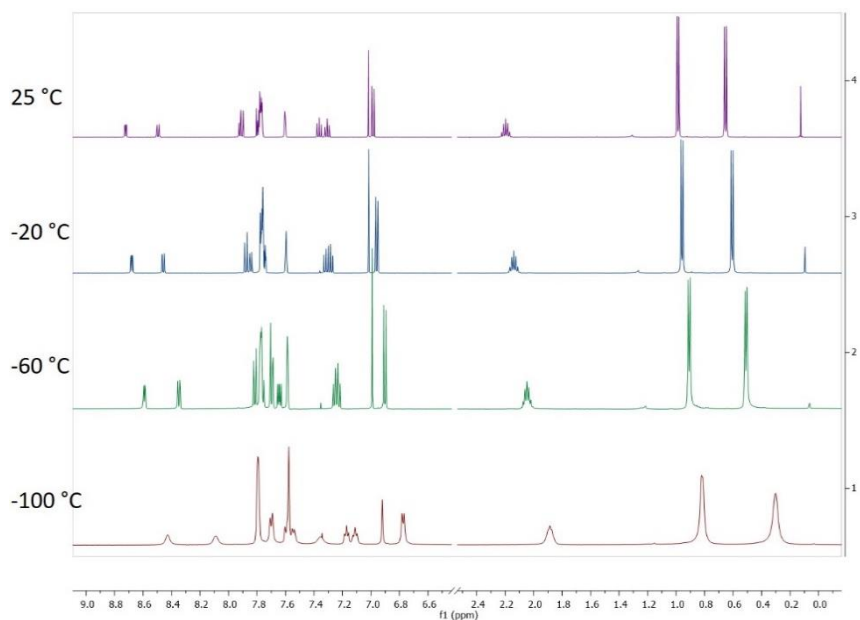


Figure 46: VT- ^1H NMR (500 MHz) spectra (25 °C to -100 °C) of a solution of **8-BArF** in CD_2Cl_2 .

We measured the ^1H NMR spectra also at $-100\text{ }^\circ\text{C}$ (Figure 40), but, unfortunately, this was still not low enough to slow down the exchange processes enough. The drift of some of the peaks might be due to a shifting equilibrium and the broadening of the signals could come from the slowed down isomerization processes, however, other reasons like increased viscosity of the solvent at low temperature or crystallization/precipitation of solids during the measurement are possible explanations too.

3.3 Gas-phase investigations on Pd-Cu transmetalation of aryl groups

For the transmetalation step in the Sonogashira reaction (Chapter 2), we experimentally obtained (only) an upper bound for the barrier of the Pd-C/Cu-C bond rearrangement and investigated its TS by means of a Pd/Cu model complex (Chapter 3.2). In a next step, we wanted to measure the kinetics of Pd/Cu transmetalation reactions in a gas-phase experiment. We anticipated that we had to go away from complexes containing chelating aryl-ligands in order to observe transmetalation of aryl groups in the gas-phase. Non-chelating diaryl Pd(II) complexes, however, are generally unstable in solution, but exceptions are complexes with fluorinated aryl ligands like e.g. $(\text{dmpe})\text{Pd}(\text{C}_6\text{F}_5)_2$ (dmpe: 1,2-bis(dimethylphosphino)ethane).¹⁴¹ We synthesized this complex, mixed it with $(\text{PPh}_3)\text{CuOTf}$ and analyzed the resulting charged species by ESI-MS. Among several mononuclear Pd- and Cu-species, a bimetallic complex with $m/z = 917$ that corresponds to $[(\text{dmpe})\text{Pd}(\text{C}_6\text{F}_5)_2\text{-CuPPh}_3]^+$ (**23**) was particularly striking. Upon CID, the bimetallic complex reacts in two pathways that both correspond to transmetalation of pentafluorophenyl from Pd to Cu. The

difference between the two reactions is that whereas in pathway **A**, PPh₃ stays bound to copper after transmetalation, in pathway **B**, PPh₃ is simultaneously exchanged with the aryl ligand (Figure 47 and 48). The two types of reaction resemble the proposed competing mechanisms of the Stille reaction (see Figure 25). The activation energy for the gas-phase reaction was measured experimentally with our customized Finnigan-MAT TSQ-700 ESI-MS/MS mass spectrometer.

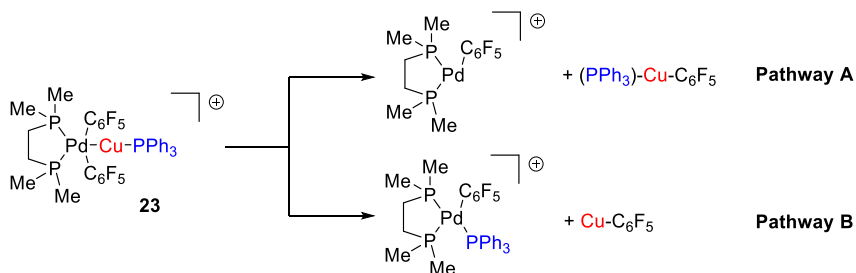


Figure 47: Reaction Pathways of **23** upon CID with Ar.

To find out if a “loose” or a “tight” TS model is appropriate as input for L-CID, and to get a more detailed mechanistic picture, the observed gas phase reactivities were modeled by DFT calculations. The lowest energy structure is calculated to be the bimetallic complex **23** with [Cu(PPh₃)]⁺ bound in the square-planar coordination sphere of Pd, similar as in the crystal structure of the related bimetallic (NN)PtPh₂/CuOTf (NN: ArNC(Me)C(Me)NAr) complex⁴⁴. In pathway **A**, aryl is being transmetalated without prior rearrangement and, thus, a “loose” TS model is best suited for pathway **A** ($E_{0,loose} = 42.7$ kcal/mol). In pathway **B**, the bimetallic complex first rearranges to INT1, an intermediate with [Cu(PPh₃)]⁺ coordinating to Pd below its square-planar coordination sphere and additionally bridged over one aryl ligand by forming an *ipso* carbon.

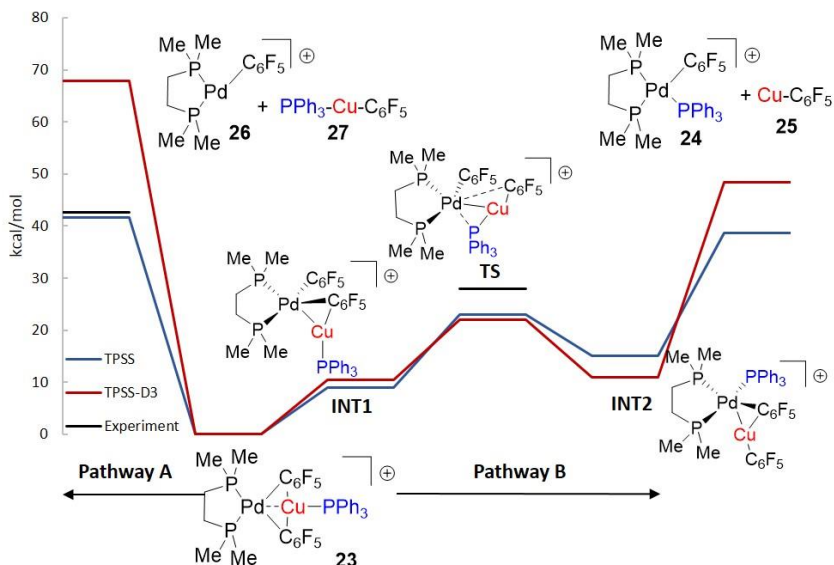


Figure 48: Potential-energy surface (TPSS(-D3)/ccPVTZ//TPSS(-D3)/SDD(d,p)) in kcal/mol for reaction pathways **A** and **B** (blue: TPSS, red: TPSS-D3, black: experimental).

This structure looks similar to the crystal structure of complex **17**. From there, it rearranges via **TS1**, a structure with a short Pd-Cu contact bridged over the phosphorus ligand, to **INT2**, an intermediated that can be seen as $[(\text{dmpm})\text{Pd}(\text{C}_6\text{F}_5)\text{PPh}_3]^+$ with $^+\text{CuC}_6\text{F}_5$ bound to Pd, PPh₃ and the aryl ligand. The last step is decooordination of CuC_6F_5 from the cationic Pd complex. Simply judging from the calculated potential energy surface, a “loose” model would also be suitable for pathway **B**, because the rate-limiting step is the decooordination of CuC_6F_5 . The discrepancy between the experimental and calculated dissociation energies in the $(\text{bhq})_2\text{Pd}\cdots\text{Cu}(\text{IPr})$ system, however, kept us alert and let us to investigate this system in more detail. Using a “loose” TS model for both reaction channels, **A** and **B**, the measured dissociation energies represent the energy difference between the bimetallic complex **23**

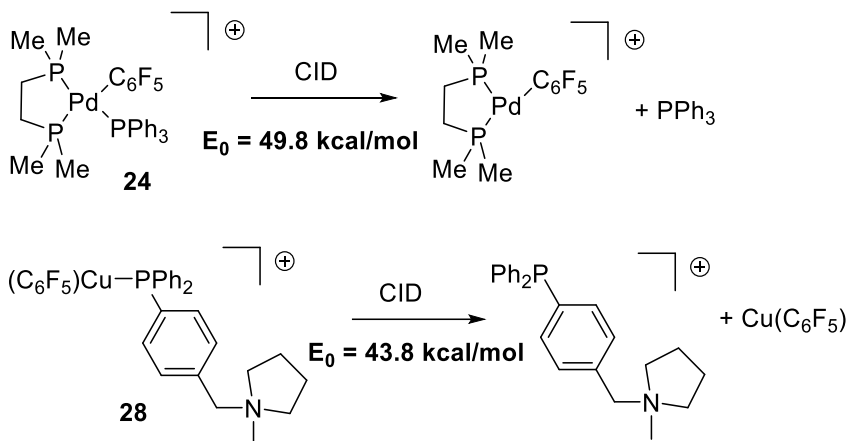


Figure 49: Complexes to measure dissociation energy of Pd-PPh₃ and Cu-PPh₂(C₆H₄R). An ammonium group was attached to make the otherwise neutral (C₆F₅)Cu(PPh₃) complex cationic.

and the products, **24 + 25** or **26 + 27**, respectively. The difference between these two “loose” dissociation energies would correspond to the difference between the [Pd]⋯PPh₃ and the [Cu]⋯PPh₃ bond energy, which could also be measured from e.g. complexes **24** and **28** in Figure 50 ($E_{0,loose} = 49.5$ kcal/mol and $E_{0,loose} = 43.7$ kcal/mol). If the “loose” TS model were correct for pathway **B**, the energy differences in the two systems would have to be the same. Because this is not the case, the differences in energy is $\Delta E = 0.7$ kcal/mol and $\Delta E = 6.0$ kcal/mol, respectively, an internal “tight” TS has to be rate-limiting in pathway **B**. The TS energies calculated with D3 correction (TPSS-D3/cc-pVTZ: 21.8 kcal/mol) and without dispersion correction (TPSS/cc-pVTZ : 23.3 kcal/mol) both match relatively well with the measured value ($E_{0,tight} = 28.0$ kcal/mol). With the TPSS functional, also pathway **A** is accurately modeled (TPSS/cc-pVTZ: $\Delta E = 41.6$ kcal/mol), however, a large discrepancy of 25.2 kcal/mol between the experimental and the calculated number was found for pathway **A** when adding

D3 correction (TPSS-D3/cc-pVTZ: $\Delta E = 67.9$ kcal/mol). This result suggests, analogous to the $(\text{bhq})_2\text{Pd}\cdots^+\text{Cu}(\text{IPr})$ system, that the stability of the bimetallic complex is substantially overestimated by DFT-D3 methods. For the internal barrier of pathway **B** this error is less distinct, perhaps because both structures, **23** and **TS1**, contain short Pd-Cu contacts.

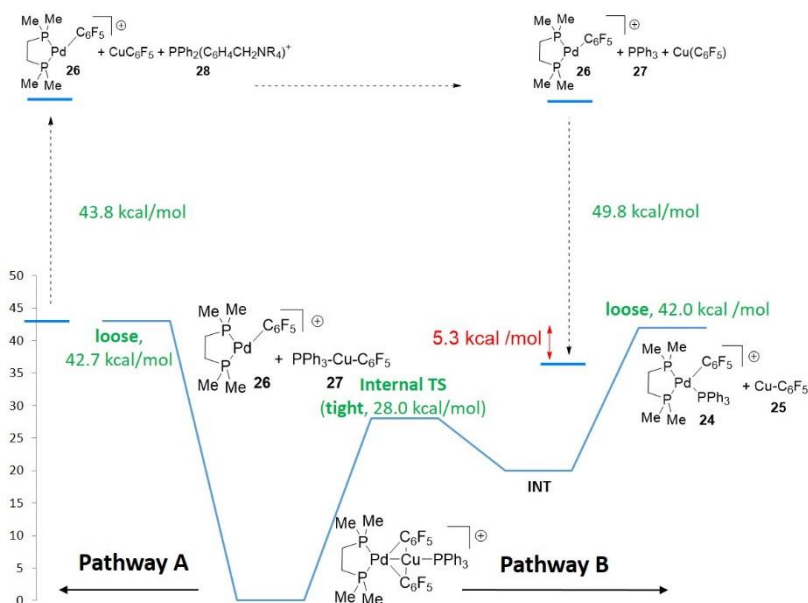


Figure 50: Schematic representation of experimental dissociation energies to determine if a “loose” or a “tight” TS model is appropriate for pathway B.

To find out more about the bonding between $(\text{dmpe})\text{Pd}(\text{C}_6\text{F}_5)_2\cdots^+\text{CuPPh}_3$ in bimetallic complex **23**, we analyzed the interaction by means of ETS-NOCV. Compared to $(\text{bhq})_2\text{Pd}\cdots^+\text{Cu}(\text{IPr})$ (see Figure 38), the bonding in $(\text{dmpe})\text{Pd}(\text{C}_6\text{F}_5)_2\cdots^+\text{CuPPh}_3$ has somewhat stronger electrostatic ($\Delta E_{\text{elstat}} = 54\%$) but weaker dispersive ($\Delta E_{\text{disp}} = 9\%$) character, the stabilization due to covalent

interactions ($\Delta E_{\text{orb}} = 37\%$) is similar in both cases. The strongest increment to the total orbital contribution comes from the $\Delta\rho(1)$ interaction (28.2 kcal/mol), which can be interpreted as the donation of electron density from the *ipso* C_{sp^2} orbitals into the Cu-C bonding regions (Figure 39). The $\Delta\rho(2)$ interaction also contributes significantly (21.2 kcal/mol) to the total orbital interaction and is

ΔE_{int}	ΔE_{Pauli}	ΔE_{elstat}	ΔE_{orb}	ΔE_{disp}
-86.7	157.3	-132.3 (54%)	-90.6 (37%)	-21.1 (9%)

Figure 51: NOCV values in kcal/mol (The percentage values in parentheses give the contribution to the total attractive interactions ($\Delta E_{\text{elstat}} + \Delta E_{\text{orb}} + \Delta E_{\text{disp}} = 244.0$ kcal/mol). The interaction energy, ΔE_{int} , is the sum of the attractive interactions and the repulsive Pauli exchange term.

best described as donation of electron density from a d-orbital of Cu into the Cu-C bond. The additional increments $\Delta\rho(3)$ - $\Delta\rho(7)$ all indicate interactions between Cu and the aryl ligands and, thus, there is no evidence for a direct Pd-Cu orbital interaction. We conclude that the bimetallic complex **23** is stabilized predominantly by the interaction of Cu with the Pd-aryl ligands and potential metal-metal interactions are of electrostatic and/or dispersive nature only. Therefore, the discrepancy between the calculated and the measured activation energy for pathway **A** could be due to incorrect treatment of the electrostatic and/or dispersion term of the interaction between the metal centers or because the bond energies of the Cu- π bonds are overestimated. The latter was not the case for $[(\text{IPr})\text{Cu-Benzene}]^+$ (see chapter 3.2.2), however, the effect of perfluorination is difficult to estimate.

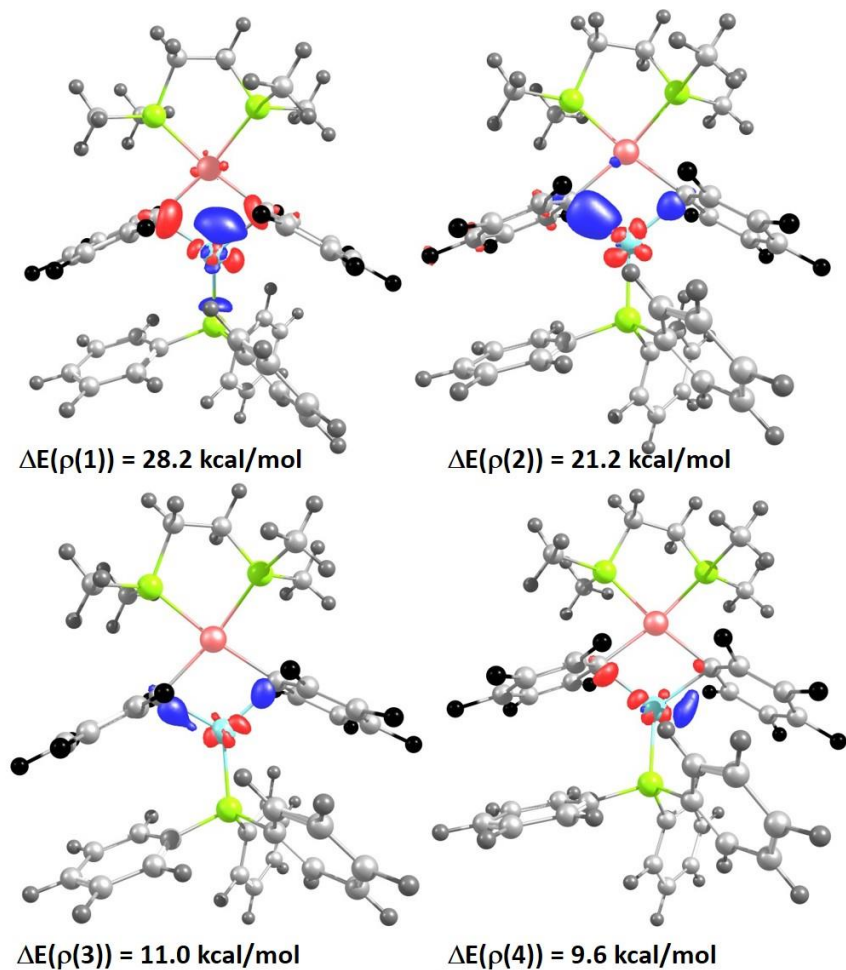


Figure 52: ETS-NOCV computed main deformation density ($\Delta\rho(1-4)$) for complex 23. Charge flows from red to blue.

4 Study of a model complex for transmetalation transition states in Negishi couplings

Eno Peanurk is acknowledged for providing Figure 57. Parts of the work presented in this chapter is published: Raphael J. Oeschger, Peter Chen, A Heterobimetallic Pd–Zn Complex: Study of a d⁸–d¹⁰ Bond in Solid State, in Solution, and in Silico *Organometallics* **2017**, 36, 1465.

4.1 Introduction

Palladium-catalyzed cross-coupling reactions have become one of the most important procedures for carbon-carbon bond formations. Among the different varieties of organometallic coupling partners, the combination of palladium catalysts with organozinc(II) reagents in the Negishi coupling is one of the most powerful protocols.¹⁴²⁻¹⁴⁴ Because of excellent functional group tolerance, combined with high reactivity and the easy synthesis of organozinc compounds, it is often the method of choice for challenging reactions involving C_{sp2}–C_{sp3} couplings.¹⁴⁵⁻¹⁴⁸ The main disadvantage is the formation of significant amounts of side-products assignable to homocoupling that are produced in competition with the desired heterocoupling products. Van Asselt and Elsevier in 1994 were the first who suggested that the homocoupling side-product could be due to transmetalation processes that exchange the organic group on Pd instead of the halide (*TM2* in Figure 54).¹⁴⁹ Some years later, also the groups of Espinet³¹ and Lei³³ found evidence that the formation of homocoupling products is the result of secondary transmetalation events. In Figure 54 a few possible side-reactions are shown, there are, however, many more imaginable. All retro-transmetalation processes that eventually lead to side-products have in common that they produce Ar-Zn compounds, which can transfer the Ar-group to a L₂Pd-Ar complex (*TM4*) to form diaryl PdL₂, an intermediate from which the

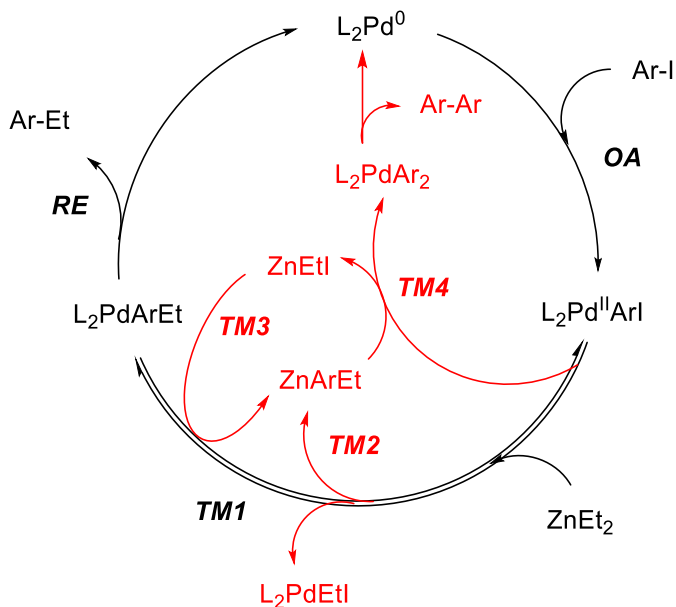


Figure 53: Simplified catalytic cycle for Negishi reaction. Steps in black lead to desired heterocoupling, steps in red to undesired homocoupling side-products.

undesired homocoupling side product ($Ar-Ar$) is released. Lei's kinetic studies show that the reductive elimination step is turnover-limiting under typical conditions of the Negishi coupling, which would render the preceding transmetalation step ($TM1$) reversible at steady-state. Both, Lei and Espinet agree that the high amount of side-product formation is most probably a result of transmetalations and their reverse processes being much faster than reductive elimination. This situation leads to accumulation of $Zn-Ar$ complexes and, subsequently, to homocoupling product formation. Furthermore, Espinet proposes that $Pd(II)-Zn(II)$ (d^8-d^{10}) interactions in the TS of the transmetalation processes are responsible for the exceptionally low energy of the barriers.³¹ Therefore, it is important to learn more about $Pd(II)-Zn(II)$ interactions so that

we will be able to tune and optimize the reaction conditions rationally. Towards this end, we investigated a bimetallic Pd/Zn model complex by X-ray analysis, in solution by NMR and in silico.

4.2 Results and Discussion

4.2.1 Structure

Complex **26** was synthesized by mixing a solution of $[(\text{bhq})_2\text{Pd}(\text{II})]^{129}$ in dichloromethane with an equimolar solution of $\text{Zn}(\text{C}_6\text{F}_5)_2^{150}$ in 1,2-difluorobenzene. Layering of the resulting solution with hexane (Figure 55) gave colorless crystals after one night at -35°C . The crystals were analyzed by X-ray diffraction and the structure is shown in Figure 56. It displays a short Pd-Zn distance¹⁵¹ of only 2.58 Å, which is shorter than the sum of the covalent radii (2.61 Å¹⁵²). The d^{10} fragment ($\text{Zn}(\text{C}_6\text{F}_5)_2$) is slightly tilted toward the bhq ligand (N-Pd-Zn: 102.5°) leading to a shortened Zn-C_{ipso} distance of 2.47 Å as compared to the other Zn-C7 (3.23 Å). The slightly distorted square-planar

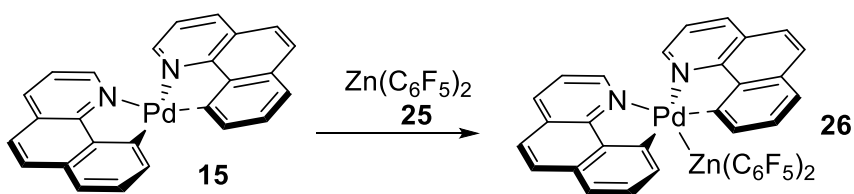


Figure 54: Synthesis of Heterobimetallic Pd-Zn Complex 3

coordination sphere around palladium in $(\text{bhq})_2\text{Pd}$ **15** (for crystal structure see Figure 28) changes only marginally upon coordination to **25**. The most striking difference between the Pd/Zn complex **26** and the isoelectronic Pd/Cu system

17 (Figure 29) is that the d^{10} fragment in **26** is significantly less tilted towards the *ipso* carbon than in **17**.

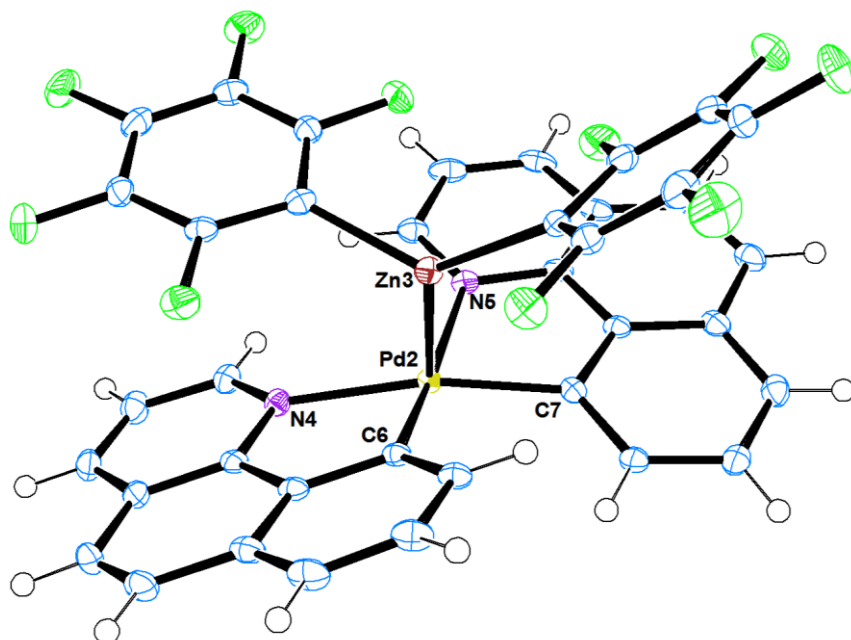


Figure 55: Thermal ellipsoid (50% probability) representation of bimetallic complex **26**. Selected bond distances [Å] and angles [°]. Pd2–Zn3 2.58, Pd2–C6 2.03, Pd2–C7 2.00, Pd2–N4 2.17, Pd2–N5 2.14, Zn3–C6 2.47, N5–Pd2–Zn3 102.5, C6–Pd2–Zn3 63.6, N5–Pd2–C6 166.1, N4–Pd2–C7 167.6.

4.2.2 Computations

For further analysis of the bonding in bimetallic complex **26** we calculated the electron density with DFT (TPSS-D3/def2-TZVP(ECP)) and analyzed it using the

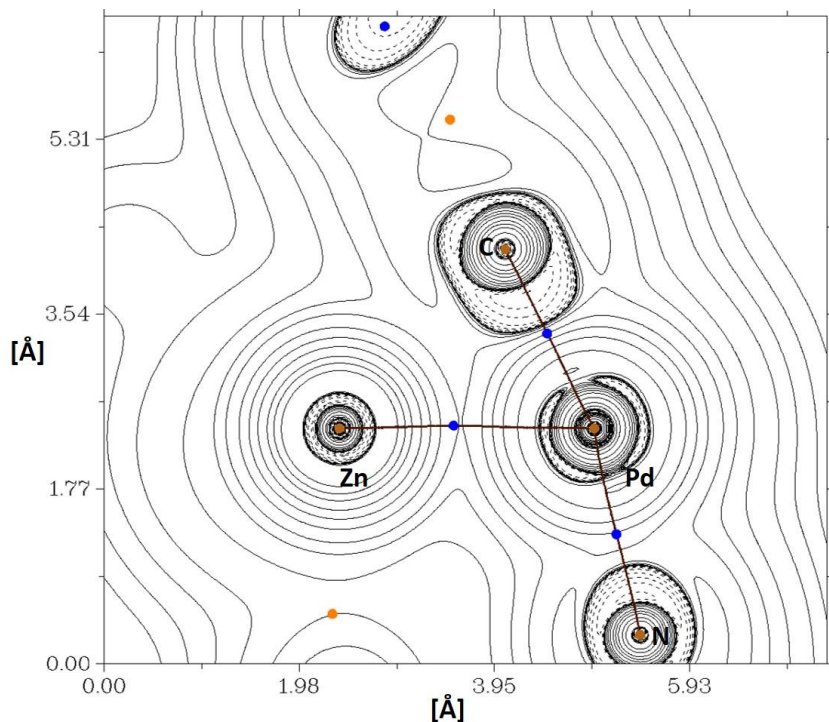


Figure 56: Contour-line diagram of $\nabla^2\rho(r)$ in the plane containing Pd, C6 and Zn, showing the bond paths (brown lines), atom critical points (ACPs, yellow points), and BCPs (blue points).

atoms-in-molecules (AIM) method.^{137, 153} The contour-line diagram of the Laplacian distribution $\nabla^2\rho(r)$ in the Pd-Zn- C_{ipso} plane is displayed in Figure 57. The AIM analysis locates a bond path and a bond critical point (BCP) between Pd-Zn and Pd- C_{ipso} but not between Zn- C_{ipso} , even though the reduced Zn- C_{ipso} distance, and the slight tipping of the Pd-Zn bond, indicate some stabilizing interaction. This result suggests that the bimetallic complex **26** is mainly stabilized by the Pd-Zn metal-metal bond and only to a minor extent by the Zn- C_{ipso} interaction. This situation is different from those in the isoelectronic Pd(II)-

Cu(I)¹⁵⁴ and Pt(II)-Au(I)⁴⁷ systems where no BCP was located between the metals, but only between M (M: Cu, Au) and the *ipso* carbons. The small $\rho = 0.31$ a.u. value and the positive $\nabla^2\rho$ value at the BCP between Pd-Zn is typical for closed-shell interactions

Additional quantitative information on the nature of the (bhq)₂Pd...Zn(C₆F₅)₂ interaction could be obtained by means of ETS-NOCV¹³⁹ analysis. The strongest contributions to the total attractive interaction were calculated to come from electrostatic ($\Delta E_{\text{elstat}} = 46\%$) and orbital ($\Delta E_{\text{orb}} = 38\%$) interactions; dispersive interactions ($\Delta E_{\text{disp}} = 16\%$) were found to be of minor importance (Figure 58). The orbital contribution was further partitioned into pairwise energy contributions for each pair of interacting orbitals (Figure 59). The strongest increment ($\Delta E(\rho(1)) = 24.8$ kcal/mol), accounting for about half of the total orbital interaction, comes from the $\Delta\rho(1)$ interaction, which can be viewed as the donation of electron density from the Pd d_{z^2} orbital into the Pd-Zn bonding region. It resembles very much the putative dative bonding interaction recently reviewed for donor-acceptor type metal-metal bonds.⁴¹ All other increments were calculated to be of much lesser importance ($\Delta E(\rho) < 6$ kcal/mol).

ΔE_{int}	ΔE_{Pauli}	ΔE_{elstat}	ΔE_{orb}	ΔE_{disp}
-58.4	76.7	-62.3 (46 %)	-51.1 (38 %)	-21.7 (16 %)

Figure 57: NOCV values in kcal/mol (The percentage values in parentheses give the contribution to the total attractive interactions ($\Delta E_{\text{elstat}} + \Delta E_{\text{orb}} + \Delta E_{\text{disp}} = 135.1$ kcal/mol). The interaction energy, ΔE_{int} , is the sum of the attractive interactions and the repulsive Pauli exchange term.

When comparing results from the ETS-NOCV analysis of the Pd/Cu **17** and the Pd/Zn **26** complexes one can see that the electrostatic interaction has the highest contribution to the total attraction between the two fragments in both

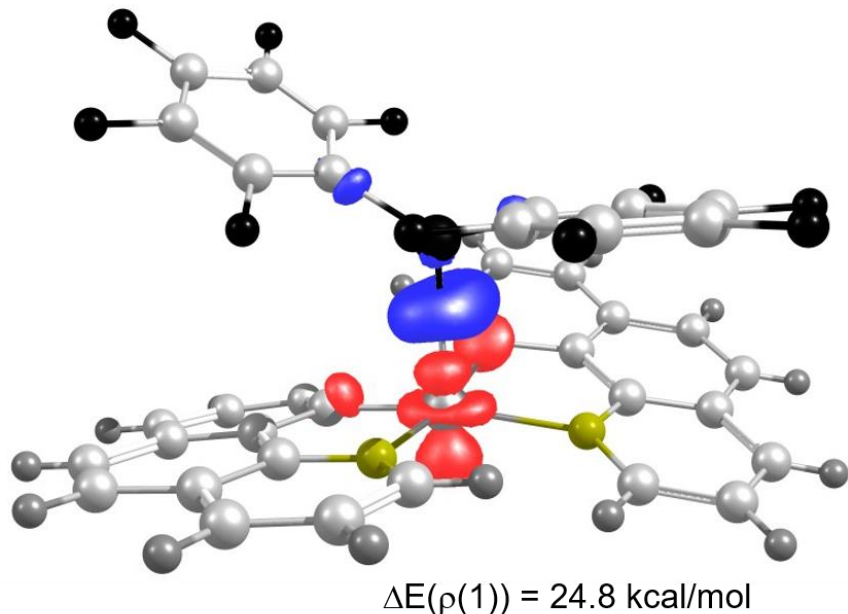


Figure 58: ETS-NOCV computed main deformation density ($\Delta\rho(1)$) for complex **26**. Charge flows from red to blue.

cases. In Pd/Cu (93 kcal/mol), however, the stabilizing energy is substantially higher than in Pd/Zn (62 kcal/mol). This result is not too surprising because the d^{10} fragment is charged in the Pd/Cu complex, whereas the Lewis acidic fragment in the Pd/Zn complex is neutral (albeit with strongly electron withdrawing substituents). The stronger electrostatic stabilization in **17** compared to **26** could be the reason for the structural difference of the coordination of the d^{10} fragment to $(\text{bhq})_2\text{Pd}$. The large electrostatic interaction of $[(\text{IPr})\text{Cu}]^+$ with the partial negative charge of the *ipso* carbon of the *bhq* ligand leads to a structure where the Cu-fragment is tilted towards the *ipso* carbon. The electrostatic interaction of neutral $\text{Zn}(\text{C}_6\text{F}_5)_2$ with the *ipso* carbon is weaker, thus, the d^{10} is less tilted towards the *bhq* ligand. The overall orbital contribution

is also higher in the case of Pd/Cu (66 kcal/mol) than in Pd/Zn (51 kcal/mol), but in both systems, the strongest orbital contribution comes from the donation of electron density of the (bhq)₂Pd fragment into the bonding region between the fragments. In the case of Pd/Cu, the donating orbital seems to be more distributed over the π -system, whereas in the Pd/Zn system, the main depletion of electron density is clearly located on the Pd d_{z²}-orbital. The difference of ΔE_{orb} of 14 kcal/mol in the two isoelectronic systems can be mainly attributed to the lack of back-donation from the d¹⁰ component in the Pd/Zn system compared to Pd/Cu ($\Delta E(\rho(2)) = 11$ kcal/mol). The reason for this variation could be that the d_{z²} orbital of the d¹⁰ fragment, which is mainly involved in the back-donation in Pd/Cu (see Figure 40), points along the C-Zn-C bond axis in Zn(C₆F₅)₂ and is, thus, not available for orbital interaction with an empty orbital of the (bhq)₂Pd fragment.¹³⁵ The contribution of dispersive interactions is relatively small in both cases.

4.2.3 Solution-Phase

The uncharged nature of bimetallic complex **26** made it unsuitable for ESI-MS/MS experiments; therefore, we studied the behavior of complex **26** in solution by NMR spectroscopy. Based on the picture of the static crystal structure, we expected 16 different signals in the ¹H- and 10 different signals in the ¹⁹F-NMR spectrum. As in the case of Pd/Cu, the spectra in CD₂Cl₂ showed only 8 signals from protons of the bhq ligands and 3 from fluorine atoms, suggesting fast exchange dynamics in solution at room temperature that render the two bhq's and the two C₆F₅-rings equivalent. In order to slow down the rates

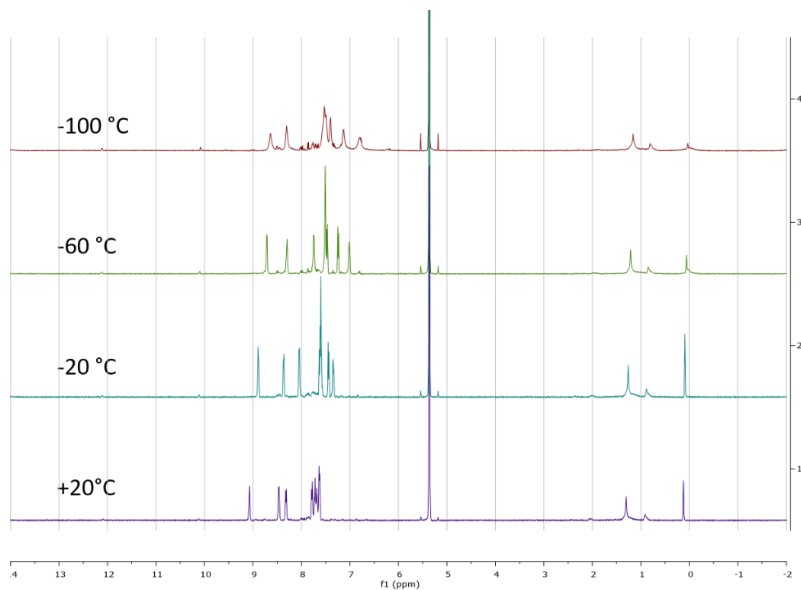


Figure 59: VT-¹H NMR spectra (-100 °C to +20 °C) of a solution of **26** in CD₂Cl₂.

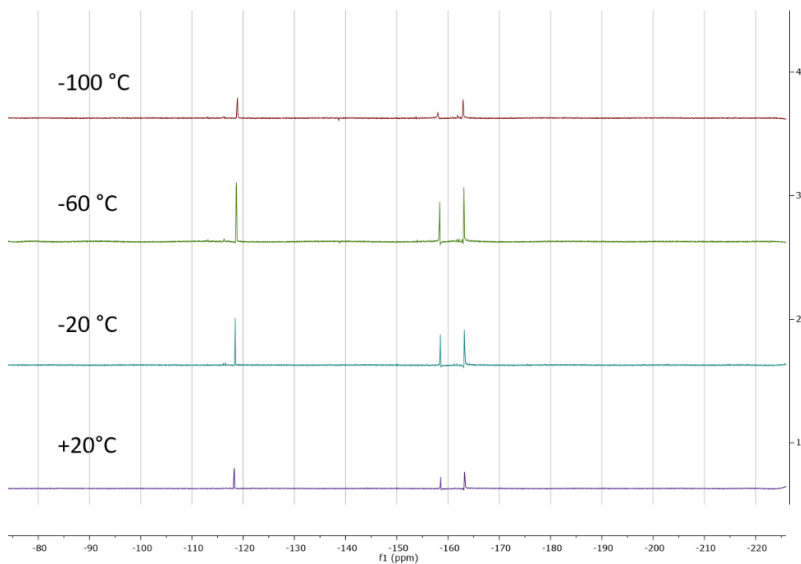


Figure 60: VT-¹⁹F NMR spectra (-100 °C to +20 °C) of a solution of **26** in CD₂Cl₂.

of exchange, the spectra were recorded at $-100\text{ }^{\circ}\text{C}$, but even at that temperature, the dynamics were too fast on the NMR time scale (see Figures 60 and 61). To find out if the observed chemical exchange phenomena are caused by dissociation of the $(\text{bhq})_2\text{Pd}$ complex from $\text{Zn}(\text{C}_6\text{F}_5)_2$, or like in the Pd-Cu system, by fast (non-dissociative) isomerization within a stable bimetallic complex, **15** was titrated into a solution of **25** (0 to 3.3 equiv) and followed by NMR. For all ratios $[\text{Pd}]:[\text{Zn}]$, ranging from substoichiometric to superstoichiometric, only one species was observed in the ^1H - and ^{19}F -NMR spectra, albeit with different chemical shifts at different stoichiometries. This lead us to the conclusion that, in solution, the bimetallic Pd-Zn complex **26** is in rapid equilibrium with unbound **15** and **25**. The dependence of the chemical shift of F_{para} on the added concentration of **15** shows typical saturation behavior and the binding constant could be determined to be $K_{\text{eq}} = (4.5 \pm 0.9) \times 10^5 \text{ mol L}^{-1}$ by nonlinear least-squares curve fitting (Figure 63) (for experimental details see chapter 6.4).¹⁵⁵⁻¹⁵⁷ From the equilibrium constant, $\Delta G = 7.7 \pm 1.5 \text{ kcal/mol}$ (at $25\text{ }^{\circ}\text{C}$) could be calculated.

Using DFT calculations (TPSS-D3//cc-pVTZ//TPSS-D3/SDD(d,p)), the gas-phase dissociation energy of $(\text{bhq})_2\text{Pd}\cdots\text{Zn}(\text{C}_6\text{F}_5)_2$ was computed to be 41.5 kcal/mol and thereby greatly exceeds the 7.7 kcal/mol dissociation energy measured in CD_2Cl_2 solution. Given that the computed values are for the gas phase, and the experiment is done in polar solvent, one should consider that dielectric shielding strongly weakens the attractive electrostatic interaction in solution (-62.3 kcal/mol in gas-phase NOCV analysis). Furthermore, substantial compensation of the attractive dispersion contribution (-21.7 kcal/mol) can be expected in solution, whereas the orbital interactions (-51.1 kcal/mol) and exchange repulsion ($+76.7 \text{ kcal/mol}$) should be less strongly affected.

Altogether, the reduction of the gas-phase dissociation energy of 41.5 kcal/mol (computed) to 7.7 kcal/mol (experimental) in polar solution is not unexpected.

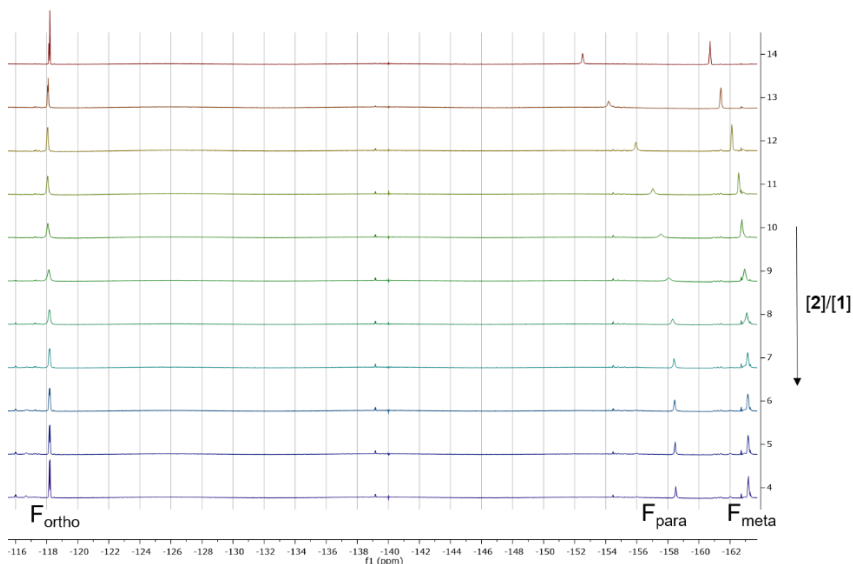


Figure 61: ^{19}F -NMR (600 MHz) titration of **15**...**25** in CD_2Cl_2 at 25°C .

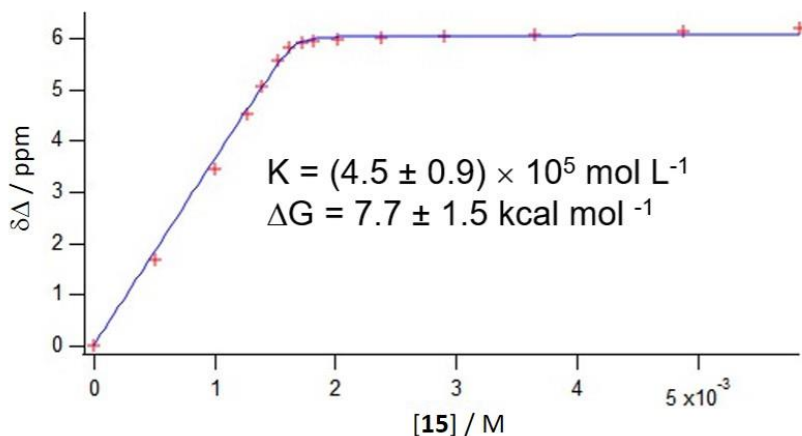


Figure 62: ^{19}F -NMR binding titration of $(\text{bhq})_2\text{Pd}$ with $\text{Zn}(\text{C}_6\text{F}_5)_2$. The complexation-induced change of chemical shift of the signals for the F atoms *para* to the Zn (F_{para}) is plotted ($C_0(\text{ZnC}_6\text{F}_5)_2 = 1.66 \text{ mM}$) and fitted to a 1:1 isotherm.

4.2.4 Discussion

Even though the Negishi coupling is often the cross-coupling protocol of choice for challenging C-C bond formations, it nevertheless suffers from major drawbacks such as formation of homocoupling side products. Mechanistic studies indicate that these problems are presumably caused by R (R = aryl, vinyl, alkyl, etc.) scrambling between Pd and Zn by secondary retro-transmetalations.^{29, 33, 149, 158} Based on results from DFT calculations, Espinet et al. proposed bimetallic PdR₂/ZnR₂ (R = C₆F₅ or Me) structures as transition states and intermediates of these undesired side reactions (Figure 64).¹³⁴ For the TS structures, they distinguished between “ligand-dependent” TSs, where a PMe₃ ligand on Pd is displaced by the incoming ZnR₂, and “ligand-independent” TSs, where the Pd-R and Zn-R bonds are being broken and formed concertedly. Whereas a concerted “ligand-independent” TS is supposed to be faster for primary transmetalations (Pd-Cl/Zn-R exchange),³⁰ a “ligand-dependent” pathway is expected to be preferred for secondary transmetalations (Pd-R/Zn-R exchange).¹³⁴ When comparing the key structural parameters of the experimental crystal structure of **26** with the DFT optimized structures of the intermediate and the “ligand-dependent” TS, it is striking how similar they are (Figure 64). Judging by the Pd-C and Zn-C bond lengths, the structure of **26** represents a point on the reaction coordinate right in-between the intermediate and the TS, **26** is being “trapped” as a minimum because the two chelating bhq ligands block the complex from going either forward or backward on the reaction coordinate.

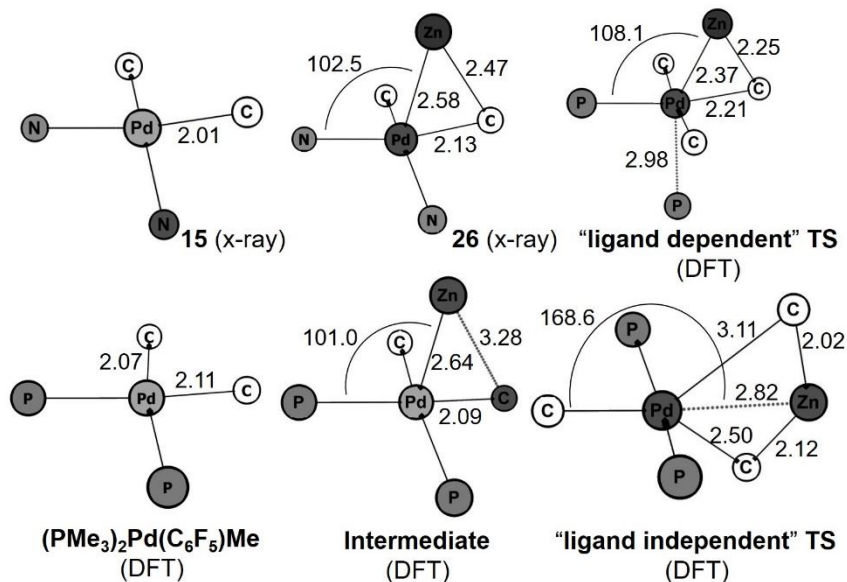


Figure 63: Comparison of the first coordination sphere of Pd (with bond distances [Å] and bond angles [°]) between crystal structures (**15** and **26**) and DFT-optimized structures, taken from reported¹³⁴ intermediates ("PMe₃)₂Pd(C₆F₅)Me", "intermediate") and TS's ("ligand (in)-dependent TS") of the Negishi reaction.

In the structure of the concerted "ligand-independent" TS, the Zn(II) fragment coordinates to Pd(II) in the plane of the square-planar complex and not perpendicular to it. The structural differences of the two TS's should make it possible to manipulate the stability of one or the other selectively. Whereas the electrostatic and dispersive part of the Pd–Zn bonding in the two TS's might be similar (small in solution), the interactions being less directional, the orbital interactions will certainly be different. The ETS-NOCV analysis in the gas-phase suggests that 38% of the attractive interactions are due to orbital interactions, in solution, the percentage orbital contribution is presumably higher (see Chapter 4.2.3.). Therefore, there may be a few kcal/mol that can be rationally altered to control the relative heights of the transmetalation barriers.

5 Conclusions and Outlook

Investigations on the transmetalation process between Pd(II) and various d^{10} metals, Cu(I), Ag(I), Au(I), and Zn(II), showed that the activation energy for the exchange of carbon fragments between these d^8 and d^{10} metals is surprisingly low. We proposed that the low barriers are due to metal-metal interactions in the TS of the transmetalations step. In literature, the bonds between square planar d^8 metals (mostly Pt(II)) and d^{10} metals are generally described as an interaction between a filled the d_{z^2} orbital and an empty s or p orbital, or assumed to be predominantly stabilized by dispersive interactions. Our results on the (bhq)₂Pd-based model system suggest that this picture of the bonding is too simplistic because the bimetallic complexes were found to be stabilized by a combination of electrostatic, orbital and dispersive interactions. The importance of the transmetalation step for the outcome of especially the Negishi reaction makes it desirable to understand how we can influence the activation energy of this step, thus, how to control the strength of Pd(II)-Zn(II) metal-metal bonds. Measuring the Pd-Zn bond strength of a series of bhq-ligands (for Pd) and aryl ligands (for Zn), substituted with σ - and π - donors and acceptors, could help to achieve this goal. The stability, the close analogy of the (bhq)₂Pd-ZnR₂ complex with the proposed structure of TS for Negishi transmetalations, as well as the practical methodology we found to quantify the dissociation energy in solution, renders this complex an ideal system to study Pd/Zn transmetalation steps. Alternatively, the dependency of the rate of the transmetalation process on electronic and steric alterations could be studied by determining the activation energy of this step for various systems in the gas-phase. Measuring the barrier for the Pd to Cu transmetalation of pentafluorophenyl in [(dmpe)Pd(C₆F₅)₂-CuPPh₃]⁺ served as a first step towards

this end. For gas-phase investigations on the bonding in $(\text{bhq})_2\text{Pd-ZnR}_2$ a charged Zn complex has to be used instead of $\text{Zn}(\text{C}_6\text{F}_5)_2$. $[\text{MeZn}][\text{Al}(\text{OR}^F)_4]^{159}$ could be a promising candidate for that purpose and its synthesis is reported.¹⁶⁰

The gas-phase investigations on the $[(\text{bhq})_2\text{Pd}\cdots\text{Cu}(\text{IPr})]^+$ demonstrate that state-of-the-art DFT methods substantially overestimate the strengths of Pd-Cu metal-metal bonds. The exact reason for this discrepancy should certainly be addressed in future investigations. If it turns out that DFT methods indeed systematically overestimate Pd(II)-M bond energies, this would have a big impact on the modeling of bimetallic reactions. It would for example imply that the potential energy surface calculated for the Sonogashira transmetalation in chapter 2 is too “flat” and that the gas-phase barrier for the internal Cu-C bond breaking, Pd-C bond forming process, is in fact around 20-30 kcal/mol higher in energy than calculated. In that case, reaction pathway **B** of the CID experiment should be fitted using a “tight” TS model, which would lead to experimental activation energies for the σ/π -rearrangement of around 35 kcal/mol for Pd/Cu and Pd/Ag, and 23 kcal/mol for Pd/Au.

For the Suzuki, Stille, and Hiyama coupling it is assumed that no metal-metal bonds are present in the TS's for transmetalations. Isolation of $(\text{bhq})_2\text{Pd-Sn/Si/B}$ complexes would indicate that this assumption is not (necessarily) generally true. The study of the interaction of $(\text{bhq})_2\text{Pd}$ with the simplest Lewis acid, a proton, could help to understand the mechanisms of protodemetalation and C-H activation processes.

Another possible research direction, more towards a synthetic application, could be to use the fast transmetalation step between Pd and Au to combine the reactivity of the two metals in one reaction and thereby overcome current

limitations of their individual applications.¹⁶¹⁻¹⁶⁴ Pd is known to catalyze C-C bond formations, however, the drawback of its application is that the organometal(loid) coupling partner needs to be preformed. Au on the other hand can be used for the catalytic hydroamination of alkynes. For alkenes, however, the last step of the cycle, the protodeauration, has generally a too high barrier and the reaction stops at the alkylgold intermediate. By combining the two reactivities, the Au intermediate could transmetalate its carbon fragment to Pd where it would be cross-coupled to form a new C-C bond. It would constitute sort of a combination of a Heck with a Negishi reaction, however, using Au(I) instead of Zn(II). Thereby, the limitations of Pd catalysts to require preformation of organometal(loid)s as well as the problem of Au catalysts with protodeaurations could be circumvent.

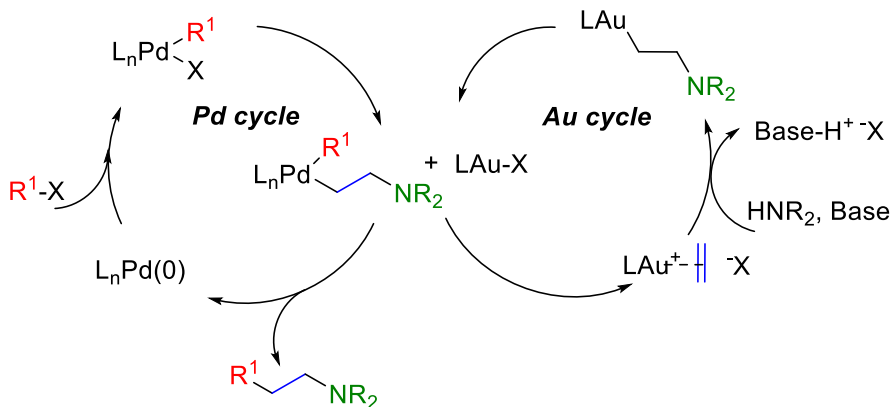


Figure 64: Hypothetical mechanism of a proposed Pd/Au catalyzed reaction.

6 Appendix

6.1 Experimental Section

Unless otherwise stated, all reactions were carried out under an atmosphere of argon using standard Schlenk techniques or in a nitrogen filled glovebox. All solvents were dried and distilled prior to use (CH_2Cl_2 / MeCN / $1,2\text{-C}_6\text{H}_4\text{F}_2$: CaH₂; Hexane, Pentane, Et₂O, THF: Na/benzophenone; Toluene: Na; MeOH: Mg) and stored over molecular sieve in a N₂-filled glovebox. Chromatographic purifications were carried out using Fluka silica gel (230-400 mesh particle size). Thin layer chromatography were carried out using Merck TLC silica gel 60 with F254. ESI-MS/MS experiments were performed on a Thermo Finnigan TSQ Quantum and on a modified Finnigan MAT TSQ-700 ESI-MS/MS. NMR were recorded on a Varian Mercury 300, Varian 500 or a Bruker 600 spectrometer. Dry NMR solvents were obtained by storing over molecular sieve for at least 3 days prior to use. The NMR spectra are reported as follows: chemical shift δ in ppm relative to TMS ($\delta = 0$ ppm), multiplicity, coupling constant (J in Hz), number of protons. The resonance multiplicity is described as s (singlet), d (doublet), t (triplet), q (quartet), or m (multiplet). Broad signals are described with br. (broad). Elemental analyses were performed by the Microanalytical Laboratorium für Organische Chemie, ETH Zürich. High resolution ESI-MS/MS was performed by the MS service für Organische Chemie, ETH Zürich.

6.2 Synthesis

(^tBuPCP)Pd-CCPh (tBuPCP: 2,6-(tBu₂PCH₂)₂C₆H₃),¹¹² (ⁱPr^OPOCOP)Pd-CCPh
 (ⁱPr^OPOCOP: 2,6-(ⁱPr₂PO)₂C₆H₃),¹¹⁵ (dmpe)Pd(Me)CCPh,¹⁶⁵ (iPr)CuOTf,¹³⁰

(IPr)AuOTf,¹¹⁶ (bhq₂)Pd,¹²⁹ (dmpe)Pd(C₆F₅)₂¹⁴¹, 7-R-benzo[h]quinoline (R: NH₂, OMe, CN, Cl, I, Me)¹³³ were synthesized according to literature procedures.

7-NO₂-benzo[h]quinoline: (This compound was synthesized under air following a modified literature procedure)¹³³. In a round bottom flask (250 mL) benzo[h]quinoline (8.00 g, 44.6 mmol, 1 eq.) was dissolved in concentrated H₂SO₄ (16 mL) at r.t.. The reaction mixture was cooled to -10 °C and a mixture of concentrated H₂SO₄ (5.5 mL) and concentrated HNO₃ (8.6 mL) was added dropwise over 8 min. The reaction mixture was subsequently poured onto ice and neutralized with aqueous NaHCO₃ and Na₂CO₃ solutions. The suspension was extracted with CH₂Cl₂ and the resulting solution was evaporated to afford a pale yellow solid. Purification by chromatography on silica gel (CH₂Cl₂/Cyclohexane 2:1) afforded the product (4.56 g, 20.4 mmol, 46 % yield). ¹H NMR (300 MHz, Chloroform-d) δ 9.71 (d, J = 8.4 Hz, 1H), 9.07 (dd, J = 4.4, 1.8 Hz, 1H), 8.48 (d, J = 9.3 Hz, 1H), 8.36 (d, J = 7.7 Hz, 1H), 8.26 (dd, J = 8.0, 1.7 Hz, 1H), 7.94 (d, J = 9.4 Hz, 1H), 7.87 – 7.75 (m, 1H), 7.64 (dd, J = 8.1, 4.4 Hz, 1H).

7-CF₃-benzo[h]quinoline: To a Schlenk flask (50 mL) were added CuCl (227.05 mg, 2.3 mmol, 2 eq.), KOtBu (257.36 mg, 2.3 mmol, 2 eq.) and 1,10-phenanthroline (413.47 mg, 2.3 mmol, 2 eq.) and extra dry DMF (6 mL). The suspension was stirred at r.t. for 37 min. Then, TMSCF₃ (0.34 mL, d. 0.962 g/mL, 2.3 mmol, 2 eq.) was added dropwise to the Schlenk flask and the reaction mixture was stirred at r.t. for 70 min. Then, a solution of 7-Iodobenzo[h]quinoline (350 mg, 1.15 mmol, 1 eq.) in extra dry DMF (2.5 mL) was added dropwise. The reaction mixture was stirred at 50 °C overnight. After cooling to r.t., it was diluted with Et₂O and filtered through a pad of celite. The organic phase was washed with saturated NaHCO₃ (aq) and brine, and dried

over Na₂SO₄. Evaporation of the solvent afforded the product (269.9 mg, NMR-purity 92 %, yield 88 %). ¹H NMR (300 MHz, Chloroform-d) δ 9.62 (d, J = 8.4 Hz, 1H), 9.06 (dd, J = 4.4, 1.8 Hz, 1H), 8.25 (dd, J = 8.0, 1.8 Hz, 1H), 8.19 (dd, J = 9.3, 2.2 Hz, 1H), 8.08 (d, J = 7.4 Hz, 1H), 7.86 (d, J = 9.3 Hz, 1H), 7.79 (dd, J = 7.9 Hz, 1H), 7.61 (dd, J = 8.1, 4.4 Hz, 1H).

7-F-benzo[h]quinoline: (The reaction was done under air.) In a round bottom flask (250 mL) 7-aminobenzo[h]quinoline (399.93 mg, 2.1 mmol, 1 eq.) was dissolved in MeOH (100 mL) and cooled to 0 °C. IsoamylNitrit (0.83 mL, 0.875 g/ml, 6.2 mmol, 3 eq.) and tetrafluoroboric acid solution (0.77 mL, 1.41 g/ml, 8M, 6.2 mmol, 3 eq.) were added dropwise and stirred at r.t. for 5.5 h. Then, the suspension was diluted with ether and filter through a frit to obtain a brown solid powder. The solid is transferred to a round bottom flask (100 ml) and suspended in *o*-xylene (35 ml). The flask was equipped with a condenser and heated to 140 °C for 14 h. The suspension was filtered and evaporated to dryness. The resulting solid was suspended in benzene, filtered through a syringe filter (CHROMAFIL Xtra PTFE 45/25 0.45 μm), and evaporated to dryness afford the product (95.14 mg, 0.48 mmol, 23 %). ¹H NMR (300 MHz, Chloroform-d) δ 9.08 (d, J = 8.3 Hz, 1H), 9.03 (dd, J = 4.4, 1.8 Hz, 1H), 8.22 (dd, J = 8.0, 1.8 Hz, 1H), 8.11 (d, J = 9.2 Hz, 1H), 7.76 (d, J = 9.0 Hz, 1H), 7.67 (td, J = 8.1, 5.6 Hz, 1H), 7.57 (dd, J = 8.0, 4.4 Hz, 1H), 7.39 (ddd, J = 10.3, 7.8, 1.1 Hz, 1H). ¹⁹F NMR (282 MHz, Chloroform-d) δ -122.94.

General procedure for bromination of substituted 7-R-benzo[h]quinolones (the reaction was done under Ar atmosphere): In a Schlenk flask, R-benzo[h]quinoline (1 eq.) and Pd(OAc)₂ (0.08 eq.) were suspended in dry CH₃CN (7 mL per mmol). N-bromosuccinimide (1.1 eq.) was added and the reaction

mixture was warmed to ca. 85 °C overnight. Then, the reaction was cooled to r.t. and the solvent was removed under reduced pressure. The residue was suspended in organic solvent. Water was added and the water phase was extracted with organic solvent. The combined organic phase was washed with brine and dried over Na₂SO₄. After filtration, the solvent was removed by evaporation.

7-Methoxy-10-bromobenzo[h]quinoline: The reaction was done according to general procedure for brominations. 7-Methoxybenzo[h]quinoline (240.59 mg, 1.1 mmol, 1 eq.), Pd(OAc)₂ (22.97 mg, 0.1 mmol, 0.09 eq.) and N-bromosuccinimide (225.06 mg, 1.3 mmol, 1.2 eq.) in dry CH₃CN (7 ml) were stirred at 90 °C overnight. Work up as described in general procedure, extraction with CH₂Cl₂ to afford the product (264.71 mg, 0.92 mmol, 80 % yield). ¹H NMR (300 MHz, Chloroform-d) δ 9.10 (dd, J = 4.3, 1.9 Hz, 1H), 8.34 (d, J = 9.1 Hz, 1H), 8.18 (dd, J = 8.1, 1.9 Hz, 1H), 8.01 (d, J = 8.6 Hz, 1H), 7.72 (d, J = 9.1 Hz, 1H), 7.56 (dd, J = 8.0, 4.3 Hz, 1H), 6.94 (d, J = 8.5 Hz, 1H).

7-Cyano-10-bromobenzo[h]quinoline: The reaction was done according to general procedure for brominations. 7-Cyanobenzo[h]quinoline (230.05 mg, 1.1 mmol, 1 eq.), Pd(OAc)₂ (15.25 mg, 0.07 mmol, 0.06 eq.) and N-bromosuccinimide (220.63 mg, 1.2 mmol, 1.2 eq.) in CH₃CN (6 mL, distill) were stirred at 90 ° overnight. Work-up as described in general procedure, extraction with Et₂O. The reaction was not over therefore it was reset again overnight. After additional work up with ether, washing with brine and drying with Na₂SO₄, the solvent was evaporated to afford the product (101.79 mg, 0.36 mmol, 32 % yield). ¹H NMR (300 MHz, Chloroform-d) δ 9.17 (dd, J = 4.3, 1.9 Hz, 1H), 8.32 –

8.23 (m, 2H), 8.19 (d, J = 8.0 Hz, 1H), 7.97 (d, J = 9.0 Hz, 1H), 7.84 (d, J = 8.0 Hz, 1H), 7.68 (dd, J = 8.1, 4.2 Hz, 1H).

7-Chloro-10-bromobenzo[h]quinoline: The reaction was done according to general procedure for brominations. 7-Chlorobenzo[h]quinoline (403.47 mg, 1.89 mmol, 1 eq.), Pd(OAc)₂ (26.09 mg, 0.012 mmol, 0.06 eq.) and N-bromosuccinimide (369.68 mg, 2.1 mmol, 1.1 eq) in CH₃CN (15 ml, distill) were stirred at 75 °C for 18 h. Work-up as described in general procedure, extraction with Et₂O to afford the product (427.94 mg, 1.46 mmol, 77 % yield). ¹H NMR (300 MHz, Chloroform-d) δ 9.13 (d, J = 4.3 Hz, 1H), 8.35 (d, J = 9.2 Hz, 1H), 8.22 (d, J = 7.0 Hz, 1H), 8.03 (d, J = 8.2 Hz, 1H), 7.85 (d, J = 9.1 Hz, 1H), 7.67 – 7.54 (m, 2H).

7-Methyl-10-bromobenzo[h]quinoline: The reaction was done according to general procedure for brominations. 7-Methylbenzo[h]quinoline (190 mg) was suspended with dry CH₃CN (2 ml). Pd(OAc)₂ (18.5 mg, 0.08 mmol, 0.08 eq.) and N-bromosuccinimide (193 mg, 1.1 mmol, 1.1 eq.) were added and the reaction is heated to 85 ° for 17 h. Work up as described in general procedure, extraction with CH₂Cl₂. Further purification by flash chromatography on silica gel eluting with CH₂Cl₂ afforded the oily product (116.84 mg, impurities remain). ¹H NMR (300 MHz, Chloroform-d) δ 9.09 (dd, J = 4.3, 1.9 Hz, 1H), 8.11 (dd, J = 8.0, 1.9 Hz, 1H), 7.96 (d, J = 7.8 Hz, 1H), 7.90 (d, J = 9.1 Hz, 1H), 7.66 (d, J = 9.2 Hz, 1H), 7.52 (dd, J = 8.0, 4.3 Hz, 1H), 7.27 (dd, J = 7.8, 0.9 Hz, 1H), 2.66 (d, J = 0.8 Hz, 3H).

7-Trifluoromethyl-10-bromobenzo[h]quinoline: The reaction was done according to general procedure for brominations. 7-Trifluoromethylbenzo[h]quinoline (223.95 mg, 0.91 mmol, 1 eq.), Pd(OAc)₂ (16.13 mg, 0.07 mmol, 0.08 eq.) and N-bromosuccinimide (176.76 mg, 1 mmol,

1.1 eq) in CH₃CN (4.5 ml) were stirred at 85 °C for 19 h. Work up as described in general procedure, extraction with Et₂O. Purification by column chromatography on silica gel eluting with CH₂Cl₂/cyclohexane 4:1 (v/v) afforded a light yellow oil (122.42 mg, 0.38 mmol, 41 % yield). ¹H NMR (300 MHz, Chloroform-d) δ 9.14 (dd, J = 4.3, 1.9 Hz, 1H), 8.24 (dd, J = 8.1, 1.9 Hz, 1H), 8.21 – 8.14 (m, 2H), 7.88 (d, J = 9.4 Hz, 1H), 7.83 (dd, J = 8.1, 0.7 Hz, 1H), 7.64 (dd, J = 8.0, 4.3 Hz, 1H). ¹⁹F NMR (282 MHz, Chloroform-d) δ -58.61.

General procedure for the palladium complex formation (the reaction was done under inert gas atmosphere): In a Schlenk flask (100 ml) substituted benzo[h]quinoline (2 eq.) was suspended in dry ether (10 mL per mmol). The suspension was cooled to -78 °C and *n*-Butyllithium (2.08 eq) was added dropwise while stirring. Then, a solution of Pd(SEt₂)Cl₂ (1 eq.) in ether (10 ml) was added. After 30 min., the suspension was poured onto water and extracted with CH₂Cl₂. The combined organic phases were washed with brine and dried over MgSO₄. Crystallization from CH₂Cl₂, layered with ether, afforded the crystalline product. The crystals were dried under high vacuum.

(bhq)₂Pd: ¹H NMR (300 MHz, Methylene Chloride-d₂) 9.10 (dd, J = 5.1, 1.5 Hz, 2H), 8.41 (t, J = 4.1 Hz, 2H), 8.33 (dd, J = 8.0, 1.4 Hz, 2H), 7.86 (d, J = 8.7 Hz, 2H), 7.69 (d, J = 4.2 Hz, 4H), 7.65 (d, J = 8.7 Hz, 2H), 7.60 (dd, J = 8.0, 5.1 Hz, 2H).

(^{Me}Obhq**)₂Pd**: ¹H NMR (300 MHz, Methylene Chloride-d₂) 9.10 (dd, J = 5.0, 1.5 Hz, 2H), 8.35 (dd, J = 8.0, 1.5 Hz, 2H), 8.29 (d, J = 8.9 Hz, 2H), 8.27 (d, J = 8.1 Hz, 2H), 7.66 (d, J = 9.0 Hz, 2H), 7.63 (dd, J = 8.0, 5.0 Hz, 2H), 7.22 (d, J = 8.1 Hz, 2H), 4.08 (s, 6H).

(^{Me}bhq)₂Pd: ¹H NMR (300 MHz, Chloroform-d) 9.09 (dd, J = 5.1, 1.5 Hz, 2H), 8.36 (d, J = 7.4 Hz, 2H), 8.32 (dd, J = 8.0, 1.4 Hz, 2H), 8.07 (d, J = 8.9 Hz, 2H), 7.66 (d, J = 8.9 Hz, 2H), 7.60 (dd, J = 8.0, 5.0 Hz, 2H), 7.56 (d, J = 7.1 Hz, 2H), 2.75 (d, J = 0.9 Hz, 6H).

Synthesis of bimetallic complexes:

(M: Cu, Au; R: H, Me, OMe): Bimetallic complexes were prepared by mixing a solution of (R-bhq)₂Pd (0.01 mM) in 0.5 mL dichloromethane with a solution of (IPr)MX (0.01 mM) (X: OTf, BArF) in 0.5 mL of dichloromethane in a vial in the glovebox. The solution was filtered, layered with n-hexane (0.2-1.0 mL) and cooled to -35 °C. Colorless needles were formed after 1-5 days.

[(bhq)₂Pd-Cu(IPr)]BArF: ¹H NMR (500 MHz, Methylene Chloride-d₂) δ 8.72 (dd, J = 5.1, 1.4 Hz, 2H), 8.49 (dd, J = 8.1, 1.3 Hz, 2H), 7.92 (d, J = 7.5 Hz, 2H), 7.91 (d, J = 8.5 Hz, 2H), 7.82 – 7.75 (m, 14H), 7.63 – 7.57 (m, 4H), 7.36 (dd, J = 7.9, 7.3 Hz, 2H), 7.33 – 7.28 (m, 2H), 7.02 (s, 2H), 6.99 (d, J = 7.8 Hz, 4H), 2.20 (p, J = 6.9 Hz, 4H), 0.99 (d, J = 6.8 Hz, 12H), 0.65 (d, J = 6.9 Hz, 12H).

[(^{OMe}bhq)₂Pd-Cu(IPr)]BArF: ¹H NMR (300 MHz, Methylene Chloride-d₂) δ 8.71 (dd, J = 5.1, 1.5 Hz, 2H), 8.47 (dd, J = 8.1, 1.4 Hz, 2H), 8.30 (d, J = 8.9 Hz, 2H), 7.82 – 7.69 (m, 14H), 7.56 (s, 4H), 7.35 – 7.20 (m, 2H), 7.01 – 6.89 (m, 6H), 6.76 (d, J = 8.1 Hz, 2H), 4.07 (s, 6H), 2.19 (p, J = 6.8 Hz, 4H), 0.96 (d, J = 6.9 Hz, 12H), 0.64 (d, J = 6.9 Hz, 12H).

[(^{Me}bhq)₂Pd-Cu(IPr)]BArF: ¹H NMR (300 MHz, Methylene Chloride-d₂) δ 8.71 (dd, J = 5.1, 1.4 Hz, 2H), 8.47 (dd, J = 8.0, 1.4 Hz, 2H), 8.07 (d, J = 8.9 Hz, 2H), 7.86 – 7.68 (m, 14H), 7.56 (s, 4H), 7.28 – 7.20 (m, 2H), 7.17 – 7.08 (m, 2H), 7.00 – 6.86

(m, 6H), 2.70 (d, $J = 0.9$ Hz, 6H), 2.15 (p, $J = 6.9$ Hz, 4H), 0.94 (d, $J = 6.8$ Hz, 12H), 0.60 (d, $J = 6.9$ Hz, 12H).

[(bhq)₂Pd-Au(IPr)]OTf: ¹H NMR (500 MHz, CD₂Cl₂) δ 8.57 (dd, $J = 5.2, 1.4$ Hz, 1H), 8.49 (dd, $J = 8.1, 1.4$ Hz, 1H), 7.89 (d, $J = 8.7$ Hz, 1H), 7.83 – 7.72 (m, 3H), 7.43 (td, $J = 7.7, 3.2$ Hz, 2H), 7.17 (s, 1H), 7.07 (d, $J = 7.8$ Hz, 2H), 2.22 (p, $J = 6.9$ Hz, 2H), 1.06 (d, $J = 6.9$ Hz, 6H), 0.76 (d, $J = 6.9$ Hz, 6H).

(bhq)₂Pd-Zn(C₆F₅)₂: (Zn(C₆F₅)₂ has to be recrystallized from toluene and dried under high vacuum prior to use) A solution of (bhq)₂Pd (4.6 mg, 10 μM) in 1 mL CH₂Cl₂ was mixed with a solution of Zn(C₆F₅)₂ (4.0 mg, 10 μM) in 1 mL 1,2-C₆H₄F₂ in a vial in the glovebox. The resulting solution was layered with 0.5 mL of Hexane and put in a glovebox fridge at -35 °C. Colorless crystals were formed overnight. ¹H NMR (500 MHz, Methylene Chloride-d₂) δ 9.01 (br. d, $J = 5.0$ Hz, 1H), 8.40 (br. d, $J = 7.0$ Hz, 1H), 8.26 (br. d, $J = 7.9$ Hz, 1H), 7.72 (br. d, $J = 8.4$ Hz, 2H), 7.69 – 7.59 (m, 1H), 7.60 – 7.53 (m, 2H). ¹⁹F NMR (471 MHz, Methylene Chloride-d₂) δ -118.24 (br. d, $J = 22.0$ Hz), -158.53 (br. t, $J = 19.7$ Hz), -162.43 – -166.35 (m). ¹³C NMR (471 MHz, Methylene Chloride-d₂) δ 154.05, 152.82, 148.00, 142.77, 138.09, 135.06, 134.35, 130.02, 129.35, 127.19, 125.50, 124.09, 121.80 (C₆F₅ resonances were not observed). El. Anal.: calc. for C₃₈H₁₆N₂F₁₀ZnPd: C 52.93, H 1.87, N 3.25, F 22.03, Zn 7.58, Pd 12.34 Found: C 52.72, H 1.86, N 3.20.

Synthesis of allyl-substitued (NHC)CuCl:

Bis(2,6-diisopropylphenyl)hept-6-ene-2,3-diimine: To a solution of Bis(2,6-diisopropylphenyl)butane-2,3-diimine (900 mg, 2.22 mmol) in pentane (4 mL) was added a solution (1.6 M) of n-BuLi (2.3 mmol, 1.44 mL) and tmeda (2.3

mmol, 0.34 mL) in pentane (8 mL) at r.t. The reaction mixture was stirred overnight. Then allyl bromide (0.78 mL, 8.9 mmol) was added and the reaction mixture was heated to 38 °C overnight. Excess allyl bromide was removed under vacuum and the residue was dissolved in pentane, filtered through a syringe filter and evaporated. Recrystallization from hot MeOH afforded the product as yellow crystals. (Yield: 72 %) ^1H NMR (300 MHz, CDCl_3) δ 7.15 (m, 6H), 5.72 (ddt, 1H), 4.91 – 4.99 (m, 2H), 2.72-2.82 (m, 4H), 2.65 – 2.70 (m, 2H), 2.26 (q, 2H), 2.10 (d, 3H), 1.15-1.25 (m, 24H). ^{13}C NMR (101 MHz, CDCl_3) δ 170.58, 168.21, 168.05, 146.08, 145.52, 137.50, 135.20, 135.08, 134.94, 123.81, 123.76, 123.70, 123.00, 122.83, 115.07, 77.35, 77.23, 77.03, 76.71, 30.52, 29.05, 28.52, 28.47, 23.27, 23.23, 23.01, 22.88, 22.73, 22.16, 17.18, 16.63, 1.05.

4-(but-3-en-1-yl)-1,3-bis(2,6-diisopropylphenyl)-5-methyl-4H-imidazolium

chloride: Bis(2,6-diisopropylphenyl)hept-6-ene-2,3-diimine (325 mg, 0.73 mmol) was dissolved in dry EtOAc (2 mL) under Ar. A solution of paraformaldehyde (28.5 mg, 0.95 mmol) in HCl in 1,4-dioxane (0.28 mL, 4M) was prepared in a vial (by means of a sonification bath) and added to the reaction mixture at 0 °C. The reaction was stirred overnight at r.t. and then filtered through a frit (Por 4), washed with ether and dried under vacuum to afford a grey solid. ^1H NMR (400 MHz, DMSO-d_6) δ 10.02 (s, 1H), 7.57 (dd, J = 7.8, 6.3 Hz, 2H), 7.34 – 7.17 (m, 4H), 5.85 – 5.67 (m, 1H), 5.02 (dd, J = 10.2, 1.8 Hz, 1H), 4.93 (dt, J = 17.2, 1.6 Hz, 1H), 3.26 (p, J = 6.7 Hz, 4H), 2.64 (t, J = 7.1 Hz, 2H), 2.37 – 2.27 (m, 2H), 2.08 (s, 3H), 1.20 (d, J = 6.7 Hz, 24H). ESI-MS m/z = 457.7

(allyl-NHC)CuCl: The imidazolium salt (170 mg, 0.35 mmol), KOTu (45 mg, 0.41 mmol) and CuCl (34 mg, 0.35 mmol) were dissolved in THF (7 mL). The mixture

was stirred under Ar for 22 h at r.t. The reaction mixture was filtered through celite and evaporated to dryness. The solid residue was washed with hexane and dried under vacuum. This compound was used without further purification.

6.3 MS-Experiments

6.3.1 Sample Preparation

Spray solutions of **4a** were prepared by mixing (PCP)PdCCPh **1** (0.6 mg, 1 μ M) with Cu(MeCN)₄BF₄ (0.3 mg, 1 μ M) and PPh₃ (0.2 mg, 1 μ M) in MeCN (0.1 mL) in a vial in the glovebox. After 1 minute, 10 μ L of the solution were added to 2 mL of MeCN and used immediately. Solutions of **4b** were prepared similarly but with AgBF₄ (0.2 mg, 1 μ M) instead of Cu(MeCN)₄BF₄.

For **4c** solutions, Ph₃PAuCl (0.5 mg, 1 μ M) was mixed with AgBF₄ (0.2 mg, 1 μ M) in 0.1 mL MeCN. After 5 minutes (PCP)PdCCPh **1** (0.6 mg, 1 μ M) were added and 10 μ L of the solution were added to 2 mL of MeCN.

Spray solutions of complex **17** and **22** were prepared by mixing (bhq)₂Pd (0.5 mg, 1 μ M) and (NHC)CuOTf (0.6 mg, 1 μ M) in 0.2 mL of Dichloromethane in a vial in the glovebox. Then 10 μ L of the solution were added to 2 mL of Acetone and used immediately.

Spray solutions of complex **21** were prepared by dissolving [IPr]CuOTf **16** (0.6 mg, 1 μ M) in 0.2 mL of Benzene in a vial in the glovebox. Then 20 μ L of the solution were added to 1 mL of Dichloroethane and used immediately.

Spray solutions of **23** and **24** were prepared by mixing $\text{dmpePd}(\text{C}_6\text{F}_5)_2$ (0.6 mg, 1 μM) with $\text{Cu}(\text{MeCN})_4\text{BF}_4$ (0.3 mg, 1 μM) and PPh_3 (0.2 mg, 1 μM) in DCE (0.1 mL) in a vial in the glovebox. After 1 minute, 10 μL of the solution were added to 2 mL of MeCN and used immediately.

Spray solutions of **25** was prepared by mixing $(1,4\text{-Dioxane})\text{Cu}(\text{C}_6\text{F}_5)$ (0.3 mg, 1 μM) with 1-Methyl-1-[4-(diphenylphosphino)benzyl]pyrrolidinium bromide (0.4 mg, 1 μM) in MeCN (0.1 mL) in a vial in the glovebox. After 1 minute, 10 μL of the solution were added to 2 mL of MeCN and used immediately.

6.3.2 Qualitative MS-Experiments

Qualitative studies were performed on a Thermo-Finnigan TSQ Quantum instrument. Spray solutions were taken into a gas-tight syringe in the glovebox and used immediately after preparation. All samples were electrosprayed with a flowrate of 5 mL/min, 4.0 – 5.0 kV spray voltage and 170 °C capillary temperature. Collision-induced dissociation (CID) experiments were done with Ar or Xe (0.1 mTorr) as collision gas and 80-120 V collision offset.

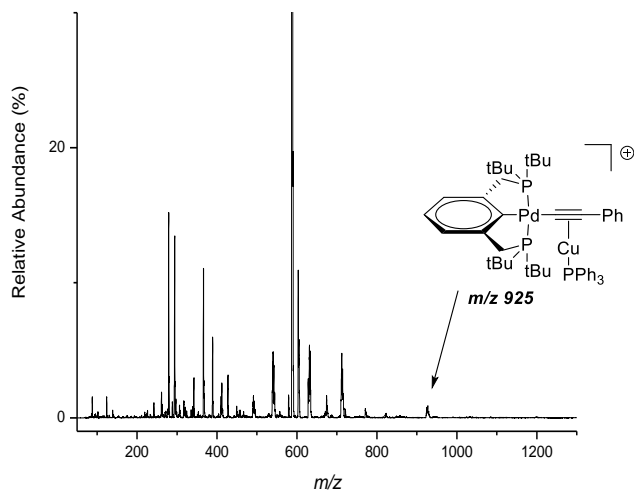


Figure 65: Full Spectrum with $[(PCP)PdCCPh-Cu(PPh_3)]^+$ ($m/z = 925$).

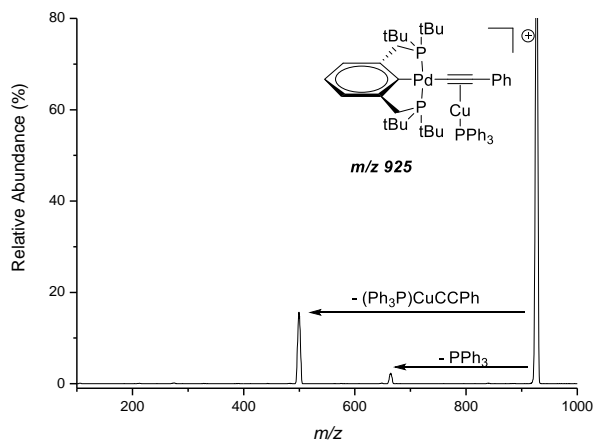


Figure 66: CID spectrum of Pd/Cu complex ($m/z = 925$) with Ar (0.1 mTorr)

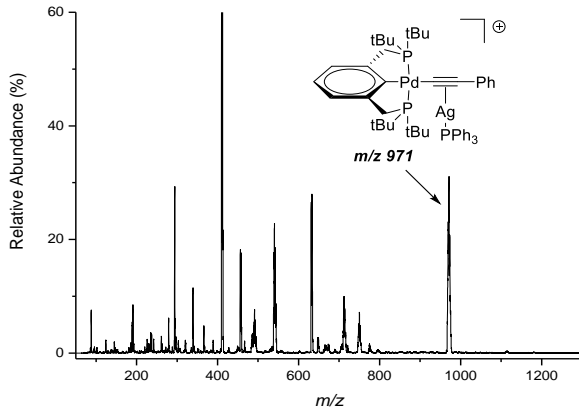


Figure 67: Full Spectrum with $[(PCP)PdCCPh-Ag(PPh_3)]^+$ ($m/z = 971$).

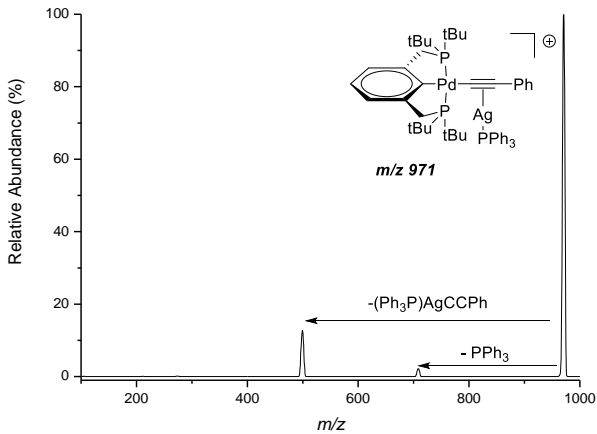
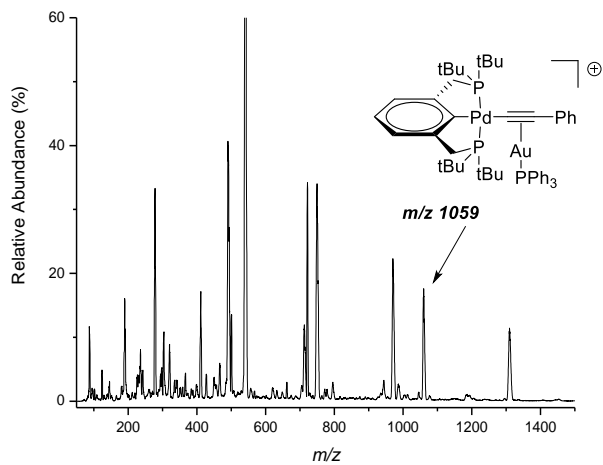
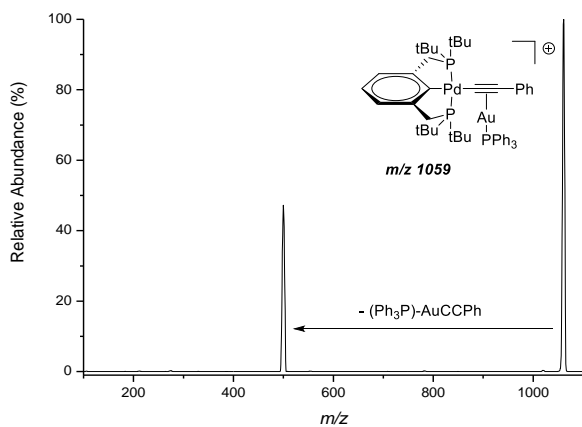


Figure 68: CID spectrum of Pd/Ag complex ($m/z = 971$) with Ar (0.1 mTorr)

Figure 69: Full Spectrum with [(PCP)PdCCPh-Au(PPh₃)]⁺ (m/z = 1059).Figure 70: CID spectrum of Pd/Au complex (m/z = 1059) with Ar (0.1 mTorr)

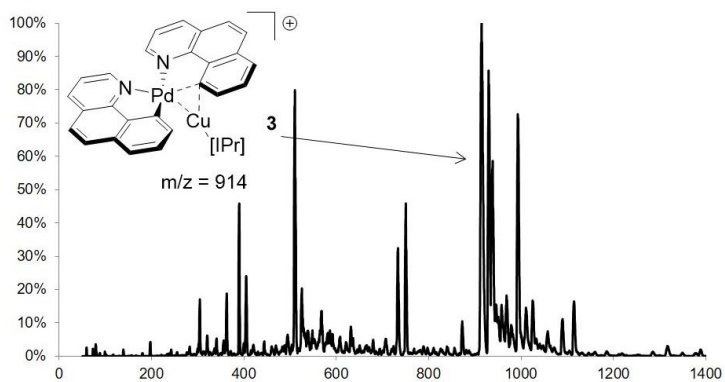


Figure 71: Full Spectrum with $[(bhq)_2Pd-Cu(IPr)]^+$ ($m/z = 914$).

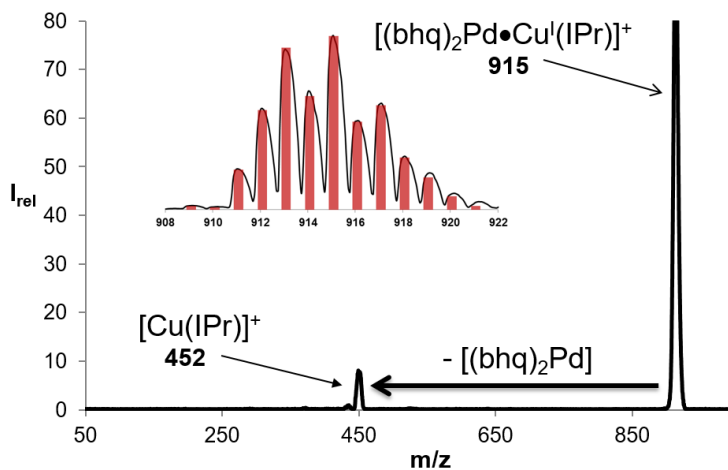


Figure 72: CID spectrum of Pd/Cu complex ($m/z = 915$) with Xe (0.1 mTorr)

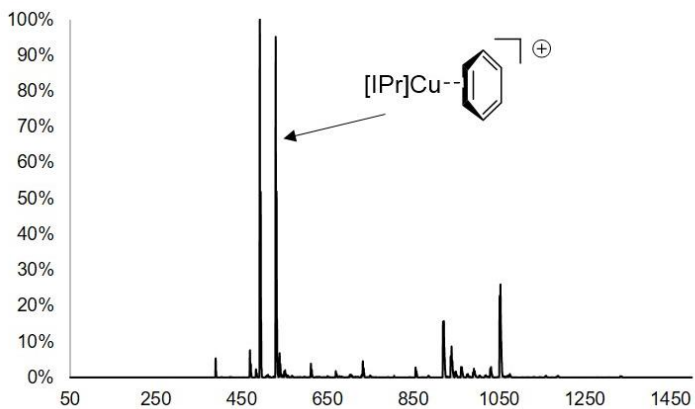


Figure 73: Full Spectrum with [IPr]Cu-Benzene ($m/z = 529$).

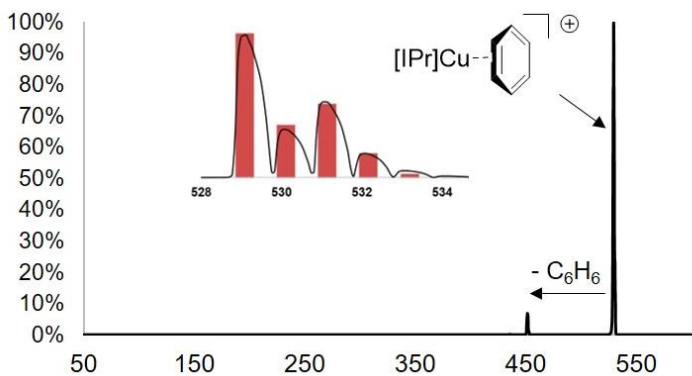
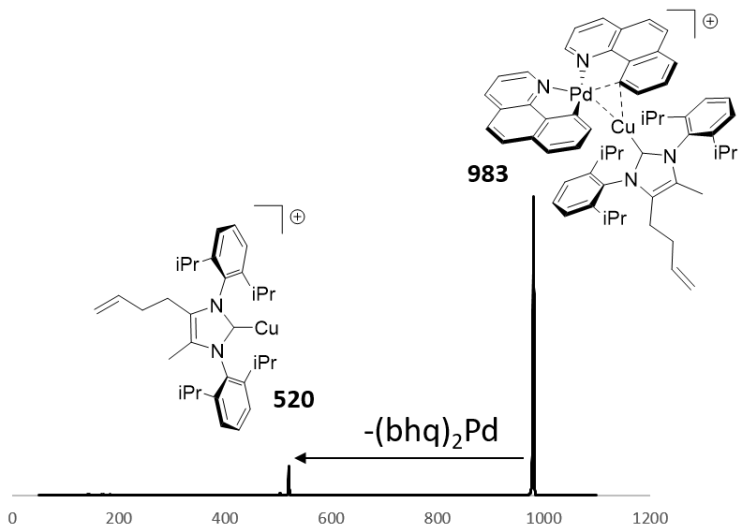
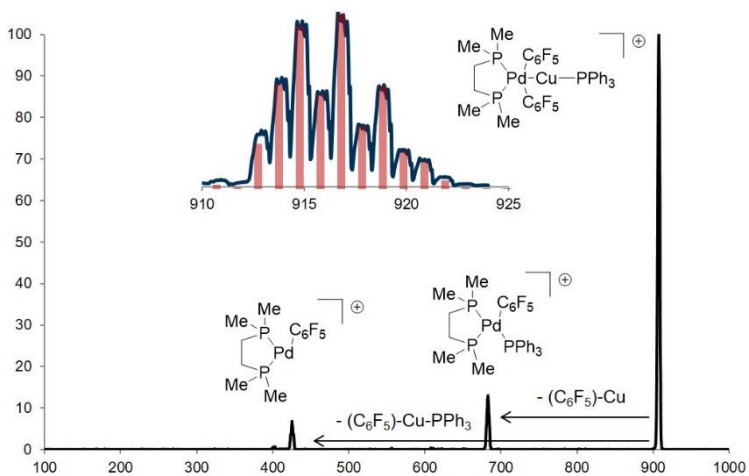


Figure 74: CID spectrum of $[\text{IPr}]_{\text{Cu}}\text{-C}_6\text{H}_6^+$ ($m/z = 529$) with Ar (0.1 mTorr)

Figure 75: CID spectrum of Pd/Cu complex ($m/z = 983$) with Ar (0.1 mTorr)Figure 76: CID spectrum of Pd/Cu complex ($m/z = 915$) with Ar (0.1 mTorr)

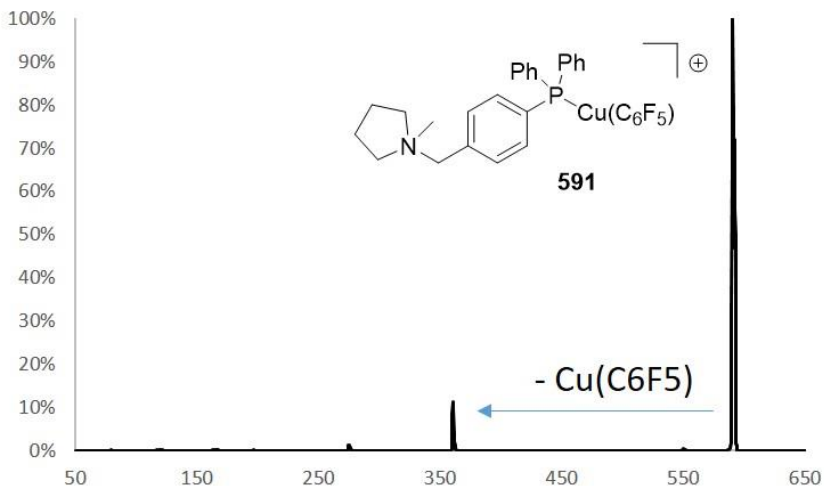


Figure 77: CID spectrum of $(\text{C}_6\text{F}_5)\text{CuPR}_3]^+$ complex ($m/z = 591$) with Ar (0.1 mTorr)

6.3.3 Quantitative MS-Experiments

T-CID (threshold collision-induced dissociation) measurements were done on a Finnigan MAT TSQ-700 mass spectrometer customized as described previously.¹ The solutions were sprayed at 3.5–4.5 kV spray voltage and capillary temperature of 170 – 190 °C. The ions were thermalized in a 24-pole ion guide to 70 °C with Argon (10 mTorr). All other lens voltages were adjusted to afford a narrow near-Gaussian distribution. The ions of interest were mass selected and collided with Argon or Xenon as collision gas at 5-7 different pressures varying from 110 to 20 mTorr.

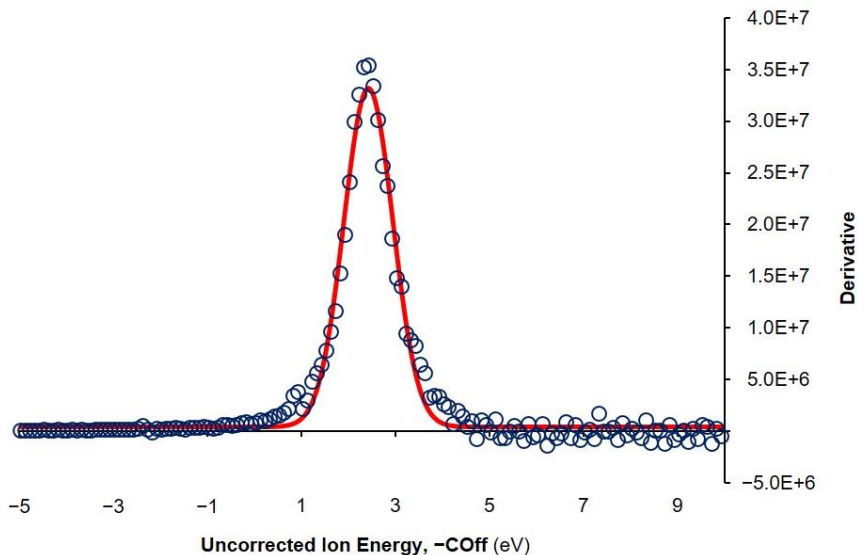


Figure 78: Ion beam kinetic energy distribution (blue) with Gaussian fit (red).

For each data set, a lab-frame ion kinetic energy scale E_{Lab} was constructed by subtracting the collision offset from V_{cen} , the average collision offset required to transmit the thermalized ions. Multiplication by $M_C / (M_C + M_R)$ – where M_C and M_R are the masses of collision gas and reactant ion, respectively – afforded a collision energy scale E_{CM} in the center-of-mass frame reflecting the maximum available activation energy.

The reactive cross-sections (σ) have been calculated, using the following formulae:

$$I_R = I_0 e^{-\sigma_{\text{tot}} \rho l}$$

I_0 and I_R are the measured transmitted intensities of ions before and after passing the collision octapole cell, σ_{tot} is the total reactive cross-section, ρ the

collision gas density and l the path length (18 cm). One obtains the rise to the product intensity $I_{p,i}$, assuming that all of the ions are detected:

$$I_0 = I_R + \sum I_P \quad \text{and} \quad \sigma_{P,i} = \frac{\sigma_{tot} I_{P,i}}{\sum I_P}$$

From the ion intensity curves at each pressure, individual product cross-sections $\sigma_{P,i}$ were determined as a function of the collision offset. In order to impose single-collision conditions, zero-pressure extrapolation was performed.

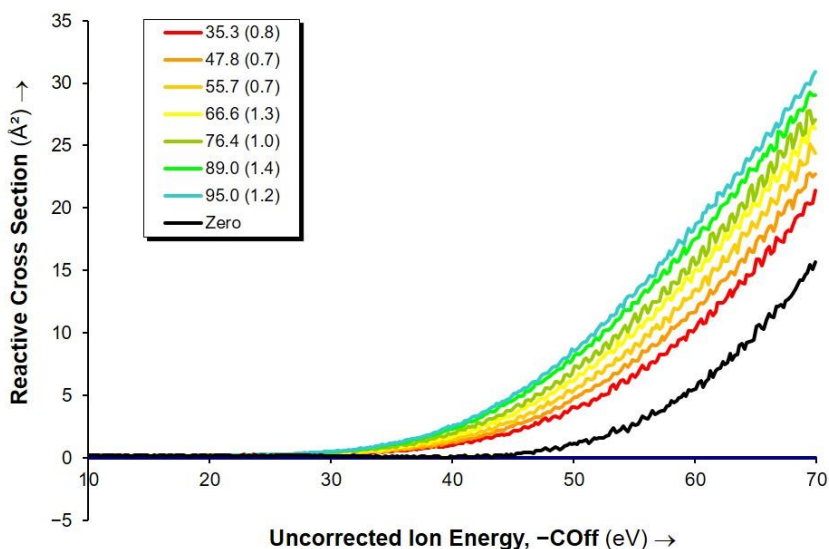


Figure 79: Typical reactive cross sections at various pressures (colored lines) and zero-pressure extrapolation (black line).

Activation energies were obtained by fitting the extrapolated reactive cross-sections with the program L-CID. Transition state parameters were set to “tight” or “loose”, depending on results from DFT calculation, chemical intuition and other arguments. For each of the data set 20 fits were selected on the basis

of visual agreement and standard deviation. The overall values and standard deviations of the parameters were obtained by reciprocal-variance weighted averaging over each of the three data sets. To the E_0 an estimated uncertainty of 0.15 V for the lab-frame energies was included. The number of internal free rotors was chosen by identifying low energy internal rotations (frequencies below around 200 cm^{-1}) from the calculated frequencies.

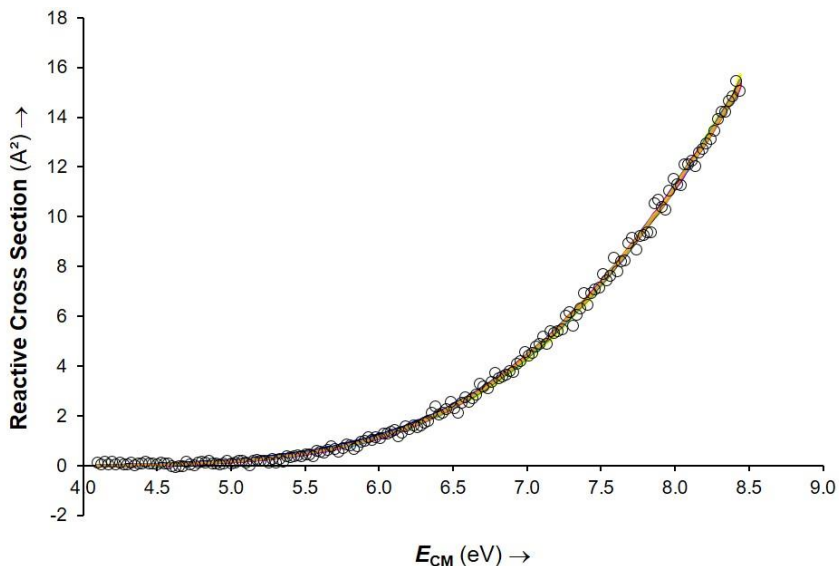


Figure 80: Typical reactive cross-sections curve in nominal collision energy (E_{cm}) of daughter ions (circles), fitted with L-CID (lines) from 4.1 to 8.5 eV in the centre of mass frame.

Appendix

<i>Data set</i>	E_0^\ddagger [eV]	V_{eff} [cm^{-1}]	α' [cm^{-1}]	E_0^\ddagger [eV]	α' [cm^{-1}]
1	1.813 ± 0.026	802 ± 49	5865 ± 298	2.027 ± 0.033	5415 ± 237
2	1.902 ± 0.056	792 ± 69	5533 ± 332	2.029 ± 0.059	5735 ± 339
3	1.827 ± 0.040	799 ± 91	56931 ± 361	2.055 ± 0.034	5872 ± 392
Overall in kcal mol ⁻¹	43.0 ± 1.1			47.0 ± 1.0	

Figure 81: Parameters for fits of [PCPPd-CCPh-CuPPh3]⁺, Number of free rotors: 0.

<i>Data set</i>	E_0^\ddagger [eV]	V_{eff} [cm^{-1}]	α' [cm^{-1}]	E_0^\ddagger [eV]	α' [cm^{-1}]
1	1.813 ± 0.057	686 ± 125	5958 ± 352	2.327 ± 0.045	5763 ± 410
2	1.857 ± 0.056	781 ± 151	5685 ± 407	2.207 ± 0.088	5762 ± 470
3	1.860 ± 0.056	786 ± 100	5625 ± 445	2.259 ± 0.060	5769 ± 463
Overall in kcal mol ⁻¹	42.5 ± 1.5			52.8 ± 1.8	

Figure 82: Parameters for fits of [PCPPd-CCPh-AgPPh3]⁺, Number of free rotors: 0.

<i>Data set</i>	E_0^\ddagger [eV]	V_{eff} [cm^{-1}]	α' [cm^{-1}]
1	1.608 ± 0.046	517 ± 19	5861 ± 396

Appendix

2	1.650 ± 0.029	549 ± 28	5971 ± 247
3	1.621 ± 0.041	529 ± 33	5823 ± 397
Overall in kcal mol ⁻¹	37.7 ± 1.0		

Figure 83: Parameters for fits of [PCPPd-CCPh-AuPPh₃]⁺, Number of free rotors: 0.

<i>Data set</i>	E_0^\ddagger [eV]	V_{eff} [cm ⁻¹]	α' [cm ⁻¹]
1	2.198 ± 0.051	904.6 ± 47.9	5881.0 ± 382.3
2	2.192 ± 0.077	855.6 ± 65.9	5794.0 ± 349.8
Overall in kcal mol ⁻¹	50.6 ± 1.4		

Figure 84: Parameters for fits of [(bmq)₂Pd-Cu(IPr)]⁺, Number of free rotors: 8.

<i>Data set</i>	E_0^\ddagger [eV]	V_{eff} [cm ⁻¹]	α' [cm ⁻¹]
1	1.821 ± 0.083	562.3 ± 58.6	5579 ± 490.6
2	1.815 ± 0.062	580.0 ± 56.3	5501 ± 474.9
Overall in kcal mol ⁻¹	42.0 ± 1.6		

Figure 85: Parameters for fits of [(Benzene)Cu(IPr)]⁺, Number of free rotors: 8.

Appendix

<i>Data set</i>	E_0^\ddagger [eV]	V_{eff} [cm^{-1}]	α' [cm^{-1}]	E_0^\ddagger [eV]	α' [cm^{-1}]
1	1.841 ± 0.08	625 ± 133	5691 ± 492	1.152 ± 0.091	239 ± 155
2	1.852 ± 0.10	608 ± 84	5763 ± 524	1.229 ± 0.1	227 ± 126
Overall in kcal mol ⁻¹	42.6 ± 2.1 (loose)			27.4 ± 2.4 (tight)	

Figure 86: Parameters for fits of [(dmpe)Pd(C₆F₅)₂-CuPPH₃]⁺, Number of free rotors: 4.

<i>Data set</i>	E_0^\ddagger [eV]	V_{eff} [cm^{-1}]	α' [cm^{-1}]
1	2.159 ± 0.031	598 ± 9	5704 ± 285
Overall in kcal mol ⁻¹	49.8 ± 0.7		

Figure 87: Parameters for fits of [(dmpe)Pd(C₆F₅)(PPH₃)]⁺, Number of free rotors: 4.

<i>Data set</i>	E_0^\ddagger [eV]	V_{eff} [cm^{-1}]	α' [cm^{-1}]	E_0^\ddagger [eV]	α' [cm^{-1}]
1	1.897 ± 0.05	638 ± 81	5687 ± 505	2.869 ± 0.185	5798 ± 447
Overall in kcal mol ⁻¹	43.8 ± 1.2 (loose)			66.2 ± 2.4 (loose)	

Figure 88: Parameters for fits of [(C₆F₅)CuPPH₂(C₆H₄CH₂NR₄)]⁺, Number of free rotors: 2.

6.4 NMR-Titration

A solution of $\text{Zn}(\text{C}_6\text{F}_5)_2$ in CD_2Cl_2 (1.663 mM) was prepared in the glovebox. This solution was used to prepare the stock solution of $(\text{bhq})_2\text{Pd}$ in order to keep the $[\text{Pd}]$ constant. Exact amounts of this solution (containing $[\text{Pd}]$ and $[\text{Zn}]$) were added by microsyringe to the solution of $(\text{bhq})_2\text{Pd}$ in a NMR-tube sealed with a septum. A ^{19}F NMR spectrum was recorded after each addition. The change in $\Delta\delta(F_{para})$ was plotted against the concentration of $(\text{bhq})_2\text{Pd}$. The data was fitted using the software IGOR Pro 7.01 according to the equation¹⁶⁶:

$$\Delta\delta = \frac{\Delta\delta_{sat}}{2} \left[\left(\frac{[\mathbf{1}]_0}{[\mathbf{2}]_0} + 1 + \frac{1}{K_a[\mathbf{2}]_0} \right) - \sqrt{\left(\frac{[\mathbf{1}]_0}{[\mathbf{2}]_0} + 1 + \frac{1}{K_a[\mathbf{2}]_0} \right)^2 - 4 \frac{[\mathbf{1}]_0}{[\mathbf{2}]_0}} \right]$$

$\Delta\delta$: change in chemical shift, relative to free $\text{Zn}(\text{C}_6\text{F}_5)_2$

$\Delta\delta_{sat}$: Calculated change in chemical shift at saturation

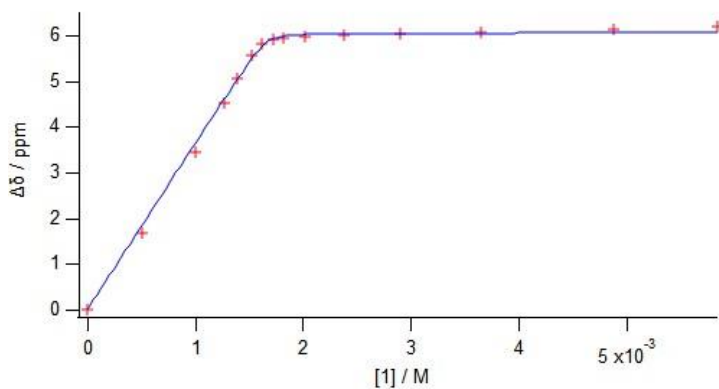
$[\mathbf{2}]_0$: concentration of complex $\text{Zn}(\text{C}_6\text{F}_5)_2$ (constant)

$[\mathbf{1}]$: concentration of complex $(\text{bhq})_2\text{Pd}$

K_a : Association constant (M^{-1})

The error in K_a was estimated to be 20%.

$[\text{bhq}_2\text{Pd}] / \text{mol L}^{-1}$	$\Delta\delta(\text{F}_{\text{para}}) / \text{ppm}$
0	0
0.000506845	1.68
0.000999859	3.44
0.001265242	4.51
0.00139378	5.04
0.001519663	5.55
0.001622596	5.8
0.001723788	5.89
0.001823282	5.93
0.002017344	5.96
0.002386868	5.99
0.002898907	6.03
0.003655603	6.07
0.004666071	6.13

Figure 89: ^{19}F NMR-Titration data in CD_2Cl_2 at 25°C Figure 90: ^{19}F NMR binding isotherm of $\text{Zn}(\text{C}_6\text{F}_5)_2$ and $(\text{bhq})_2\text{Pd}$ in CD_2Cl_2 at 25°C . $K_a = (4.5 \pm 0.9) \times 10^5 \text{ mol L}^{-1}$ and $\delta_{\text{sat}} = 6.05 \text{ ppm}$

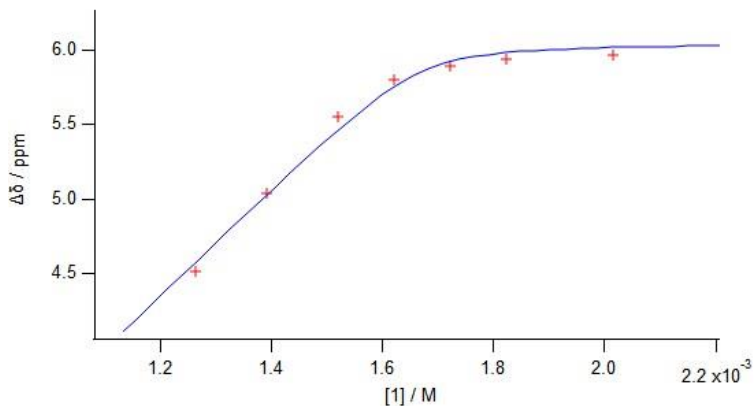


Figure 91: Zoomed-in region of Figure 77.

6.5 DFT Calculations

Chapter 2: Geometry optimizations were performed using Gaussian 09 package. The M06-L functional was used with SDD basis set and an effective core potential for transition metals and D95(d,p) basis set on all other atoms. Energies were computed using the ADF suite using the M06-L functional and a TZP basis set without frozen core. Relativistic effects including spin-orbit coupling were treated via the Zero Order Regular Approximation (ZORA) formalism.

Chapters 3 and 4: The geometries were optimized using the Gaussian 09 package with TPSS or TPSS-D3 and SDD basis set for Pd, Cu, Zn and D95(d,p) basis set on all other atoms. Single point energies were calculated using the TPSS or TPSS-D3 functional and SDD basis set with 2f and g polarization for Pd, Cu, Zn, and cc-pVTZ basis set for H,C,N (TPSS(-D3)/cc-pVTZ//TPSS(-D3)/SDD(d,p)).

The electron density for the AIM analysis was calculated with the coordinates from the crystal structures and the Gaussian09 suite using the TPSS-D3 functional and the def2-TZVP basis set (ECP on Pd).

The EDA-NOCV calculations were done with the geometries from the crystal structure or optimized geometries. The ADF 2012.01 program package was used with the TPSS-D3 functional and a triple- ζ -quality basis set augmented with one set of polarization functions. Scalar relativistic effects were incorporated by applying the zeroth-order regular approximation (ZORA).

7 References

1. Köhler, K.; Wussow, K.; Wirth, A. S., Palladium-Catalyzed Cross-Coupling Reactions – A General Introduction. In *Palladium-Catalyzed Coupling Reactions*, Wiley-VCH Verlag GmbH & Co. KGaA: 2013; pp 1-30.
2. Negishi, E.-i.; Wang, G.; Rao, H.; Xu, Z., Alkyne Elementometalation–Pd-Catalyzed Cross-Coupling. Toward Synthesis of All Conceivable Types of Acyclic Alkenes in High Yields, Efficiently, Selectively, Economically, and Safely: “Green” Way. *The Journal of Organic Chemistry* **2010**, *75* (10), 3151-3182.
3. Johansson Seechurn, C. C. C.; Kitching, M. O.; Colacot, T. J.; Snieckus, V., Palladium-Catalyzed Cross-Coupling: A Historical Contextual Perspective to the 2010 Nobel Prize. *Angew. Chem. Int. Ed.* **2012**, *51* (21), 5062-5085.
4. Echavarren, A. M.; Homs, A., Mechanistic Aspects of Metal-Catalyzed C,C- and C,X-Bond Forming Reactions. In *Metal-Catalyzed Cross-Coupling Reactions and More*, Wiley-VCH Verlag GmbH & Co. KGaA: 2014; pp 1-64.
5. Stille, J. K., Oxidative addition and reductive elimination. In *The Metal—Carbon Bond (1985)*, John Wiley & Sons, Ltd.: **2010**; 625-787.
6. Braga, A. A. C.; Ujaque, G.; Maseras, F., Mechanism of Palladium-Catalyzed Cross-Coupling Reactions. In *Computational Modeling for Homogeneous and Enzymatic Catalysis*, Wiley-VCH Verlag GmbH & Co. KGaA: **2008**; 109-130.
7. Rudolph, A.; Lautens, M., Secondary Alkyl Halides in Transition-Metal-Catalyzed Cross-Coupling Reactions. *Angew. Chem. Int. Ed.* **2009**, *48* (15), 2656-2670.
8. Stille, J. K.; Lau, K. S. Y., Mechanisms of oxidative addition of organic halides to Group 8 transition-metal complexes. *Acc. Chem. Res.* **1977**, *10* (12), 434-442.
9. Ananikov, V. P.; Musaev, D. G.; Morokuma, K., Transition Metal Catalyzed Carbon-Carbon Bond Formation: The Key of Homogeneous Catalysis. In *Computational Modeling for Homogeneous and Enzymatic Catalysis*, Wiley-VCH Verlag GmbH & Co. KGaA: **2008**; 131-148.

10. Moravskiy, A.; Stille, J. K., Mechanisms of 1,1-reductive elimination from palladium: elimination of ethane from dimethylpalladium(II) and trimethylpalladium(IV). *J. Am. Chem. Soc.* **1981**, *103* (14), 4182-4186.
11. Miyaura, N.; Suzuki, A., Palladium-Catalyzed Cross-Coupling Reactions of Organoboron Compounds. *Chem. Rev.* **1995**, *95* (7), 2457-2483.
12. Lennox, A. J. J.; Lloyd-Jones, G. C., Transmetalation in the Suzuki–Miyaura Coupling: The Fork in the Trail. *Angew. Chem. Int. Ed.* **2013**, *52* (29), 7362-7370.
13. Miyaura, N., Cross-coupling reaction of organoboron compounds via base-assisted transmetalation to palladium(II) complexes. *J. Organomet. Chem.* **2002**, *653* (1–2), 54-57.
14. Braga, A. A. C.; Ujaque, G.; Maseras, F., A DFT Study of the Full Catalytic Cycle of the Suzuki–Miyaura Cross-Coupling on a Model System. *Organometallics* **2006**, *25* (15), 3647-3658.
15. Matos, K.; Soderquist, J. A., Alkylboranes in the Suzuki–Miyaura Coupling: Stereochemical and Mechanistic Studies. *The Journal of Organic Chemistry* **1998**, *63* (3), 461-470.
16. Carrow, B. P.; Hartwig, J. F., Distinguishing Between Pathways for Transmetalation in Suzuki–Miyaura Reactions. *J. Am. Chem. Soc.* **2011**, *133* (7), 2116-2119.
17. Amatore, C.; Jutand, A.; Le Duc, G., Kinetic Data for the Transmetalation/Reductive Elimination in Palladium-Catalyzed Suzuki–Miyaura Reactions: Unexpected Triple Role of Hydroxide Ions Used as Base. *Chemistry – A European Journal* **2011**, *17* (8), 2492-2503.
18. Schmidt, A. F.; Kurokhtina, A. A.; Larina, E. V., Role of a base in Suzuki-Miyaura reaction. *Russ. J. Gen. Chem.* **2011**, *81* (7), 1573.
19. Thomas, A. A.; Wang, H.; Zahrt, A. F.; Denmark, S. E., Structural, Kinetic, and Computational Characterization of the Elusive Arylpalladium(II)boronate Complexes in the Suzuki–Miyaura Reaction. *J. Am. Chem. Soc.* **2017**, *139* (10), 3805-3821.
20. Thomas, A. A.; Denmark, S. E., Pre-transmetalation intermediates in the Suzuki-Miyaura reaction revealed: The missing link. *Science* **2016**, *352* (6283), 329-332.

21. Cordovilla, C.; Bartolomé, C.; Martínez-Ilarduya, J. M.; Espinet, P., The Stille Reaction, 38 Years Later. *ACS Catalysis* **2015**, *5* (5), 3040-3053.
22. Espinet, P.; Echavarren, A. M., The Mechanisms of the Stille Reaction. *Angew. Chem. Int. Ed.* **2004**, *43* (36), 4704-4734.
23. Stille, J. K., The Palladium-Catalyzed Cross-Coupling Reactions of Organotin Reagents with Organic Electrophiles [New Synthetic Methods (58)]. *Angewandte Chemie International Edition in English* **1986**, *25* (6), 508-524.
24. Labadie, J. W.; Stille, J. K., Mechanisms of the palladium-catalyzed couplings of acid chlorides with organotin reagents. *J. Am. Chem. Soc.* **1983**, *105* (19), 6129-6137.
25. Ye, J.; Bhatt, R. K.; Falck, J. R., Stereospecific palladium/copper cocatalyzed cross-coupling of .alpha.-alkoxy- and .alpha.-aminostannanes with acyl chlorides. *J. Am. Chem. Soc.* **1994**, *116* (1), 1-5.
26. Nova, A.; Ujaque, G.; Maseras, F.; Lledós, A.; Espinet, P., A Critical Analysis of the Cyclic and Open Alternatives of the Transmetalation Step in the Stille Cross-Coupling Reaction. *J. Am. Chem. Soc.* **2006**, *128* (45), 14571-14578.
27. Casado, A. L.; Espinet, P.; Gallego, A. M., Mechanism of the Stille Reaction. 2. Couplings of Aryl Triflates with Vinyltributyltin. Observation of Intermediates. A More Comprehensive Scheme. *J. Am. Chem. Soc.* **2000**, *122* (48), 11771-11782.
28. Casado, A. L.; Espinet, P., Mechanism of the Stille Reaction. 1. The Transmetalation Step. Coupling of R1I and R2SnBu3 Catalyzed by trans-[PdR1IL2] (R1 = C6Cl2F3; R2 = Vinyl, 4-Methoxyphenyl; L = AsPh3). *J. Am. Chem. Soc.* **1998**, *120* (35), 8978-8985.
29. Casares, J. A.; Espinet, P.; Fuentes, B.; Salas, G., Insights into the Mechanism of the Negishi Reaction: ZnRX versus ZnR2 Reagents. *J. Am. Chem. Soc.* **2007**, *129* (12), 3508-3509.
30. García-Melchor, M.; Fuentes, B.; Lledós, A.; Casares, J. A.; Ujaque, G.; Espinet, P., Cationic Intermediates in the Pd-Catalyzed Negishi Coupling. Kinetic and Density Functional Theory Study of Alternative Transmetalation Pathways in the Me–Me Coupling of ZnMe2

- and trans-[PdMeCl(PMePh₂)₂]. *J. Am. Chem. Soc.* **2011**, *133* (34), 13519-13526.
31. Fuentes, B.; García-Melchor, M.; Lledós, A.; Maseras, F.; Casares, J. A.; Ujaque, G.; Espinet, P., Palladium Round Trip in the Negishi Coupling of trans-[PdMeCl(PMePh₂)₂] with ZnMeCl: An Experimental and DFT Study of the Transmetalation Step. *Chemistry – A European Journal* **2010**, *16* (29), 8596-8599.
32. Xin, J.; Zhang, G.; Deng, Y.; Zhang, H.; Lei, A., Which one is faster? A kinetic investigation of Pd and Ni catalyzed Negishi-type oxidative coupling reactions. *Dalton Transactions* **2015**, *44* (46), 19777-19781.
33. Liu, Q.; Lan, Y.; Liu, J.; Li, G.; Wu, Y.-D.; Lei, A., Revealing a Second Transmetalation Step in the Negishi Coupling and Its Competition with Reductive Elimination: Improvement in the Interpretation of the Mechanism of Biaryl Syntheses. *J. Am. Chem. Soc.* **2009**, *131* (29), 10201-10210.
34. Serra, D.; Moret, M.-E.; Chen, P., Transmetalation of Methyl Groups Supported by PtII–Aul Bonds in the Gas Phase, in Silico, and in Solution. *J. Am. Chem. Soc.* **2011**, *133* (23), 8914-8926.
35. Moret, M.-E.; Serra, D.; Bach, A.; Chen, P., Transmetalation Supported by a PtII–CuI Bond. *Angew. Chem. Int. Ed.* **2010**, *49* (16), 2873-2877.
36. Oeschger, R. J.; Chen, P., The First Heterobimetallic Pd–Zn Complex: Study of a d8–d10 Bond in Solid State, in Solution, and in Silico. *Organometallics* **2017**.
37. Van der Ploeg, A. F. M. J.; Van Koten, G.; Vrieze, K.; Spek, A. L.; Duisenberg, A. J. M., Crystal structure and molecular geometry of a square-pyramidal platinum(II) complex [{2,6-(Me₂NCH₂)₂C₆H₃}Pt(μ-((p-tol)NC(H)N(i-Pr)))HgBrCl] containing a PtII-to-HgII donor bond. *Organometallics* **1982**, *1* (8), 1066-1070.
38. Van der Ploeg, A. F. M. J.; Van Koten, G.; Brevard, C., INEPT silver-109 NMR evidence for direct platinum-to-silver bonding in dinuclear [[2,6-(Me₂NCH₂)₂C₆H₃][p-toINC(H)NR]PtAgBr]. *Inorg. Chem.* **1982**, *21* (7), 2878-2881.
39. Arsenault, G. J.; Anderson, C. M.; Puddephatt, R. J., Complexes with platinum-gold and -silver bonds: catalysis by silver(I) of alkyl

- exchange reactions between platinum centers. *Organometallics* **1988**, *7* (10), 2094-2097.
40. Usón, R.; Forniés, J.; Tomás, M.; Casas, J. M.; Cotton, F. A.; Falvello, L. R., New compounds with platinum to silver bonds unsupported by covalent bridges. *J. Am. Chem. Soc.* **1985**, *107* (8), 2556-2557.
41. Bauer, J.; Braunschweig, H.; Dewhurst, R. D., Metal-Only Lewis Pairs with Transition Metal Lewis Bases. *Chem. Rev.* **2012**, *112* (8), 4329-4346.
42. Moret, M.-E., Organometallic Platinum(II) and Palladium(II) Complexes as Donor Ligands for Lewis-Acidic d¹⁰ and s² Centers. In *Higher Oxidation State Organopalladium and Platinum Chemistry*, Canty, J. A., Ed. Springer Berlin Heidelberg: Berlin, Heidelberg, **2011**; 157-184.
43. Fuertes, S.; Woodall, C. H.; Raithby, P. R.; Sicilia, V., Heteropolynuclear Pt(II)–M(I) Clusters with a C₂N₂C Biscyclometalated Ligand. *Organometallics* **2012**, *31* (11), 4228-4240.
44. Moret, M.-E.; Chen, P., Interaction of Organoplatinum(II) Complexes with Monovalent Coinage Metal Triflates. *J. Am. Chem. Soc.* **2009**, *131* (15), 5675-5690.
45. Forniés, J.; Ibáñez, S.; Martín, A.; Sanz, M.; Berenguer, J. R.; Lalinde, E.; Torroba, J., Influence of the Pt→Ag Donor–Acceptor Bond and Polymorphism on the Spectroscopic and Optical Properties of Heteropolynuclear Benzoquinolateplatinum(II) Complexes. *Organometallics* **2006**, *25* (18), 4331-4340.
46. Yamaguchi, T.; Yamazaki, F.; Ito, T., A Helical Metal–Metal Bonded Chain via the Pt→Ag Dative Bond. *J. Am. Chem. Soc.* **2001**, *123* (4), 743-744.
47. Baya, M.; Belío, Ú.; Fernández, I.; Fuertes, S.; Martín, A., Unusual Metal–Metal Bonding in a Dinuclear Pt–Au Complex: Snapshot of a Transmetalation Process. *Angew. Chem. Int. Ed.* **2016**, *55* (24), 6978-6982.
48. Liberman-Martin, A. L.; Levine, D. S.; Ziegler, M. S.; Bergman, R. G.; Tilley, T. D., Lewis acid-base interactions between platinum(ii) diaryl complexes and bis(perfluorophenyl)zinc: strongly accelerated reductive

- elimination induced by a Z-type ligand. *Chem. Commun.* **2016**, 52 (43), 7039-7042.
49. Ma, M.; Sidiropoulos, A.; Ralte, L.; Stasch, A.; Jones, C., Metal-only Lewis pairs featuring unsupported Pt[\rightarrow]M (M = Zn or Cd) dative bonds. *Chem. Commun.* **2013**, 49 (1), 48-50.
50. Forniés, J.; Martín, A.; Sicilia, V.; Villarroya, P., Reactivity of [M(CAP)(S2CNMe2)] [M = Pt, Pd; CAP = CH2-C6H4-P(o-tolyl)2- κ C,P] toward Mercury(II) Carboxylates. X-ray Molecular Structures of [Pt(CAP)(S2CNMe2)(O2CCF3)Hg(O2CCF3)] and [Pd(S2CNMe2){ μ -P(o-tolyl)2-C6H4-CH2-} μ -O2CCH3}Hg(O2CCH3)]. *Organometallics* **2000**, 19 (6), 1107-1114.
51. Falvello, L. R.; Forniés, J.; Martín, A.; Navarro, R.; Sicilia, V.; Villarroya, P., Reactivity of [M(CAP)(S2C-R)] (M = Pd, Pt; CAP = CH2-C6H4-P(o-tolyl)2- κ C,P; R = NMe2, OEt) toward HgX2 (X = Br, I). X-ray Crystal Structures of [Pt{CH2-C6H4P(o-tolyl)2- κ C,P}(S2CNMe2)HgI(μ -I)]2 and [PdBr(S2COEt){ μ -P(o-tolyl)2-C6H4-CH2-}HgBr]·0.5HgBr2·C2H4Cl2. *Inorg. Chem.* **1997**, 36 (27), 6166-6171.
52. Yamaguchi, T.; Yamazaki, F.; Ito, T., The First Examples of Platinum(II)-Cadmium(II) Bonds: The Role of Strong Field Ligands in Making Dative Pt \rightarrow M Bonds. *J. Am. Chem. Soc.* **1999**, 121 (32), 7405-7406.
53. Crespo, O.; Gimeno, M. C.; Laguna, A.; Lehtonen, O.; Ospino, I.; Pyykkö, P.; Villacampa, M. D., Structural and Photophysical Study on Heterobimetallic Complexes with d8-d10 Interactions Supported by Carborane Ligands: Theoretical Analysis of the Emissive Behaviour. *Chemistry - A European Journal* **2014**, 20 (11), 3120-3127.
54. Arias, A.; Forniés, J.; Fortuño, C.; Martín, A.; Mastroilli, P.; Gallo, V.; Latronico, M.; Todisco, S., Donor Behaviour of Anionic and Asymmetric Phosphanido Derivatives of Platinum and Palladium. *Eur. J. Inorg. Chem.* **2014**, 2014 (10), 1679-1693.
55. Heckenroth, M.; Kluser, E.; Neels, A.; Albrecht, M., Neutral Ligands with Exceptional Donor Ability for Palladium-Catalyzed Alkene Hydrogenation. *Angew. Chem. Int. Ed.* **2007**, 46 (33), 6293-6296.
56. Braunstein, P.; Frison, C.; Oberbeckmann-Winter, N.; Morise, X.; Messaoudi, A.; Bénard, M.; Rohmer, M.-M.; Welter, R., An Oriented 1D

- Coordination/Organometallic Dimetallic Molecular Wire with Ag@Pd Metal–Metal Bonds. *Angew. Chem. Int. Ed.* **2004**, *43* (45), 6120–6125.
57. Reitsamer, C.; Schuh, W.; Kopacka, H.; Wurst, K.; Peringer, P., Synthesis and Structure of the First Heterodinuclear PCP–Pincer–CDP Complex with a Pd–Au d8–d10 Pseudo-Closed-Shell Interaction. *Organometallics* **2009**, *28* (22), 6617–6620.
58. Kim, M.; Taylor, T. J.; Gabbai, F. P., Hg(II)···Pd(II) Metallophilic Interactions. *J. Am. Chem. Soc.* **2008**, *130* (20), 6332–6333.
59. Pyykkö, P., Strong Closed-Shell Interactions in Inorganic Chemistry. *Chem. Rev.* **1997**, *97* (3), 597–636.
60. Burdett, J. K., Substitution reactions at square-planar d8 metal centers and the kinetic cis and trans effects. A general molecular orbital description. *Inorg. Chem.* **1977**, *16* (12), 3013–3025.
61. Zumdahl, S. S.; Drago, R. S., A molecular orbital study of the trans influence and kinetic trans effect in square-planar platinum(II) complexes. *J. Am. Chem. Soc.* **1968**, *90* (24), 6669–6675.
62. Pyykkö, P.; Li, J.; Runeberg, N., Predicted ligand dependence of the Au(I)···Au(I) attraction in (XAuPH₃)₂. *Chem. Phys. Lett.* **1994**, *218* (1), 133–138.
63. Xia, B.-H.; Zhang, H.-X.; Che, C.-M.; Leung, K.-H.; Phillips, D. L.; Zhu, N.; Zhou, Z.-Y., Metal–Metal Interactions in Heterobimetallic d8–d10 Complexes. Structures and Spectroscopic Investigation of [M′M′′(μ-dcpm)₂(CN)₂]⁺ (M′ = Pt, Pd; M′′ = Cu, Ag, Au) and Related Complexes by UV–vis Absorption and Resonance Raman Spectroscopy and ab Initio Calculations. *J. Am. Chem. Soc.* **2003**, *125* (34), 10362–10374.
64. Aullón, G.; Alvarez, S., Axial Bonding Capabilities of Square Planar d8–ML₄ Complexes. Theoretical Study and Structural Correlations. *Inorg. Chem.* **1996**, *35* (11), 3137–3144.
65. Mealli, C.; Pichierri, F.; Randaccio, L.; Zangrando, E.; Krumm, M.; Holtenrich, D.; Lippert, B., Theoretical Aspects of the Heterobimetallic Dimers with the T Over Square Structural Motif. Synthesis and Structure of a Heteronuclear Platinum and Palladium Complex with 1-Methylcytosinato Bridging Ligands. *Inorg. Chem.* **1995**, *34* (13), 3418–3424.

66. Ziegler, T.; Nagle, J. K.; Snijders, J. G.; Baerends, E. J., Theoretical study of the electronic structures and absorption spectra of tetracyanoplatinate(2-) and dithallium tetracyanoplatinate(2-) based on density functional theory including relativistic effects. *J. Am. Chem. Soc.* **1989**, *111* (15), 5631-5635.
67. Nagle, J. K.; Balch, A. L.; Olmstead, M. M., $\text{Ti}_2\text{Pt}(\text{CN})_4$: a non-columnar, luminescent form of $\text{Pt}(\text{CN})_4^{2-}$ containing platinum-thallium bonds. *J. Am. Chem. Soc.* **1988**, *110* (1), 319-321.
68. Grimme, S.; Djukic, J.-P., Cation–Cation “Attraction”: When London Dispersion Attraction Wins over Coulomb Repulsion. *Inorg. Chem.* **2011**, *50* (6), 2619-2628.
69. Xia, B.-H.; Zhang, H.-X.; Jiao, Y.-Q.; Pan, Q.-J.; Li, Z.-S.; Sun, C.-C., Metallophilic attractions between d8–d10 heterometallic compounds $\text{trans}[\text{Pt}(\text{PH}_3)_2(\text{CN})_2]$ and $\text{M}(\text{PH}_3)_2^+$ (M=Ag or Cu): Ab initio study. *The Journal of Chemical Physics* **2004**, *120* (24), 11487-11492.
70. Crespo, O.; Laguna, A.; Fernández, E. J.; López-de-Luzuriaga, J. M.; Jones, P. G.; Teichert, M.; Monge, M.; Pyykkö, P.; Runeberg, N.; Schütz, M.; Werner, H.-J., Experimental and Theoretical Studies of the d8–d10 Interaction between Pd(II) and Au(I): Bis(chloro[(phenylthiomethyl)diphenylphosphine]gold(I))–dichloropalladium(II) and Related Systems. *Inorg. Chem.* **2000**, *39* (21), 4786-4792.
71. Zhugralin, A. R.; Kobylanskii, I. J.; Chen, P., Experimental Gas-Phase and in Silico Investigation of β -Methyl Elimination from Cationic Palladium Alkyl Species. *Organometallics* **2015**, *34* (7), 1301-1306.
72. Vikse, K. L.; Chen, P., Elementary Reactions at Organocopper(III): A Gas-Phase and Theoretical Study. *Organometallics* **2015**, *34* (7), 1294-1300.
73. Oeschger, R. J.; Ringger, D. H.; Chen, P., Gas-Phase Investigations on the Transmetalation Step in Sonogashira Reactions. *Organometallics* **2015**, *34* (15), 3888-3892.
74. Ringger, D. H.; Kobylanskii, I. J.; Serra, D.; Chen, P., Quantitative Description of Structural Effects on the Stability of Gold(I) Carbenes. *Chemistry – A European Journal* **2014**, *20* (44), 14270-14281.

75. Couzijn, E. P. A.; Kobylanskii, I. J.; Moret, M.-E.; Chen, P., Experimental Gas-Phase Thermochemistry for Alkane Reductive Elimination from Pt(IV). *Organometallics* **2014**, *33* (11), 2889-2897.
76. Batiste, L.; Chen, P., Coinage-Metal Mediated Ring Opening of cis-1,2-Dimethoxycyclopropane: Trends from the Gold, Copper, and Silver Fischer Carbene Bond Strength. *J. Am. Chem. Soc.* **2014**, *136* (26), 9296-9307.
77. Kobylanskii, I. J.; Widner, F. J.; Kräutler, B.; Chen, P., Co–C Bond Energies in Adenosylcobinamide and Methylcobinamide in the Gas Phase and in Silico. *J. Am. Chem. Soc.* **2013**, *135* (37), 13648-13651.
78. Fedorov, A.; Batiste, L.; Bach, A.; Birney, D. M.; Chen, P., Potential Energy Surface for (Retro-)Cyclopropanation: Metathesis with a Cationic Gold Complex. *J. Am. Chem. Soc.* **2011**, *133* (31), 12162-12171.
79. Fedorov, A.; Couzijn, E. P. A.; Nagornova, N. S.; Boyarkin, O. V.; Rizzo, T. R.; Chen, P., Structure and Bonding of Isoleptic Coinage Metal (Cu, Ag, Au) Dimethylaminonitrenes in the Gas Phase. *J. Am. Chem. Soc.* **2010**, *132* (39), 13789-13798.
80. Couzijn, E. P. A.; Zocher, E.; Bach, A.; Chen, P., Gas-Phase Energetics of Reductive Elimination from a Palladium(II) N-Heterocyclic Carbene Complex. *Chemistry – A European Journal* **2010**, *16* (18), 5408-5415.
81. Narancic, S.; Bach, A.; Chen, P., Simple Fitting of Energy-Resolved Reactive Cross Sections in Threshold Collision-Induced Dissociation (T-CID) Experiments. *The Journal of Physical Chemistry A* **2007**, *111* (30), 7006-7013.
82. Pérez-Temprano, M. H.; Casares, J. A.; Espinet, P., Bimetallic Catalysis using Transition and Group 11 Metals: An Emerging Tool for C-C Coupling and Other Reactions. *Chemistry – A European Journal* **2012**, *18* (7), 1864-1884.
83. Hirner, J. J.; Shi, Y.; Blum, S. A., Organogold Reactivity with Palladium, Nickel, and Rhodium: Transmetalation, Cross-Coupling, and Dual Catalysis. *Acc. Chem. Res.* **2011**, *44* (8), 603-613.
84. Sonogashira, K.; Tohda, Y.; Hagihara, N., A convenient synthesis of acetylenes: catalytic substitutions of acetylenic hydrogen with

- bromoalkenes, iodoarenes and bromopyridines. *Tetrahedron Lett.* **1975**, 16 (50), 4467-4470.
85. Weibel, J.-M.; Blanc, A.; Pale, P., Ag-Mediated Reactions: Coupling and Heterocyclization Reactions. *Chem. Rev.* **2008**, 108 (8), 3149-3173.
86. Létinois-Halbes, U.; Pale, P.; Berger, S., Ag NMR as a Tool for Mechanistic Studies of Ag-Catalyzed Reactions: Evidence for in Situ Formation of Alkyn-1-yl Silver from Alkynes and Silver Salts. *The Journal of Organic Chemistry* **2005**, 70 (23), 9185-9190.
87. Halbes, U.; Bertus, P.; Pale, P., The first direct coupling of 1-trialkylsilyl-1-alkynes with vinyl triflates; a new access to enynes. *Tetrahedron Lett.* **2001**, 42 (49), 8641-8644.
88. Bertus, P.; Halbes, U.; Pale, P., Pd/Ag-Catalyzed Direct Coupling of 1-Trimethylsilyl Alkynes with Vinyl Triflates. *Eur. J. Org. Chem.* **2001**, 2001 (23), 4391-4393.
89. Bertus, P.; Pale, P., Silver salts as new catalyst for coupling reactions; synthesis of epoxyenynes. *Tetrahedron Lett.* **1996**, 37 (12), 2019-2022.
90. Jones, L. A.; Sanz, S.; Laguna, M., Gold compounds as efficient co-catalysts in palladium-catalysed alkyne alkylation. *Catal. Today* **2007**, 122 (3-4), 403-406.
91. Lauterbach, T.; Livendahl, M.; Rosellon, A.; Espinet, P.; Echavarren, A. M., *Org. Lett.* **2010**, 12, 3006.
92. Panda, B.; Sarkar, T. K., On the catalytic duo PdCl₂(PPh₃)₂/AuCl(PPh₃) that cannot effect a Sonogashira-type reaction: a correction. *Tetrahedron Lett.* **2010**, 51 (2), 301-305.
93. Panda, B.; Sarkar, T. K., Gold and palladium combined for the Sonogashira-type cross-coupling of arenediazonium salts. *Chem. Commun.* **2010**, 46 (18), 3131-3133.
94. Panda, B.; Sarkar, T. K., Gold and Palladium Combined for the Sonogashira Coupling of Aryl and Heteroaryl Halides. *Synthesis* **2013**, 45 (06), 817-829.
95. Bakherad, M., Recent progress and current applications of Sonogashira coupling reaction in water. *Appl. Organomet. Chem.* **2013**, 27 (3), 125-140.

96. Chinchilla, R.; Najera, C., Recent advances in Sonogashira reactions. *Chem. Soc. Rev.* **2011**, *40* (10), 5084-5121.
97. Marsden, J. A.; Haley, M. M., Cross-Coupling Reactions to sp Carbon Atoms. In *Metal-Catalyzed Cross-Coupling Reactions*, Wiley-VCH Verlag GmbH: 2008; pp 317-394.
98. Doucet, H.; Hierso, J.-C., Palladium-Based Catalytic Systems for the Synthesis of Conjugated Enynes by Sonogashira Reactions and Related Alkynylations. *Angew. Chem. Int. Ed.* **2007**, *46* (6), 834-871.
99. Chinchilla, R.; Nájera, C., The Sonogashira Reaction: A Booming Methodology in Synthetic Organic Chemistry†. *Chem. Rev.* **2007**, *107* (3), 874-922.
100. Brandsma, L., 16 - Transition Metals-Catalysed Couplings of Acetylenes with sp²-Halides. In *Synthesis of Acetylenes, Allenes and Cumulenes*, Brandsma, L., Ed. Academic Press: Oxford, 2004; pp 293-317.
101. Tykwinski, R. R., Evolution in the Palladium-Catalyzed Cross-Coupling of sp- and sp²-Hybridized Carbon Atoms. *Angew. Chem. Int. Ed.* **2003**, *42* (14), 1566-1568.
102. Sonogashira, K., Development of Pd-Cu catalyzed cross-coupling of terminal acetylenes with sp²-carbon halides. *J. Organomet. Chem.* **2002**, *653* (1-2), 46-49.
103. Sonogashira, K., 2.4 - Coupling Reactions Between sp² and sp Carbon Centers. In *Comprehensive Organic Synthesis*, Fleming, B. M. T., Ed. Pergamon: Oxford, 1991; pp 521-549.
104. Osakada, K.; Yamamoto, T., Transmetalation of alkynyl and aryl complexes of Group 10 transition metals. *Coord. Chem. Rev.* **2000**, *198* (1), 379-399.
105. Osakada, K.; Sakata, R.; Yamamoto, T., Preparation and Properties of trans-Pd(Ar)(C:CPh)(PEt₃)₂. Intermolecular Alkynyl Ligand Transfer between Copper(I) and Palladium(II) Complexes Relevant to Palladium Complex Catalyzed Cross-Coupling of Terminal Alkyne with Haloarene in the Presence of Cu(I) Cocatalyst. *Organometallics* **1997**, *16* (24), 5354-5364.
106. Osakada, K.; Takizawa, T.; Yamamoto, T., Alkynylcopper(I) Complexes with PPh₃ Ligands. Preparation, Structure, and Alkyne Ligand

- Transfer to Palladium(II) Complexes. *Organometallics* **1995**, *14* (7), 3531-3538.
107. Meana, I.; Espinet, P.; Albéniz, A. C., Heterometallic Complexes by Transmetalation of Alkynyl Groups from Copper or Silver to Allyl Palladium Complexes: Demetalation Studies and Alkynyl Homocoupling. *Organometallics* **2014**, *33* (1), 1-7.
108. He, C.; Ke, J.; Xu, H.; Lei, A., Synergistic Catalysis in the Sonogashira Coupling Reaction: Quantitative Kinetic Investigation of Transmetalation. *Angew. Chem. Int. Ed.* **2013**, *52* (5), 1527-1530.
109. Pérez-Temprano, M. H.; Casares, J. A.; de Lera, Á. R.; Álvarez, R.; Espinet, P., Strong Metallophilic Interactions in the Palladium Arylation by Gold Aryls. *Angew. Chem. Int. Ed.* **2012**, *51* (20), 4917-4920.
110. Hansmann, M. M.; Pernpointner, M.; Döpp, R.; Hashmi, A. S. K., A Theoretical DFT-Based and Experimental Study of the Transmetalation Step in Au/Pd-Mediated Cross-Coupling Reactions. *Chemistry – A European Journal* **2013**, *19* (45), 15290-15303.
111. Additionally, L-CID can only treat up to two reaction channels.
112. Moulton, C. J.; Shaw, B. L., Transition metal-carbon bonds. Part XLII. Complexes of nickel, palladium, platinum, rhodium and iridium with the tridentate ligand 2,6-bis[(di-*t*-butylphosphino)methyl]phenyl. *J. Chem. Soc., Dalton Trans.* **1976**, (11), 1020-1024.
113. ADF2012, S., Theoretical Chemistry, Vrije Universiteit, Amsterdam, The Netherlands, <http://www.scm.com>.
114. Frisch, M. J.; Trucks, G. W.; Schlegel, H. B.; Scuseria, G. E.; Robb, M. A.; Cheeseman, J. R.; Scalmani, G.; Barone, V.; Mennucci, B.; Petersson, G. A.; Nakatsuji, H.; Caricato, M.; Li, X.; Hratchian, H. P.; Izmaylov, A. F.; Bloino, J.; Zheng, G.; Sonnenberg, J. L.; Hada, M.; Ehara, M.; Toyota, K.; Fukuda, R.; Hasegawa, J.; Ishida, M.; Nakajima, T.; Honda, Y.; Kitao, O.; Nakai, H.; Vreven, T.; Montgomery Jr., J. A.; Peralta, J. E.; Ogliaro, F.; Bearpark, M. J.; Heyd, J.; Brothers, E. N.; Kudin, K. N.; Staroverov, V. N.; Kobayashi, R.; Normand, J.; Raghavachari, K.; Rendell, A. P.; Burant, J. C.; Iyengar, S. S.; Tomasi, J.; Cossi, M.; Rega, N.; Millam, N. J.; Klene, M.; Knox, J. E.; Cross, J. B.; Bakken, V.; Adamo, C.; Jaramillo, J.; Gomperts, R.; Stratmann, R. E.; Yazyev, O.; Austin, A. J.; Cammi, R.; Pomelli, C.; Ochterski, J. W.; Martin, R. L.; Morokuma, K.; Zakrzewski, V.

- G.; Voth, G. A.; Salvador, P.; Dannenberg, J. J.; Dapprich, S.; Daniels, A. D.; Farkas, Ö.; Foresman, J. B.; Ortiz, J. V.; Cioslowski, J.; Fox, D. J. *Gaussian 09*, Gaussian, Inc.: Wallingford, CT, USA, 2009.
115. Adhikary, A.; Schwartz, J. R.; Meadows, L. M.; Krause, J. A.; Guan, H., Interaction of alkynes with palladium POCOP-pincer hydride complexes and its unexpected relation to palladium-catalyzed hydrogenation of alkynes. *Inorganic Chemistry Frontiers* **2014**, *1* (1), 71-82.
116. Tsui, E. Y.; Müller, P.; Sadighi, J. P., Reactions of a Stable Monomeric Gold(I) Hydride Complex. *Angew. Chem. Int. Ed.* **2008**, *47* (46), 8937-8940.
117. Gaillard, S.; Slawin, A. M. Z.; Nolan, S. P., A N-heterocyclic carbene gold hydroxide complex: a golden synthon. *Chem. Commun.* **2010**, *46* (16), 2742-2744.
118. Toledo, A.; Meana, I.; Albéniz, A. C., Formal Gold-to-Gold Transmetalation of an Alkynyl Group Mediated by Palladium: A Bisalkynyl Gold Complex as a Ligand to Palladium. *Chemistry – A European Journal* **2015**, *21* (38), 13216-13220.
119. Bondi, A., van der Waals Volumes and Radii. *The Journal of Physical Chemistry* **1964**, *68* (3), 441-451.
120. Calculated TSa–c are lower in energy than intermediates 6a–c. Geometry optimizations were done at a lower level of accuracy, M06-L/SDD(d,p), followed by more precise single points at M06 L/TZP. Such an approach leads to minor inconsistencies due to the distinct flatness of the potential-energy surface.
121. Hallinan, N.; Besancon, V.; Forster, M.; Elbaze, G.; Ducommun, Y.; Merbach, A. E., High-pressure NMR kinetics. 47. Solvent-exchange mechanisms of nonaqueous square-planar tetrasolvates: a high-pressure proton NMR investigation. *Inorg. Chem.* **1991**, *30* (5), 1112-1114.
122. Hellquist, B.; Elding, L. I.; Ducommun, Y., Mechanism for formation and aquation of palladium(II) acetonitrile complexes in aqueous solution. Variable-temperature and variable pressure study of stabilities and kinetics. *Inorg. Chem.* **1988**, *27* (20), 3620-3623.

123. Roulet, R.; Gray, H. B., Mechanisms of substitution reactions of axially blocked palladium(II) complexes in different solvents. *Inorg. Chem.* **1972**, *11* (9), 2101-2104.
124. Marino, J. P.; Long, J. K., New strategies for annulations: a highly convergent and stereoselective synthesis of an octahydronaphthalene synthon for dihydrocompactin. *J. Am. Chem. Soc.* **1988**, *110* (23), 7916-7917.
125. Liebeskind, L. S.; Fengl, R. W., 3-Stannylcyclobutenediones as nucleophilic cyclobutenedione equivalents. Synthesis of substituted cyclobutenediones and cyclobutenedione monoacetals and the beneficial effect of catalytic copper iodide on the Stille reaction. *The Journal of Organic Chemistry* **1990**, *55* (19), 5359-5364.
126. Deng, J. Z.; Paone, D. V.; Ginnetti, A. T.; Kurihara, H.; Dreher, S. D.; Weissman, S. A.; Stauffer, S. R.; Burgey, C. S., Copper-Facilitated Suzuki Reactions: Application to 2-Heterocyclic Boronates. *Org. Lett.* **2009**, *11* (2), 345-347.
127. Bürgi, H. B.; Dunitz, J. D.; Lehn, J. M.; Wipff, G., Stereochemistry of reaction paths at carbonyl centres. *Tetrahedron* **1974**, *30* (12), 1563-1572.
128. Schweizer, W. B.; Procter, G.; Kaftory, M.; Dunitz, J. D., Structural Studies of 1,8-Disubstituted Naphthalenes as Probes for nucleophile-electrophile interactions. *Helv. Chim. Acta* **1978**, *61* (8), 2783-2808.
129. Jolliet, P.; Gianini, M.; von Zelewsky, A.; Bernardinelli, G.; Stoeckli-Evans, H., Cyclometalated Complexes of Palladium(II) and Platinum(II): cis-Configured Homoleptic and Heteroleptic Compounds with Aromatic C \wedge N Ligands. *Inorg. Chem.* **1996**, *35* (17), 4883-4888.
130. Fructos, M. R.; de Frémont, P.; Nolan, S. P.; Díaz-Requejo, M. M.; Pérez, P. J., Alkane Carbon-Hydrogen Bond Functionalization with (NHC)MCl Precatalysts (M = Cu, Au; NHC = N-Heterocyclic Carbene). *Organometallics* **2006**, *25* (9), 2237-2241.
131. Cordero, B.; Gomez, V.; Platero-Prats, A. E.; Reves, M.; Echeverria, J.; Cremades, E.; Barragan, F.; Alvarez, S., Covalent radii revisited. *Dalton Transactions* **2008**, (21), 2832-2838.
132. delPozo, J.; Carrasco, D.; Pérez-Temprano, M. H.; García-Melchor, M.; Álvarez, R.; Casares, J. A.; Espinet, P., Stille Coupling

Involving Bulky Groups Feasible with Gold Cocatalyst. *Angew. Chem. Int. Ed.* **2013**, *52* (8), 2189-2193.

133. Furuya, T.; Benitez, D.; Tkatchouk, E.; Strom, A. E.; Tang, P.; Goddard, W. A.; Ritter, T., Mechanism of C–F Reductive Elimination from Palladium(IV) Fluorides. *J. Am. Chem. Soc.* **2010**, *132* (11), 3793-3807.

134. del Pozo, J.; Salas, G.; Álvarez, R.; Casares, J. A.; Espinet, P., The Negishi Catalysis: Full Study of the Complications in the Transmetalation Step and Consequences for the Coupling Products. *Organometallics* **2016**, *35* (20), 3604-3611.

135. delPozo, J.; Gioria, E.; Casares, J. A.; Álvarez, R.; Espinet, P., Organometallic Nucleophiles and Pd: What Makes ZnMe₂ Different? Is Au Like Zn? *Organometallics* **2015**, *34* (13), 3120-3128.

136. Collins, L. R.; Riddlestone, I. M.; Mahon, M. F.; Whittlesey, M. K., A Comparison of the Stability and Reactivity of Diamido- and Diaminocarbene Copper Alkoxide and Hydride Complexes. *Chemistry – A European Journal* **2015**, *21* (40), 14075-14084.

137. Bader, R. F. W., *Atoms in Molecules: A Quantum Theory*. Oxford University Press: Oxford, U.K., 1990.

138. Mann, K. R.; Gordon, J. G.; Gray, H. B., Characterization of oligomers of tetrakis(phenyl isocyanide)rhodium(I) in acetonitrile solution. *J. Am. Chem. Soc.* **1975**, *97* (12), 3553-3555.

139. Frenking, G.; Matthias Bickelhaupt, F., The EDA Perspective of Chemical Bonding. In *The Chemical Bond*, Wiley-VCH Verlag GmbH & Co. KGaA: **2014**; 121-157.

140. BDEs of C–C bonds. In *Comprehensive Handbook of Chemical Bond Energies*, CRC Press: **2007**; 147-210.

141. Hughes, R. P.; Ward, A. J.; Golen, J. A.; Incarvito, C. D.; Rheingold, A. L.; Zakharov, L. N., Synthesis, molecular structures, and chemistry of some new palladium(II) and platinum(II) complexes with pentafluorophenyl ligands. *Dalton Transactions* **2004**, (17), 2720-2727.

142. Haas, D.; Hammann, J. M.; Greiner, R.; Knochel, P., Recent Developments in Negishi Cross-Coupling Reactions. *ACS Catalysis* **2016**, *6* (3), 1540-1552.

143. Negishi, E.-i., Magical Power of Transition Metals: Past, Present, and Future (Nobel Lecture). *Angew. Chem. Int. Ed.* **2011**, *50* (30), 6738-6764.
144. Jana, R.; Pathak, T. P.; Sigman, M. S., Advances in Transition Metal (Pd,Ni,Fe)-Catalyzed Cross-Coupling Reactions Using Alkyl-organometallics as Reaction Partners. *Chem. Rev.* **2011**, *111* (3), 1417-1492.
145. Krasovskiy, A.; Thomé, I.; Graff, J.; Krasovskaya, V.; Konopelski, P.; Duplais, C.; Lipshutz, B. H., Cross-couplings of alkyl halides with heteroaromatic halides, in water at room temperature. *Tetrahedron Lett.* **2011**, *52* (17), 2203-2205.
146. Hadei, N.; Achonduh, G. T.; Valente, C.; O'Brien, C. J.; Organ, M. G., Differentiating C-Br and C-Cl Bond Activation by Using Solvent Polarity: Applications to Orthogonal Alkyl-Alkyl Negishi Reactions. *Angew. Chem. Int. Ed.* **2011**, *50* (17), 3896-3899.
147. Duplais, C.; Krasovskiy, A.; Lipshutz, B. H., Organozinc Chemistry Enabled by Micellar Catalysis. Palladium-Catalyzed Cross-Couplings between Alkyl and Aryl Bromides in Water at Room Temperature. *Organometallics* **2011**, *30* (22), 6090-6097.
148. Bernhardt, S.; Manolikakes, G.; Kunz, T.; Knochel, P., Preparation of Solid Salt-Stabilized Functionalized Organozinc Compounds and their Application to Cross-Coupling and Carbonyl Addition Reactions. *Angew. Chem. Int. Ed.* **2011**, *50* (39), 9205-9209.
149. van Asselt, R.; Elsevier, C. J., Rigid bidentate nitrogen ligands in organometallic chemistry and homogeneous catalysis. 8. On the Mechanism of Formation of Homocoupled Products in the Carbon-Carbon Cross-Coupling Reaction Catalyzed by Palladium Complexes Containing Rigid Bidentate Nitrogen Ligands: Evidence for the Exchange of Organic Groups between Palladium and the Transmetalating Reagent. *Organometallics* **1994**, *13* (5), 1972-1980.
150. Guerrero, A.; Martin, E.; Hughes, D. L.; Kaltsoyannis, N.; Bochmann, M., Zinc(II) η^1 - and η^2 -Toluene Complexes: Structure and Bonding in $\text{Zn}(\text{C}_6\text{F}_5)_2 \cdot (\text{toluene})$ and $\text{Zn}(\text{C}_6\text{F}_4\text{-2-C}_6\text{F}_5)_2 \cdot (\text{toluene})$. *Organometallics* **2006**, *25* (14), 3311-3313.

151. Fafard, C. M.; Chen, C.-H.; Foxman, B. M.; Ozerov, O. V., Covalent palladium-zinc bonds and their reactivity. *Chem. Commun.* **2007**, (43), 4465-4467.
152. Cordero, B.; Gómez, V.; Platero-Prats, A. E.; Reyes, M.; Echeverría, J.; Cremades, E.; Barragan, F.; Alvarez, S., Covalent radii revisited. *Dalton Transactions* **2008**, (21), 2832-2838.
153. Bader, R. F. W., A Bond Path: A Universal Indicator of Bonded Interactions. *The Journal of Physical Chemistry A* **1998**, *102* (37), 7314-7323.
154. Oeschger, R. J.; Chen, P., Structure and Gas-Phase Thermochemistry of a Pd/Cu Complex: Studies on a Model for Transmetalation Transition States. *J. Am. Chem. Soc.* **2017**, *139* (3), 1069-1072.
155. Thordarson, P., Determining association constants from titration experiments in supramolecular chemistry. *Chem. Soc. Rev.* **2011**, *40* (3), 1305-1323.
156. Fielding, L., Determination of Association Constants (K_a) from Solution NMR Data. *Tetrahedron* **2000**, *56* (34), 6151-6170.
157. Macomber, R. S., An introduction to NMR titration for studying rapid reversible complexation. *J. Chem. Educ.* **1992**, *69* (5), 375.
158. Gioria, E.; Martínez-Ilarduya, J. M.; Espinet, P., Experimental Study of the Mechanism of the Palladium-Catalyzed Aryl-Alkyl Negishi Coupling Using Hybrid Phosphine-Electron-Withdrawing Olefin Ligands. *Organometallics* **2014**, *33* (17), 4394-4400.
159. Petersen, T. O.; Simone, D.; Krossing, I., From Ion-Like Ethylzinc Aluminates to $[\text{EtZn}(\text{arene})_2]^+[\text{Al}(\text{ORF})_4]^-$ Salts. *Chemistry – A European Journal* **2016**, *22* (44), 15847-15855.
160. Petersen, T. O.; Tausch, E.; Schaefer, J.; Scherer, H.; Roesky, P. W.; Krossing, I., Ethyl-Zinc(II)-Cation Equivalents: Synthesis and Hydroamination Catalysis. *Chemistry – A European Journal* **2015**, *21* (39), 13696-13702.
161. Pye, D. R.; Mankad, N. P., Bimetallic catalysis for C-C and C-X coupling reactions. *Chemical Science* **2017**, *8* (3), 1705-1718.
162. Hashmi, A. S. K.; Lothschütz, C.; Döpp, R.; Ackermann, M.; De Buck Becker, J.; Rudolph, M.; Scholz, C.; Rominger, F., On Homogeneous

- Gold/Palladium Catalytic Systems. *Adv. Synth. Catal.* **2012**, *354* (1), 133-147.
163. Shi, Y.; Roth, K. E.; Ramgren, S. D.; Blum, S. A., Catalyzed Catalysis Using Carbophilic Lewis Acidic Gold and Lewis Basic Palladium: Synthesis of Substituted Butenolides and Isocoumarins. *J. Am. Chem. Soc.* **2009**, *131* (50), 18022-18023.
164. García-Domínguez, P.; Nevado, C., Au–Pd Bimetallic Catalysis: The Importance of Anionic Ligands in Catalyst Speciation. *J. Am. Chem. Soc.* **2016**, *138* (10), 3266-3269.
165. Kim, Y.-J.; Osakada, K.; Yamamoto, A., Preparation and properties of alkylpalladium(II) and -platinum(II) alkynyl complexes. *J. Organomet. Chem.* **1993**, *452* (1), 247-250.
166. Biedermann, F.; Schneider, H.-J., Experimental Binding Energies in Supramolecular Complexes. *Chem. Rev.* **2016**, *116* (9), 5216-5300.

8 Curriculum Vitae

Raphael Joseph Oeschger

Born on April 26, 1987 in Basel, Switzerland

Education

03/2012 – 08/2017	Ph.D. thesis in the group of Prof. Dr. Peter Chen ETH Zurich, Switzerland
2010 – 2012	Master of Science ETH in Chemistry, ETH Zurich
2007 – 2010	Bachelor of Science ETH in Chemistry, ETH Zurich
2003 – 2007	Gymnasium Interlaken, Switzerland

Research and Teaching Experience

2012 – 2017	Ph.D. research with Prof. Peter Chen, ETH Zurich Project: <i>Development of Model Complexes for Study of Transmetalation Step in Palladium Catalyzed Cross-Coupling Reactions</i>
2013 – 2017	Teaching Assistant, ETH Zurich <ul style="list-style-type: none">• Assistant of lecture “Organic Chemistry VIII: Reactive Intermediates”• Assistant for organic chemistry exercises• Assistant for practical synthetic organic chemistry courses• Supervision of five undergraduate students